Modeling the contribution of infra-gravity and incident band swash on wave run-up on East coast South-Korean beaches

with XBeach

K. R. Koudstaal

Technische Universiteit Delft

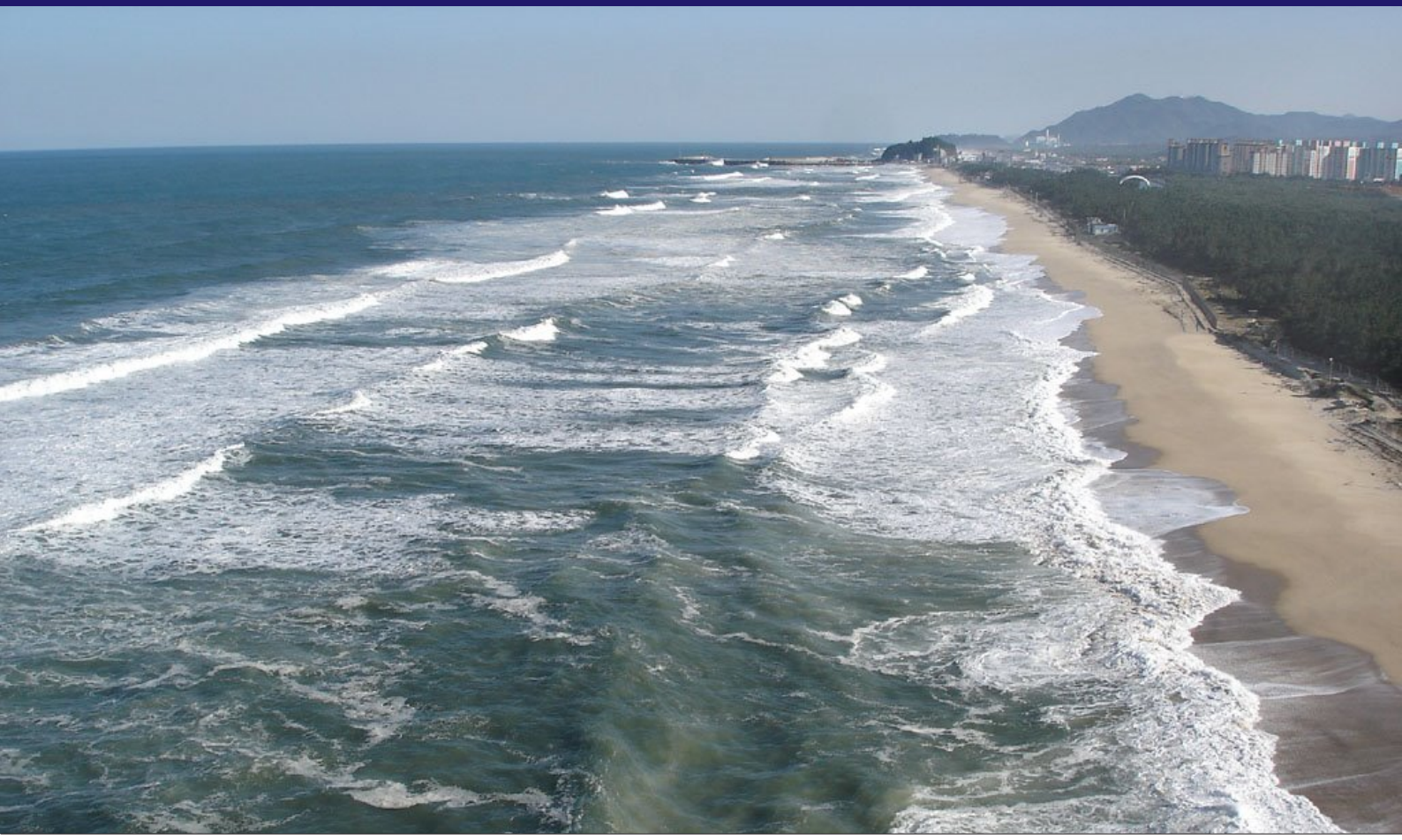

TU Delft Delft University of Technology

Challenge the future

Modeling the contribution of infragravity and incident band swash on wave run-up on East coast South-Korean beaches

With XBeach

by

K. R. Koudstaal

in partial fulfillment of the requirements for the degree of

Master of Science

in Coastal Engineering

at the Delft University of Technology,

to be defended publicly on Tuesday December 6, 2016 at 15:00 AM.

Student number:	4146735	
Supervisor:	Prof. dr. ir. A. J. H. M. Reniers,	TU Delft
Thesis committee:	Dr. R. T. McCall,	Deltares
	Dr. M. A. De Schipper,	TU Delft
	Dr. M. F. S. Tissier,	TU Delft

Deltares
Enabling Delta Life

TU Delft Delft University of Technology

"The sea, once it casts its spell, holds on in its net of wonder forever."

Jacques-Yves Cousteau

SUMMARY

The maximum wave run-up on a beach is an important factor in the design of coastal protection measures. Therefore, it is desired to predict this run-up based on numerical models. In this thesis, this is done with the use of the model XBeach.

Wave run-up consists of multiple components: a swash height, S, and a wave set-up, $<\eta>$. The swash height can be divided in a high frequency (incident) and low frequency (infragravity) part. Which of these two frequencies prevail depends on multiple factors such as offshore wave energy and local bathymetry. In general, it is expected that on low sloping beaches or dissipative coasts, low frequency swash is dominant. Steep beaches or reflective coasts experience a dominance of high frequency swash motions. Intermediate beaches experience both high and low frequency motions, and thus lie somewhere between these two extremes. This report uses a case study, which is such an intermediate beach, with an alongshore varying bathymetry and topography: Anmok beach in South-Korea.

This report also shows that the prevailing frequency band determines what type of (simplified) model can be used. This is done with the use of both 1D and 2DH models. As no data are available, all conclusions are made based on the model results only.

The main part of this thesis consists of 1D results, as this required less computational time. Therefore, many synthetic storms could be analysed. Their analysis showed that low frequency motions prevail in the wave run-up and that the use of a simplified model is allowed.

Even though a 1D model requires less computational demand, the question can arise whether it is valid to use it, since the case study showed a strongly alongshore varying coast. To research this, a 2DH model of the case study site has been analysed as well. The analysis is limited to one storm condition, that was also used in the 1D model, due to time constraints. The results showed differences between the 1D and 2DH model in the generation of low frequency motions, which lead to differences in the maximum wave run-up as well. The low frequency motions do not prevail as was seen in the 1D model. Contrary to the 1D model, very low frequency motions could also be found in the wave run-up of the 2DH model.

As the 2DH model results are assumed to be closest to reality, the results suggest that a more simplified approach in the determination of wave run-up is not allowed for this particular case study. However, since the results are based on a single storm condition, further research is necessary to provide more insight and better conclusions.

PREFACE

This thesis marks the final step to complete the master Hydraulic engineering at the Technical University Delft. The research has been conducted in collaboration with Deltares in Delft and is part of their CoMIDAS project.

Firstly, I would like to thank my entire committee; Ad Reniers, Marion Tissier, Matthieu de Schipper and Robert McCall. Thank you for your guidance and constructive feedback throughout this project, as well for the sympathy and patience when I fell ill for a month. Special thanks go to Robert McCall for his efforts and daily supervision, it was great working with you!

I would like to thank the CoMIDAS project members for the interesting meetings and opportunity to contribute to this project. Thanks go also out to my fellow students at Deltares for interesting discussions and feedback, but also for the "gezellige" coffee breaks.

Lastly, I would like to thank my dear friends and family for their support, wise words, smiles and laughs and much needed distractions throughout these months. Special thanks go to Maxime, for always being there when I needed you the most.

K. R. Koudstaal
Delft, November 2016

CONTENTS

List of Figures

LIST OF TABLES

NOMENCLATURE

SYMBOLS

Symbol	|Units |	Description
S	$[m]$	Vertical swash height
S_{IG}	$[m]$	Vertical swash height at infragravity frequencies
S_{inc}	$[m]$	Vertical swash height at incident frequencies
$R_{2\%}$	$[m]$	Wave run-up with a 2% exceedance level
$<\eta>$	$[m]$	Mean run-up at the shoreline, vertically
f	$[Hz]$	Wave frequency
f_{split}	$[Hz]$	Split frequency for division between lf and hf
g	$[m/s^2]$	Gravitational constant (9.81 m/s^2)
$T_{m-1,0}$	$[s]$	Mean spectral wave period
H_{m0}	$[m]$	Significant wave height
HF	$[Hz]$	High frequency ($> f_{split}$)
inc	$[Hz]$	Incident frequency band, same as hf
LF	$[Hz]$	Low frequency ($0.004Hz < f < f_{split}$)
IG	$[Hz]$	Infragravity frequency band, same as lf
vlf	$[Hz]$	Very low frequency ($< 0.004Hz$)
H_0	$[m]$	Offshore wave height
L_0	$[m]$	Offshore wave length
s_0	$[-]$	Offshore wave steepness
c	$[m/s]$	Wave celerity
ω	$[rad/s]$	Radial frequency ($2\pi f$)
k	$[rad/m]$	Wave number ($2\pi/L$)
β_f	$[-]$	Beach face slope
β	$[-]$	Same as β_f
β_H	$[-]$	Surf similarity parameter
ξ	$[-]$	Iribarren number
T_p	$[s]$	Peak wave period
m_n	$[m^2/s^n]$	nth order variance moment
D_w	$[m^2]$	Dissipation by wave breaking
α	$[-]$	Wave dissipation coefficient
T_{rep}	$[s]$	Representative wave period
Q_b	$[-]$	Fraction of breaking waves
E_w	$[m^2]$	Wave energy
H_{rms}	$[m]$	Root-mean-square wave height
H_{max}	$[m]$	Maximum wave height
h	$[m]$	Water depth
γ	$[-]$	Breaking threshold in breaker formulation (H_{rms}/h)
γ_2	$[-]$	Second breaking threshold in breaker formulation (H_{rms}/h)
R^2	$[-]$	Coefficient of determination
SS_{res}		Residual sum of squares dimension depends on evaluated data
SS_{tot}		Total sum of squares, dimension depends on evaluated data

ABBREVIATIONS

Abbreviations	Description
JONSWAP	Joint North Sea WAve Project
HISWA	Hindcastinf of waves in shallow water, by Holthuijsen *et al.* [8]
NSWE	Non-linear Shallow Water Equations
CE	Cusp Embayment
CH	Cusp Horn
RMSE	Root-mean-square-error
SWL	Still water level
WL	Water level
Surf.def.	Surf-beat mode of XBeach, default breaker formulation
Surf.rd.	Surf-beat mode of XBeach, Roelvink-Daly breaker formulation
Surf.rd.adap.	Surf-beat mode of XBeach, calibrated Roelvink-Daly breaker formulation
Non-h.	Non-hydrostatic mode of XBeach

1

INTRODUCTION

1.1. BACKGROUND

The coastal zone is the place where the sea and land meet. A lot of characteristics meet and interact with each-other in this zone; waves, tides, currents, sea level rise, sedimentation and erosion are just a few examples. How they interact depends on their location within the coastal zone. One of these zones is called the swash zone: A highly dynamic zone, just after the surf zone (figure 1.1), where the waves wash up and run down the beach. The maximum run-up level is important in coastal zones, since it influences the extent of a habitable zone near the coast.

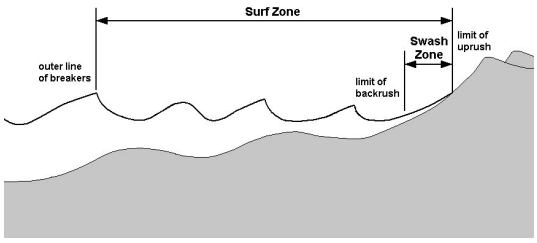

Figure 1.1: Different zones within the coastal zones [1]

Run-up and the swash zone
Run-up on a beach consists of multiple components: a swash height amplitude, S, and a wave set-up, $< \eta >$. The swash height amplitude can be divided in a high frequency (incident) and low frequency (infragravity) part [7]. Whether the high or low frequency swash motions are dominant depends on the bathymetry, as explained in chapter 2. In general, it is expected that on low sloping beaches or dissipative coasts, low frequency swash is dominant. Steep beaches or reflective coasts experience a dominance of high frequency swash motions. Intermediate beaches experience both high and low frequency motions, and thus lie somewhere between these two extremes. However, other research by Baldock *et al.* [9] and Brocchini and Baldock [10] states that low frequency swash can dominate on reflective coasts as well, which would probably result in a dominance of infragravity motions on an intermediate beach as well. The uncertainty as to which motions prevail forms the foundation of research subquestion 1.

The main part of this thesis revolves around the applicability of a 1D model for run-up on an intermediate beach with a rhythmic bar and beach state. Masselink *et al.* [11] found for example that a system with a cusping beach shows a difference in run-up, with higher run-up at the cusp horn than in the cusp embayment. Therefore, in the 1D part, two cross sections are modeled: the cusp horn and the cusp embayment, as shown in figure 1.3. The results will give an indication whether longshore variability can be neglected. In the 2DH model, the run-up at the same locations is compared to see the effect refraction has on the wave run-up at these locations. It thus shows the applicability of a 1D model for this beach system. During this last part of

the thesis, it is assumed that the 2DH model gives results closest to reality.

Case study location

The case study location is Amnok beach in Gangneung, South-Korea. This part of South-Korea is characterized by a micro-tidal environment, with a varying tidal-range between $0.1m$ and $0.3m$. Seasonal variations fall in the same range as the tidal-range [12]. The beach is wave dominated, with most of the time low significant wave heights (less than $1.5m$) and peak periods (less than $7.5s$). During extreme events however, the significant wave height can reach over $8m$ with peak periods of more than $15s$. Per season the dominant wave direction changes, but on average it can be concluded that they come from NE-NNE direction [12].

The beach shows some alongshore variation with cusp horns and embayments, as well as cresentic bars. According to Swinkels *et al.* [12], the rhytmic cusps appear to correlate with these cresentic shaped bars. When combined with a beach face gradient around the WL of approximately $\tan\beta_f = 0.13$ for the cusp horn and $\tan\beta_f = 0.098$ for the cusp embayment[1] (based on bathymetry, as shown in figure 1.3, the beaches can be classified as intermediate beaches with a rhythmic bar and beach state.

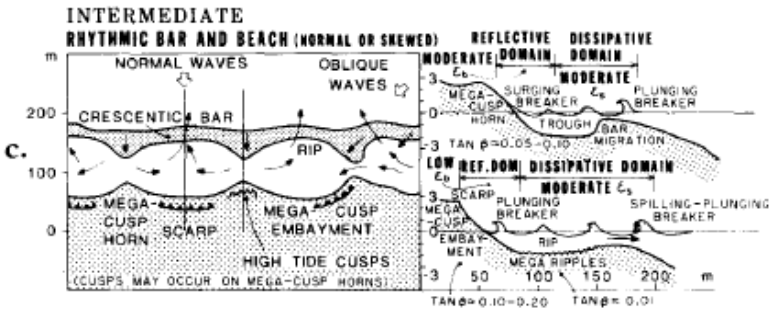

Figure 1.2: Characteristic of the classification of an intermediate beach with a rhythmic bar and beach state, image taken from Wright and Short [2]

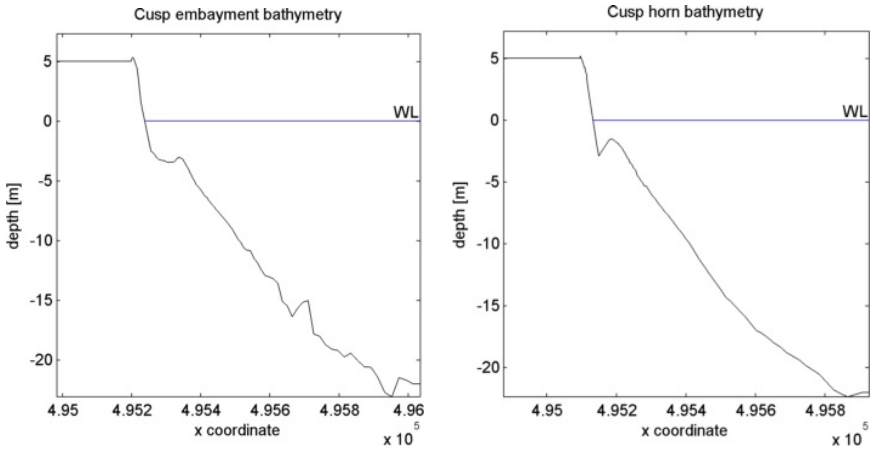

(a) Bathymetry at a cusp embayment (CE) (b) Bathymetry at a cusp horn (CH)

Figure 1.3: Both bathymetries

[1] Above WL the beach face slope of the CE increases to $\tan\beta_f = 0.1792$

Scope of this project
In this thesis the focus will be on this swash zone and the hydraulic processes that occur there. However, the scope of the project is confined to South-Korean intermediate beaches with a rhythmic bar and beach state, which will be modeled with the use of a wave model called XBeach. The explanation of the classification can be found in section 2.5. This location is so specific, as this research is part of an existing project called *CoMIDAS - East Coast Case*.

The scope of this report is confined to the beaches Anmok and Namhangjin of the city Gangneung, in the Gangwon-do Province, South-Korea. These beaches are relatively small ($25-50m$) and show a rhythmic cusp and bar system, as can be seen in figure 1.4.

A range of fictitious storm conditions will be used to answer the main research question of this report. These storm conditions cover the variety of storm conditions that can be found at this location.

As no data are available for this research, the results of a numerical model (XBeach) will be used instead. This model has several modes, of which 2 will be used in this thesis. Firstly, the *Non-hydrostatic mode* will be used. This mode solves all hydrodynamic processes and behaves closest to reality. It has been validated in the past, thus forming a good basis for this research. Secondly, the *Surf-beat mode* will be used. This mode is based on the separation of the high frequency wave groups and the low frequency waves that are generated by them. It is known that this type of model underestimates the incident motions as it does not resolve the intra-wave motions of the short waves [13]. More information about the model and its modes can be found in section 2.7. Finally, the focus of this research lies on the hydrodynamics in the swash zone. Therefore, the models are run without a morphological update.

Modeling the run-up and its components correctly is not only important for the design height of coastal structures, but also forms the basis of a correct representation of overtopping and sediment dynamics in the swash zone. This lies, however, outside of the scope of this thesis.

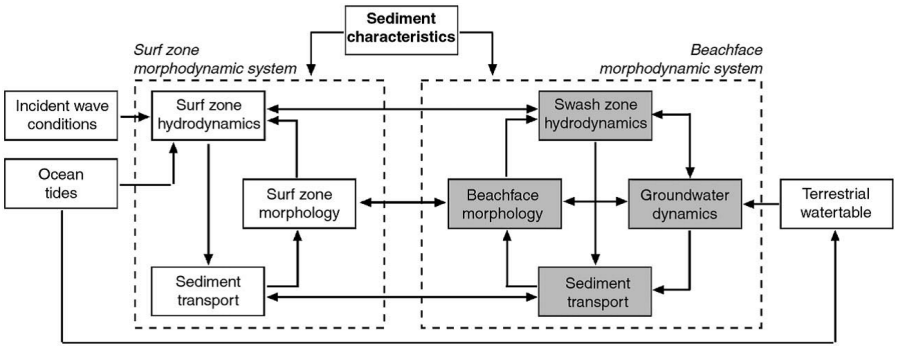

Figure 1.5: The interconnecting complex processes that affect the coastal region, taken from Masselink and Puleo [3]

(a)

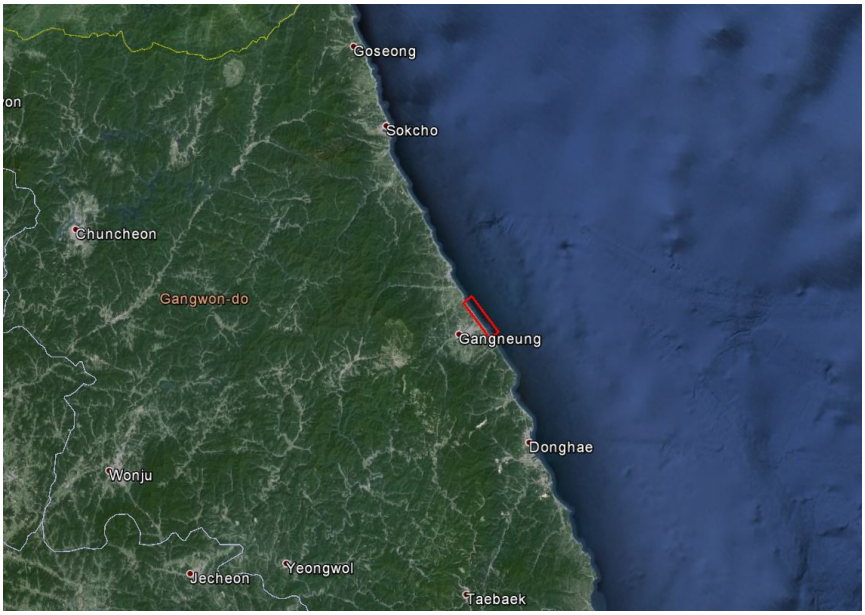

(b)

(c)

Figure 1.4: FTTB: a) Location of the Gangwon-do province in South-Korea, b) Location of research within the province of Gangwon-do, c) Overview of Anmok (left of port) and Namhangjin (right of port) beach. Images taken with Google Earth

1.2. RESEARCH GOALS

1.2.1. RESEARCH QUESTIONS

The focus of this research will be the applicability of the model XBeach to simulate wave run-up on East coast South-Korean intermediate beaches. To this end, the roles of infragravity (IG) and incident (inc) band swash will be researched, by comparing their influence on the wave run-up on these beaches. The effect of longshore variability will also be included in the research. The final research question will be:

"Under what conditions can wave run-up be modeled sufficiently well for engineering purposes, by a 1D Surf-beat model of intermediate beaches"

As explained in the introduction, this question is based on a working hypothesis that the Surf-beat mode of XBeach can not model incident swash correctly.

In order to narrow down the research, the different parts of the main question are described below.

- *Conditions*: only three different conditions will be examined, namely
  - the bathymetry,
  - the offshore wave steepness and
  - offshore wave height
- *Sufficiently well for engineering purposes*: a maximum relative difference of 10% between the Surf-beat and Non-hydrostatic mode is accepted
- *Intermediate beaches*: only one beach will be regarded and explained in the introduction, this will be Anmok beach in South Korea

To answer the main research question, the following sub-questions need to be answered as well;

1. How do the contributions of setup, incident (HF) and infragravity (LF) band swash vary under the aforementioned conditions?
2. What are the differences in the predictions of the swash motions between the Non-hydrostatic and the Surf-beat mode, and are these differences a function of the aforementioned conditions?

In order to check until what extent an 1D model is justified, another sub-question will be researched: sub-question 3. As the 1D model will not include processes such as the refraction between the cusp horn and embayment, this sub-question has to be answered using a 2DH model.

3. Are there differences in the predictions of the swash dynamics between the 2DH and 1D model, and are they caused by the alongshore varying bathymetry and topography of the research location?

The hydrodynamics of the model are handled differently by the two modes, especially in 2DH [6]. This leads to the final sub-question 4.

4. Is the (dis)similarity between simulated swash dynamics in the non-hydrostatic and surf-beat mode different for 1D and 2DH models?

1.2.2. HYPOTHESIS

The generation of LF motions depends on multiple variables, such as offshore wave steepness, foreshore slope and offshore wave height. As explained in chapter 2, whether HF or LF motions prevail in the swash zone, depends on the beach state. This research surrounds an intermediate beach state, thus indicating to have a mix of both LF and HF motions. As explained in chapter 3, a mix of storm conditions will be used in this report. Therefore, the hypothesis for sub-question 1 is as follows:

With increasing offshore wave height and decreasing offshore wave steepness, the role of LF motions in the swash zone is mainly dominant

This hypothesis brings about another theory. In some run-up formulations (for example by Stockdon *et al.* [7]) it is stated that low frequency motions in the swash zone are not affected by the beach face slope. On the other hand, Guedes *et al.* [14] states that a change in beach face slope affects the high frequency swash and that this slope is the main reason for alongshore changes in swash characteristics. Therefore, in the case

where low frequency motions are highly dominant before entering the swash zone, little change in dominance is expected within the swash-zone. Larger differences are expected when high frequency motions are dominant, as these motions are subjected to changes while running up the beach. Thus a second hypothesis for sub-research question 1 is:

The respective roles of incident and infragravity band swash are determined by the respective significant high frequency and low frequency wave-height at the toe of the beach.

This will be researched qualitatively (how much of the total energy is for the low frequency motions) and quantitatively (parameterization of the swash with hydrodynamic parameters at the toe). The latter could result in a parameterization of the incident swash motions, which can be used for the Surf-beat model, as incident swash is expected to not be modelled correctly. This is right away also the foundation for the hypothesis for sub-research question 2:

Surf-beat estimates all LF motions sufficiently well for engineering purposes. When LF motions are dominant in the swash zone, the underestimation of HF motions becomes negligible, thus correctly estimating the Non-hydrostatic run-up.

For the last two sub-research questions, there are two hypothesis. The first one can partially be answered by the 1D models. Both are based on they theory in section 2.6. For research question 3, the hypothesis is:

The wave run-up in a 2DH model will be higher at the cusp horn and lower at the embayment compared to the run-up at these locations in a 1D model, due to non-uniform refraction.

For research question 4 the hypothesis is:

Due to the alongshore uniformity assumption in 1D models, the LF wave growth will be stronger in 1D models than 2DH models. Therefore the difference between the Non-hydrostatic and Surf-beat modes will increase in a 2DH model as the LF contribution to the modeled swash decreases.

1.2.3. APPROACH

An important step in the approach is the assumption that the Non-hydrostatic mode is taken as "reality" as no data is available throughout this report. The Non-hydrostatic 2DH model results are taken as closest to reality, as it also includes 2D processes.

The first part of this thesis involves modeling with a 1D Non-hydrostatic model. Two bathymetries are used, a *cusp horn* and a *cusp embayment* as well as varying offshore conditions. The offshore conditions both vary in wave height and steepness. Even though processes such as refraction between the cusp horn and embayment are not part of a 1D model, it is expected to see differences in run-up. This is due to the difference in bar shape and beach face slope, as can be seen in figures 3.2b and 3.2a. In order to answer the first hypothesis, an output is generated for both the run-up signal, as well as at the toe of the beach face. For both bathymetries this will be at the same depth. Both the output of the run-up and at the toe undergo a spectral analysis and are then qualitatively and quantitatively compared to each other. More information about the methodology of the Non-hydrostatic model can be found in section 3.3. The Surf-beat model undergoes a similar approach, including the testing of multiple breaker formulations. The final part of the 1D modeling involves the comparison of the two models.

When the first two research questions have been answered, sub-questions 3 and 4 are researched for a 2DH case. Due to time constraints, only one storm condition is modeled. The choice of storm condition depends on the 1D results. Both a Surf-beat and Non-hydrostatic calculation are made. The focus lies on the analysis of longshore variability in run-up and its long and high frequency components, but also in the evaluation of any differences between the 1D and 2DH models. It will show if long-shore variability can be neglected when it comes to run-up.

Important to note is that all models will be executed without a morphological update. The main topic is the influence of the intermediate beach state on the hydrodynamics and which parts of these hydrodynamics prevail for which conditions.

1.3. OUTLINE

Contents of the rest of the report is as follows:

Chapter 2: Includes an explanation the physics in the swash-zone
Chapter 3: Explains the methodology of the 1D model
Chapter 4: Contains an overview of the 1D results and their analysis
Chapter 5: Gives an overview of all 1D conclusions and answers to the first two research sub-questions
Chapter 6: Includes the methodology of the 2DH model, its results and analysis
Chapter 7: Provides an overall discussion, conclusion and recommendations of this report

Finally, the Appendix contains an overview of all 1D results on which the analysis in chapter 4 is based, in Appendix A. Appendix B includes extra figures to support the analysis in chapter 6. Appendix C gives an analysis of the current method of analyzing the swash zone. Lastly, in Appendix D an example of an XBeach input file can be found.

2

PHYSICS IN THE SWASH ZONE

The swash zone is a dynamic zone that moves as the water levels vary [15]. It extends from the limit of run-down (backwash) to the limit of run-up (up rush). Due to wave interactions, these limits vary as well, causing an intermittent behaviour of the swash zone. Gaining insight about this behaviour is crucial for a continuous advance of accurate models.

This chapter provides some insights of processes that are important for this thesis. It is however assumed that the reader already has some familiarity with the topic of coastal engineering. Section 2.1 explains shortly some essential coastal terminology. After this, section 2.2 will cover the type of waves that can occur, in both the nearshore and swash zone. Section 2.4 shows some examples of parameterization of run-up parameters. Finally, section 2.5 covers the different types of beach states and the relative importance of different waves on the different types of beaches.

2.1. ZONES

To understand a bit more about the swash zone, it is important to know where it is located and what other processes occur prior to this zone.

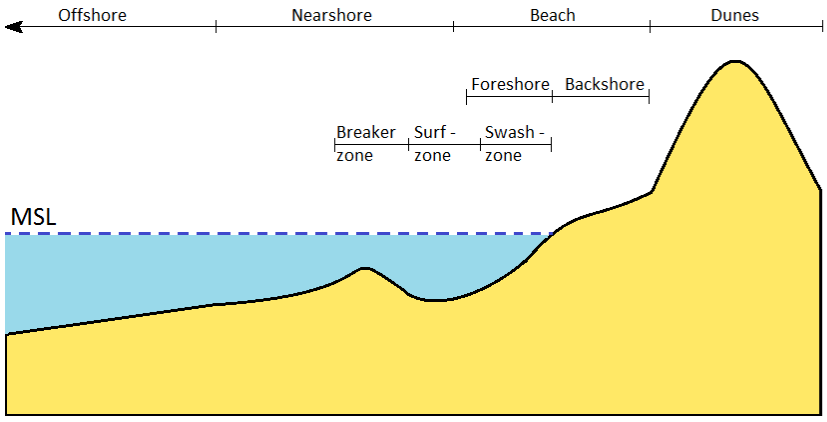

Figure 2.1: Different zones within the coastal region [1]

The waves come into the system from the *offshore* region, where, if the depth is large enough, they do not interact with the bottom. As they start approaching the coast, the waves start to shoal due to the reduction in depth and the conservation of wave energy flux. The increase in wave-height will continue until the waves reach a point of breaking in the *breaker zone*. This breaking causes the wave to become a bore, which continues into the *swash zone* where it collapses and runs up the *foreshore* and runs down again. Therefore, swash is defined by USACE [16] as: "The rush of water up onto the beach face following the breaking of a wave".

2.2. WAVE TYPES

Waves can be described by their length and type of generation. They can be generated by gravitational forces (tides), earthquakes (tsunamis), wind (swell and wind waves, also called surface wave [16]) or by waves themselves (infragravity or low frequency waves). As mentioned in chapter 1, the tide and seasonal variability at the research location are negigible. Therefore, this section will only focus on wind waves and wave-induced motions. This means that the focus lies on high frequency (HF) or short waves, and low frequency (LF) or long waves. The separation between these bands is based on the split frequency (f_{split}). More information about this parameter can be found in section 3.3.2.

2.2.1. HIGH FREQUENCY

The term, high frequency waves, is another name for the types of surface waves: wind and swell. The first type of waves are, as the name suggest, generated by the wind itself and therefore depend on the wind characteristics such as velocity, fetch and the duration, but also depend on the waterdepth. The HF waves are defined as such, that their period lies between about 0.25 and 25 to 30 seconds.

Whereas wind waves are often irregular and random, with their energy spread out over multiple frequencies, swell waves are more regular, with their energy confined to a smaller amount of frequencies. This is because of frequency dispersion: As the storm ceases and the waves propagate, they are sorted on their frequency, as different frequencies propagate with different celerities. As the shorter waves dissipate the fastest, the remaining swell waves are often relatively long. A secondary effect is that the sorted waves then travel in wave groups, which is important for the generation of LF waves. [17]

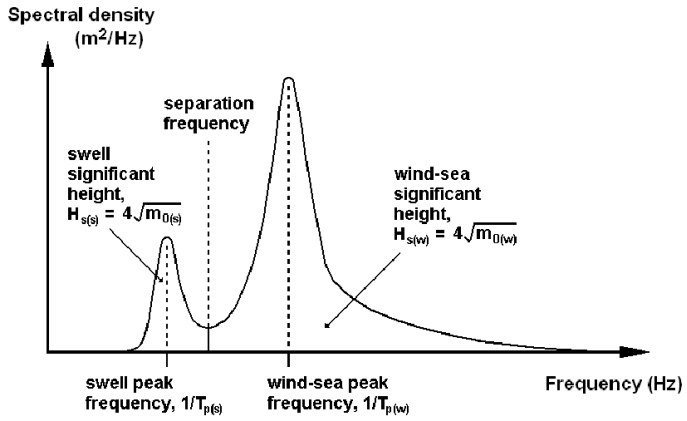

Figure 2.2: Example of a spectral differences between wind and swell waves, from Hawkes *et al.* [4]

2.2.2. LOW FREQUENCY

On the other end of the spectrum, in the range of ($0.004Hz - f_{split}$) lie the LF motions. The discussion of f_{split} (0.0375 Hz) can be found in section 3.3.2. As mentioned before, the LF motions are induced by the waves themselves, as first seen by Munk [18]. Later on, this phenomenon was explained by Longuet-Higgins and Stewart [19] (LHS62) by radiation stresses and mass flux. They also stated that as the LF motion travels with the wave group velocity, they are bound to the wave group, hence the name: *bound long wave*. Furthermore they discussed that this long wave becomes free as the HF waves start to break.

This is however, not the only mechanism that can force a free long wave. As explain by Brocchini and Baldock [10], other mechanisms are:

1. Interacting short waves inside the swash zone: an interaction between incident waves and the swash motions of the foregoing waves [9];
2. Generation by a moving breakpoint, where it is also assumed that no bound long waves are present. [20]

These long waves partially dissipate and reflect at the shoreline. Battjes [21] and further on Van Dongeren *et al.* [22] discussed that the surf-similarity parameter β_H controls these reflections and dissipations. This parameter is directly linked to the Iribarren number, ξ, a breaking parameter for regular waves by Battjes [23]. Both are shown in equations 2.1 and 2.2. The formulas are composed of the beach face slope, β, significant wave height, H and the wave length, L_0. They found, based on experimental data, that from about a value of $\xi = 2.5$ a maximum reflection occurs, for both long and regular waves.

$$\xi = \frac{\tan\beta}{(\frac{H}{L_0})^{\frac{1}{2}}} \tag{2.1}$$

$$\xi = \sqrt{2\pi}\beta_H \tag{2.2}$$

The Iribarren number is one of the parameters used to define a beach state. More information about beach states and the importance of HF and LF motions can be found in section 2.5. In short, it can be said that a high value for ξ indicates a reflective beach. This indicates that either the beach slope has to be large, or the incoming wave must have a low wave steepness to experience the beach slope as reflective. Analogous the opposite occurs for a dissipative beach.

2.3. SWASH DYNAMICS

As waves approach the coast, the majority of them will break and release their energy. Some of this energy is converted into run-up on the beach [7]. This run-up, is followed by a run-down of the wave, completing the *swash cycle*. In this cycle, and just as in the other zones in the nearshore region, both HF and LF motions occur. These are often referred to as incident (*inc*) and infra-gravity (*IG*) swash motions. The separation between the *inc* and *IG* motions is the same split frequency as mentioned before.

However, these motions do not necessarily occur perfectly one after the other. It can happen that a next wave approaches, as the previous wave is still in its swash cycle. This results in either the absorption of the first wave by the second wave, or in a collision between the two waves. This is called swash-swash [24] interaction and an example is given in figure 2.3

Because of this phenomenon, errors in a spectral analysis could occur as high frequency motions are enforced to be able to represent the swash-swash interactions correctly. Also, a spectral analysis is often based on Eulerian measurements, where the wave signal can be described by a superposition of harmonious waves. In the swash zone however, the results are acquired by Langrangian measurements, thus making it uncertain if the frequency analysis is in agreement with the incoming waves. However, as this form of analysing the swash zone is frequently used in literature (for example Stockdon *et al.* [7] and Hughes *et al.* [5]), a high correlation can be assumed. Therefore, it is used in this report as well.

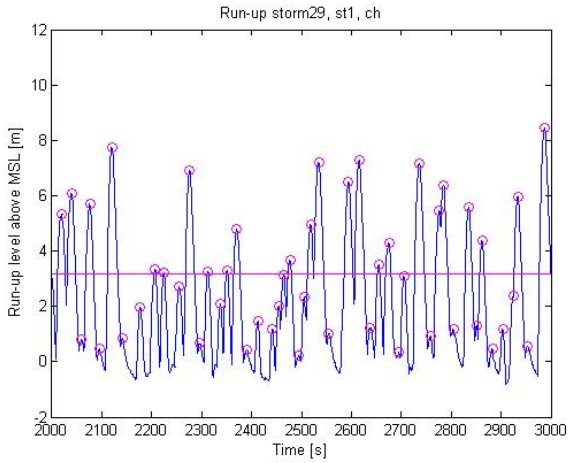

Figure 2.3: Example of interacting swash motions: as one cycle runs up and (partially) down the beach, the next cycle already starts. This is in particularly visible between 2500-2700 s.

2.4. RUN-UP IN THE SWASH ZONE

All swash motions combined form the wave run-up: the maximum level reached by a wave on a beach, relative to still water level [16]. The wave run-up height that is used to design structures for example, is defined as $R_{2\%}$. This is the wave run-up level, measured vertically from the still water line, which is exceeded by 2% of the number of incoming waves [25].

One of the first suggested parameterizations for run-up was by Hunt [26] for smooth slopes in relatively deep water, as visible in equation 2.3. In this equation, the run-up is composed of the offshore wave height, H, the Iribarren number, ξ and a constant factor K.

$$\frac{R}{H} = K\xi \tag{2.3}$$

Stockdon *et al.* [7] proposed a formulation for this wave run-up level as a combination of the maximum wave setup η and the significant swash excursion S. The spectrum of the significant swash excursion can be decomposed into incident (HF) and infragravity (LF) frequency bands, as is shown in equation 2.5

$$R_2 = 1.1\left[<\eta> + \frac{S}{2}\right], where \tag{2.4}$$

$$\begin{aligned} &S = \sqrt{S_{inc}^2 + S_{IG}^2}, and \\ &<\eta>, S_{inc}, S_{IG} = f\left(H_0, T_0, \beta_f\right) \end{aligned} \tag{2.5}$$

These expressions depend on wave height H, the deep-water wave length L_0, the wave period T, and the beach steepness β_f[1]. Stockdon *et al.* [7] found, based on their data set, a general expression for run-up on all beaches;

$$R_2 = 1.1\left(0.35\beta_f\left(H_0L_0\right)^{\frac{1}{2}} + \frac{\left[H_0L_0\left(0.563\beta_f^2 + 0.004\right)\right]^{\frac{1}{2}}}{2}\right) \tag{2.6}$$

When compared to equation 2.4, it can be seen that the left part within the brackets of equation 2.6 is an expression for the wave setup, whereas the right part is an expression for the significant swash excursion.

Another study, [27], found a parameterization for wave run-up on reflective beaches, which also included wind and tide;

$$R_2 = 0.503\beta\left(H_0L_0\right)^{\frac{1}{2}} + 0.878\xi\frac{H_0^3}{L_0} - 0.016U_(w,x) + 0.188\eta_(tide) + 0.457 \tag{2.7}$$

It can be seen that all equations depend on an Iribarren (like) parameter; however equation 2.6 uses the foreshore beach slope parameter instead of the beach gradient. This number has been frequently used in expressions for wave run-up (eg as mentioned in [25]).

2.5. BEACH STATES

Wright and Short [2] describe beaches according to their morphology and how they affect the waves. There are 3 main types of beaches, namely:

1. Reflective beaches: This type of beach has a very steep slope with a narrow surf and swash zone. It lacks any dissipative elements, which results in either collapsing waves on the beach itself, or waves that get reflected. As less waves break, there are both high and low frequency motions present, with the first being assumed dominant and the latter being assumed very weak to negligible. Other research (Baldock and Holmes [28]), however, showed that LF motions can still be dominant on steep reflective beaches, although generated by other mechanisms.
2. Dissipative beaches: This type of beach represents the other end of the classification, as it has a very long, low sloping beach and fully consists of dissipative elements. Therefore most short waves break and their energy is dissipated in a saturated surf zone. This mechanism releases the bound long waves, which results in dominance of low frequency motions at the shoreline.

[1] Most parameterizations use the beach face slope, since this area is more accessible for surveying than the submerged profile [27]. This could possibly lead to errors, but the formulation by Stockdon *et al.* [7] proved to work quite well for their data set.

3. Intermediate beaches: As the name indicates, this type of beach represents the intermediate shape between a reflective and dissipative condition. Wright and short classify 4 different intermediate shapes, ranging from more reflective to more dissipative behaviour. Therefore they have both high and low frequency motions at the shoreline, but their relative importance cannot be defined in advance.

2.6. INTERMEDIATE BEACHES

In the previous section, some details about intermediate beaches have been shortly mentioned. This section goes slightly deeper into the current knowledge of intermediate beaches (with a rhythmic bar and beach state).

Bradshaw [29] stated that an alternating intermediate beach shows more reflective to dissipative behaviour, depending on the offshore wave height. Increasing the offshore wave height resulted in a more dissipative behaviour, thus where low frequency motions prevail more. A similar result has been found by Hughes *et al.* [5] as shown in figure 2.4. The lower offshore conditions, the grey graph, show lower energies in the LF part of the spectrum and higher energies in the HF part of the spectrum. With increasing conditions, the role of LF motions become more dominant, resulting in the black graph.

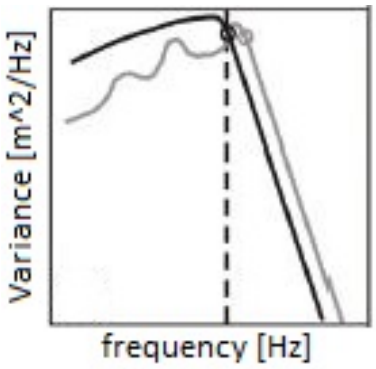

Figure 2.4: Schematic example of swash spectra for an intermediate beach with rhythmic bar and beach state. It respresents the log-log spectrum, with variance on the vertical axis and frequency on the horizontal axis. The grey graph is a representation of lower energy offshore conditions, the black graph is a representation of high energy offshore conditions. The dotted line represents the split frequency, f_{split}. Taken and adapted from Hughes *et al.* [5].

Due to the longshore variability in the beach state, also a longshore variability in wave run-up has been found in multiple occasions, but not always with a clear statement where, in alongshore sense, the run-up is the highest [30][7][14]. Bradshaw [29] however does state that in a system with transverse bars and troughs, a more reflective type of run-up can be found where shoals are not present. Thus, a higher amount of HF motions is expected at that location. This coincides with the cusp embayment in a rhythmic bar and beach system, although not to the same extent. Guedes *et al.* [14] found a longshore variability in run-up in a midly varying bathymetry. This variability is mainly due to changes in incident or HF motions. The infragravity or LF motions are found to be relatively consistent alongshore, as there is a similar foreshore slope throughout the bathymetry. The HF motions are found to vary mainly due to differences beach face slope, but differences in breaking over nearshore bars contributed as well. Therefore, for the research location of this thesis, longshore variability in run-up is expected, as a larger alongshore variability is found. Lastly, a paper by Masselink *et al.* [11] does indicate that the vertical wave run-up at the cusp horn is higher than at the cusp embayment. It has to be noted that his research is based on a location without a rhythmic bar system.

Overall it can be concluded that the behaviour of a intermediate beach with a rhythmic bar and beach state is very dependent on offshore conditions and that longshore variability in run-up can be expected.

2.7. NUMERICAL MODELLING WITH XBEACH

In this section, the two modes of the model XBeach are described, which will be used in this report. The explanation of model in this chapter is based on the XBeach manual, Kingsday version [6], a paper by [31] and the website xbeach.org. XBeach is a numerical, open-source, and two dimensional model (depth-averaged), that includes multiple processes such as[2];

- Refraction, shoaling and breaking of short waves
- Generation, propagation and dissipation of LF waves
- Wave-induced set-up
- Sediment transport
- Dune face avalanching

This study will use the XBeach model to resolve the research questions mentioned in chapter 1.2. Two wave modes of the model will be used:

- The Surf-beat wave mode
- The Non-hydrostatic wave mode

Surf-beat mode This instationary mode resolves the wave height on the scale of wave groups, with the use of the HISWA equations. The variations on this scale induce radiation stress gradients [19], which generate the LF or infragravity waves, which on their turn are solved by the nonlinear shallow water equations (NSWE). A schematic representation of this process is given in figure 2.5. Dissipation is accounted for, as well as other mechanisms such as; wave-driven and wind-driven currents, run-up and backwash of LF waves.

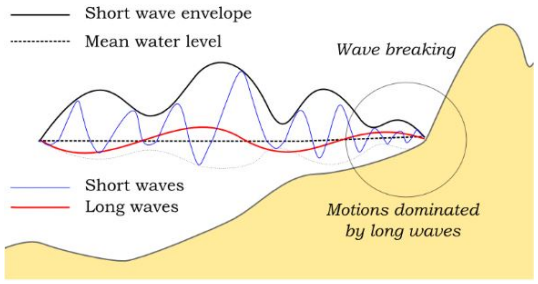

Figure 2.5: Schematic representation of the surf-beat mode, taken from Roelvink *et al.* [6]. The text, *dominated by long waves*, is only valid for dissipative conditions

The dissipation can be modelled by selecting different breaker formulations. In this report, the following 3 cases are used, all based on the same dissipation formulation, as shown by equation 2.8.

$$\bar{D_w} = 2\frac{\alpha}{T_{rep}} Q_b E_w \frac{H_{rms}}{h} \tag{2.8}$$

1. **The default breaker model**, *Roelvink2*: This formulation uses the idea to calculate the dissipation by multiplying the fraction of breaking waves (Q_b) with the dissipation per breaking event.

$$Q_b = 1 - \exp\left(-\left(\frac{H_{rms}}{H_{max}}\right)^n\right) \tag{2.9}$$

2. **Formulation by Daly *et al.* [32],** $Roelvink\_Daly$: This breaker model is based on the idea that waves fully break if a threshold is exceeded (γ) and stop breaking when the wave height is lower than a second threshold (γ_2). primary tests showed that Surf-beat underestimated the low frequency motions. This breaker model has been found to increase those motions in Roelvink *et al.* [33].

$$\begin{cases} Q_b = 1 \; if \; H_{rms} > \gamma h \\ Q_b = 0 \; if \; H_{rms} < \gamma_2 h \end{cases} \tag{2.10}$$

[2] A more complete list can be found in the manual [6].

3. **Calibrated** $Roelvink\_Daly$: Instead of using the default values from formulation 2, they have been changed to induce more LF motions (by trial and error) as primary tests proved this was necessary for some cases. The conditions of these tests are shown in table 3.1. Further in this report, this breaker formulation will be referred to as *Roelvink-Daly, adapted*. The tests resulted in the use of $\gamma = 0.6 \, and \, \gamma_2 = 0.25$, which means that compared to the default values, the waves start breaking later, and stop breaking later.

One of the assumptions of the Surf-beat mode, is that no short wave motions are reflected at the shore. They are all assumed to dissipate at the shoreline. This is therefore the working hypothesis throughout this report. Hence, it is expected that the Surf-beat mode will not model the S_{inc} and outgoing $H_{m0,hf}$ correctly for non-dissipative conditions.

Non-hydrostatic mode This mode uses the non-linear shallow water equations, with a non-hydrostatic pressure correction by Stelling and Zijlema [34]. This pressure correction is similar to the method in the one layer version of the model SWASH. This mode can solve all processes: all incoming waves, both HF and LF motions, are resolved individually, contrary to the Surf-beat mode. Therefore, it is a more reliable method to solve individual wave breaking. Moreover, it allows HF motions to reflect at the shoreline, whereas the Surf-beat mode assumes all wave groups to dissipate there. The Non-hydrostatic mode does however, require more computational demand as a higher spatial resolution is required, which implies smaller time steps, thus a longer computation time.

As the mode has been calibrated (for example by McCall *et al.* [35] and validation reports from `xbeach.org`), it is expected that the results are accurate enough to use as a reference as no data is available. The use of a model such as SWASH could be more accurate, due to the vertical layering, but is not chosen here, as using the same program (XBeach) would reduce the time to set up the models.

3

1D METHODOLOGY

As mentioned in chapter 1.2, the first research sub-questions will be researched using 1D models. These 1D models are cross-shore sections of the full bathymetry at two locations, as shown in figure 3.1. These precise locations are chosen to already see if the rhythmic bar and beach state have an influence on the highest 2% of the run-up, or the $R_{2\%}$. It has to be noted however, that the 1D model does not take all processes into account, so no full conclusions about their influence can be drawn yet.

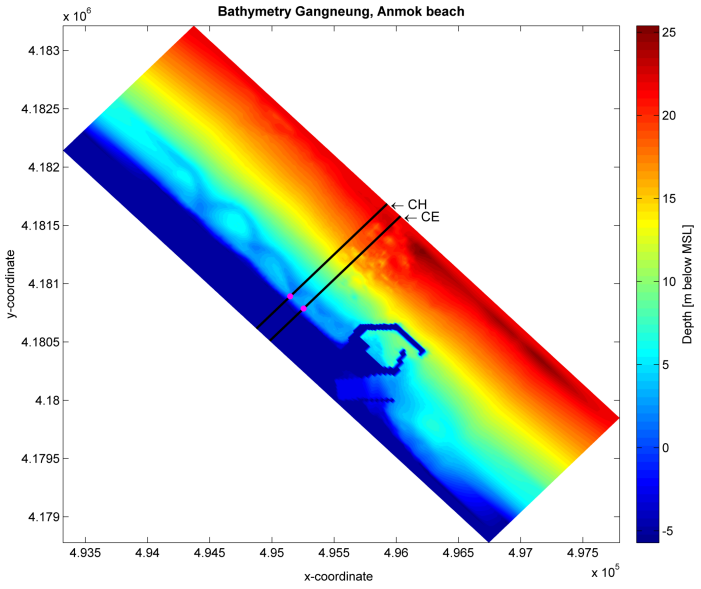

Figure 3.1: The locations of the 1D bathymetries within the 2DH model

In this chapter, firstly a short overview is given of the first offshore conditions used in this thesis. The conditions are limited to a range of 1-8,5 meters input significant wave height. This range is used to get an idea of the different processes during different storms. Their results showed a general overestimation of high frequency and an underestimation of low frequency motions, using default model parameters in the Surf-beat mode, compared to the Non-hydrostatic mode. Therefore, other breaker formulations of the Surf-beat mode have been tested to lower the under- and overestimations. The *Roelvink-Daly* breaker formulation has been calibrated to increase the amount of LF motions, as explained in section 2.7.

The second part of this chapter consists of the methodology behind the final computations for the 1D modeling. This section contains an overview of new storm conditions and the Non-hydrostatic methodology. Lastly, a section is dedicated to the differences in the methodology for the Surf-beat mode and an overview of the changed parameters compared to the default settings.

3.1. WAVE BREAKER CALIBRATION SIMULATIONS

The first computed storm conditions are given as a boundary conditions in the form of a *jons-table*, as can be seen in table 3.1. This means that this table consists of the offshore wave input parameters to generate a JONSWAP spectrum at the offshore boundary: the significant wave height, H_{m0}, the peak wave period, T_p and the angle of entry of the incoming waves and the spreading, *s*. *Gamma-jsp* defines the shape of the spectrum, where a value of 3.3 coincides with a JONSWAP spectrum. The total storm duration for these first computed storms equals 1 hour. Table 3.1 shows the main conditions of the different storms, which are based on the CoMIDAS report of Swinkels *et al.* [12]. The results of these first calculations have been used to calibrate the breaker formulations mentioned in section 2.7.

Table 3.1: The different primary storm conditions used in this research

	H_{m0} [m]	T_p [s]	Main angle [°]	gamma-jsp [-]	s [-]
1	8.5	15.00	44.5	3.3	20.000
2	7.29104	13.5836	31.6673	3.3	6.8957183
3	4.62480	10.3825	45.1565	3.3	5.8208188
4	2.81449	9.203654	51.6075	3.3	5.1939126
5	1.0	7.00	44.5	3.3	20.000

3.2. GRID GENERATION

As can be seen in sections 3.1 and 3.3, each storm condition has a different H_{m0} and T_p. Since the resolution of the computational grid partially depends on these parameters, it would indicate that each computational grid is different. To avoid discrepancies in run-up due to these differences, each storm is therefore computed with the same grid resolution. This resolution is the smallest resolution that can still be used for the lowest storm. Figures 3.2a and 3.2b show an example of a cross-section of the research location. From this figure, it can be seen that the dune crest is at 5 m above MSL. Since the storms are extreme conditions with large $H_{m0}s$, the bathymetry is changed in order to be able to compute run-up only. The bathymetry cross-section can be found in figures 3.2a and 3.2b, where it can be seen that the slope of the original beach/back shore (red line) is extended (black line). These figures also show the beach face slope, $tan(\beta)$. This parameter is obtained by determining the beach face slope around WL, over a distance of about 20 m. At the cusp embayment (figure 3.2b), this is also conducted where the beach face slope showed a transition into a steeper section, about 2.5 m above WL.

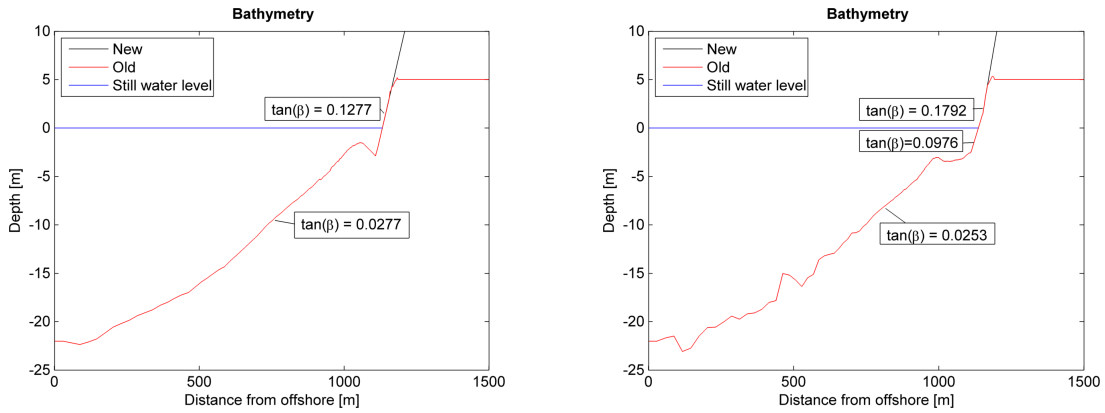

(a) Changed bathymetry for the cusp horn

(b) Changed bathymetry for the cusp embayment

Figure 3.2: Changed bathymetries

3.3. NON-HYDROSTATIC METHODOLOGY

3.3.1. INPUT CONDITIONS

Based on first computations with the 5 different conditions, it was clear that the role of HF and LF waves differs per storm condition. Therefore, in order to answer research sub question 2, new synthetic storm conditions have been made for the two bathymetries. They are computed for 130 minutes. These storm conditions consist of 3 different offshore steepnesses (s_0): 1%, 2% (swell waves) and 4% (wind waves).

$$\begin{aligned} s_0 &= \frac{H_0}{L_0} \qquad where, \\ L_0 &= \frac{g*T^2}{2\pi} \qquad therefore, \\ T_{p,offshore} &= sqrt(\frac{H_0*2\pi}{s_0*g}) \end{aligned} \tag{3.1}$$

Each steepness criterion consists of 29 storms in the range of an offshore wave height (H_0) between 2 and 9 meters. From this range and the steepness criteria, offshore peak periods ($T_{p,offshore}$) for the model input can be calculated from formula 3.1. It results in a range of incident wave periods between 5.66 s ($H_0 = 2m, s_0 =$ 4%) to 24 s ($H_0 = 9m, s_0 = 1\%$), as shown in table 3.2. This maximum $T_{p,offshore}$ lies very close to the split frequency mentioned in 3.3.2 and lies just within the domain of wind waves. Table 3.3 shows an overview of the new values of the other parameters. There is now a single value for the main angle, based on the dominant wave direction as mentioned by Swinkels *et al.* [12], and a single value for the spreading parameter s, based on the average of the storms used in the same report. As explained in section 1.1, both the seasonal variations as the tidal range are both very small. Therefore, both are excluded from the models.

Table 3.2: Minimum and maximum peak periods per offshore wave steepness

	$T_{p,s_0=1\%}[s]$	$T_{p,s_0=2\%}[s]$	$T_{p,s_0=4\%}[s]$
Min.	11.32	8.00	5.66
Max.	24.01	16.98	12.00

Table 3.3: Set parameters for the offshore boundary condition

Main angle [°]	gamma-jsp [-]	s [-]	duration [s]
40.00	3.3	5.00	7801

3.3.2. SPECTRAL ANALYSIS

As the main research question mentioned, this thesis focuses on the swash zone. Therefore, both bathymetries are analysed based on the instantaneous water level at the toe of the beach, where the depth equals 2.4 meters, and on the run-up signal of every storm condition.

The instantaneous water level is composed of a sum of a large number of harmonic wave components, known as Fourier series [17]. In order to perform a spectral analysis, a variance density spectrum has to be made of this water level elevation. The first 6 minutes of every water level signal is neglected, as this is part of the spin-up time. This can be done with a Fast Fourier Transformation (FFT), which results in a graph where the variance density is spread out over the frequencies.

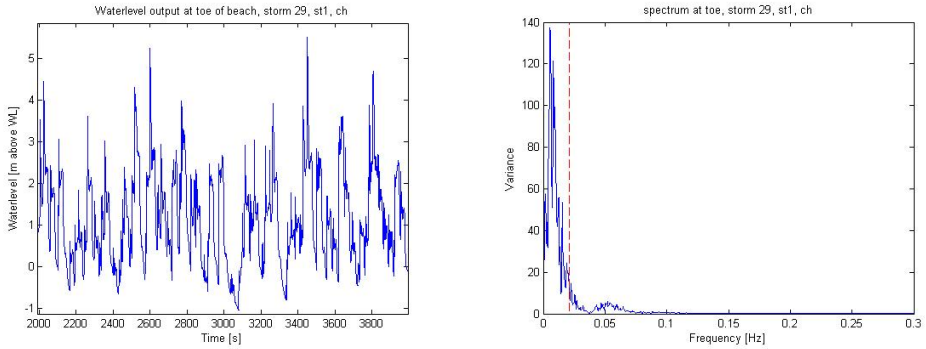

(a) Water level signal example at the toe

(b) Spectrum of the example storm, where the red dashed line represents the split frequency

Figure 3.3: Water level signal example and its variance density spectrum

The total spectrum can then be split in a HF and LF spectrum. There are multiple split frequencies used in papers, such as $f_{split} = 0.05Hz$ by Stockdon *et al.* [7], $f_{split} = 0.04Hz$ by de Schipper *et al.* [36], or $f_{split} = 0.5 * f_{peak,offshore}$ by Roelvink and Stive [37]. Cutting off at the wrong location may give an erroneous idea of the amount of HF and LF energy. Thus, based on all spectra of the total signal at the toe, a split frequency of $f_{split} = 0.0375Hz$ is chosen. The upper limit of the spectrum is based on the Nyquist frequency (f_N) of 2 Hz[1]. This is in agreement of the theory in section 2.2.1. The spectra of the total signal at the toe, as well as the used split frequency can be seen in figure 3.4.

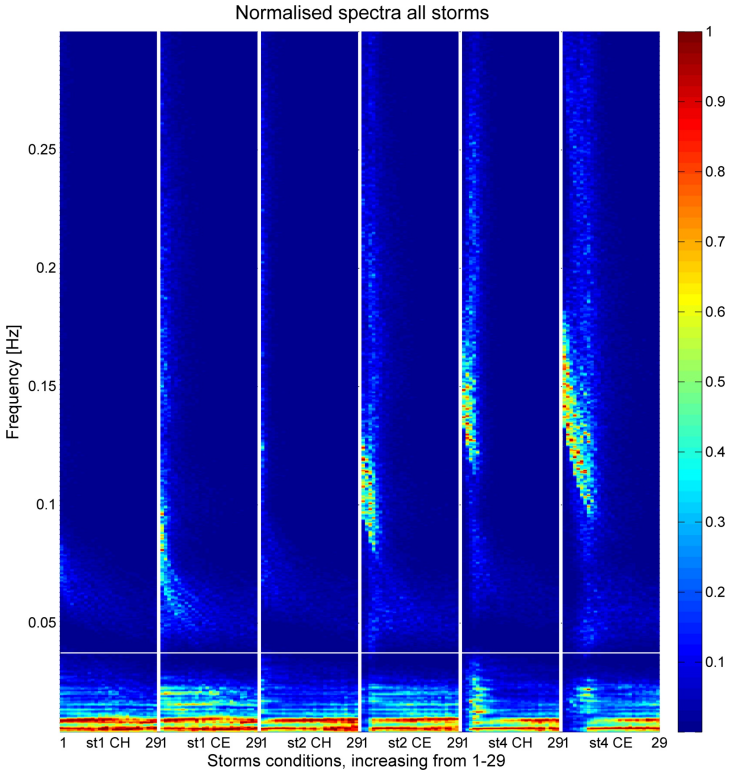

Figure 3.4: Spectra of storm conditions at the toe of the beach. On the x-axis the storm conditions are given for both 1D models (CH and CE). On the y-axis, the frequencies from 0-0.3 Hz are shown, as any above that barely contain any energy. The split frequency is shown as a white line at 0.0375 Hz.

From the spectra, parameters such as H_{m0} and the mean energy spectrum period ($T_{m-1,0}$) can be deter-

[1] Based on equation C.1 and a sample frequency of 4 Hz

mined. These two parameters are based on the variance moments of the spectra, as can be seen in formula 3.2 and 3.3. The variance moments are defined according to formula 3.4, [17], where n is the n^{th} order moment.

$$H_{m0} = 4\sqrt{m_0} \tag{3.2}$$

$$T_{m-1,0} = \frac{m_{-1}}{m_0} \tag{3.3}$$

$$m_n = \int_0^\infty f^n E(f) df \tag{3.4}$$

These parameters are determined in order to compare and relate the wave signal at the toe with the swash height signal. As explained in section 2.4, the swash height amplitude is composed of an infragravity (LF) and incident (HF) part, as shown in formulas 2.4 and 2.5. They are LF and HF motions respectively and are split by the same split frequency as at the toe. Therefore, the motions at the toe can be qualitatively (percentage of total energy for LF motions) and quantitatively (using the parameters at the toe for a parameterization of the run-up components) compared to the motions in the swash. More information about the quantitative comparison can be found in section 4.1.4. In the case that a correct parameterization for the incident (HF) swash motions is found, and the results of the Surf-beat mode show large deviations because of a misrepresentation of the HF motions, this paramerization can be use to improve the Surf-beat results.

The run-up is determined by using the shoreline signal from XBeach. Firstly, the highest points of each swash cycle are determined. Then, from these points the highest 2% value is taken and the mean is determined. Composing run-up into a mean and swash height amplitude, according to formula 2.4, has a good fit with a slightly steeper slope than shown in that formula.

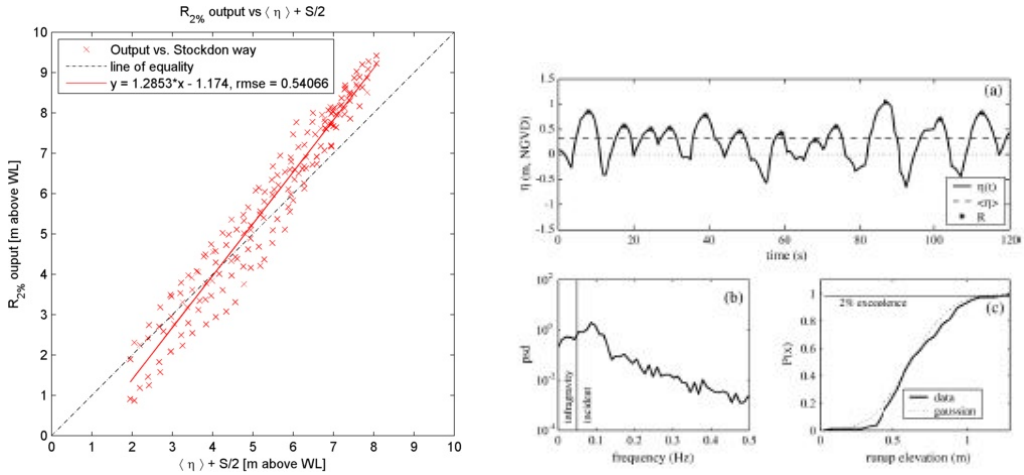

(a) Stockdon's method compared to the run-up output by the XBeach Non-hydrostatic mode

(b) Stockdon's method for a spectral analysis of the vertical swash signal

Figure 3.5: Stockdon's method and result compared to XBeach output. Figure 3.5b taken from Stockdon *et al.* [7].

3.3.3. SPLITTING OF TOTAL SIGNAL

The separation is done by a MATLAB script based on the separation technique by Guza *et al.* [38], where the in and out component are based on a characteristic shown in formula 3.5. It separates the incoming and outgoing waves by using a relationship between the surface elevation and the cross-shore depth average velocity.

$$C_\pm = (\eta c \pm hn)/2c \tag{3.5}$$

Here η represents the surface elevation, n the depth averaged current vector and h the local water depth. The original formula uses the shallow water wave celerity $c = \sqrt{gh}$. A wide range of conditions is used in this thesis, but not all of them fall under the shallow water range. Therefore, instead the wave celerity is based on the spectrum: $c = \omega/k$ where radial frequency equals $\omega = 2f\pi$ and the wave number, k is based on the dispersion relationship. The spectral analysis of the incoming and outgoing signal is then computed in the same manner as in section 3.3.2.

3.4. SURF-BEAT METHODOLOGY

The methodology of the Surf-beat mode mostly follows the methodology of the Non-hydrostatic mode. To avoid potential extra differences between the two modes, the same grid and offshore boundary conditions are used for both modes.

3.4.1. SPECTRAL ANALYSIS OF A SURF-BEAT MODE

The spectral analysis of the Surf-beat mode differentiates from the Non-hydrostatic mode, due to the differences in method of wave resolving as mentioned in section 2.7. For the Surf-beat mode, this results in a water level elevation on the wavegroup scale and a separate short wave water level elevation. To be able to analyse the results in a similar manner to the Non-hydrostatic approach, firstly spectra have to be made of the separate water level elevations. This is illustrated in the following flowchart.

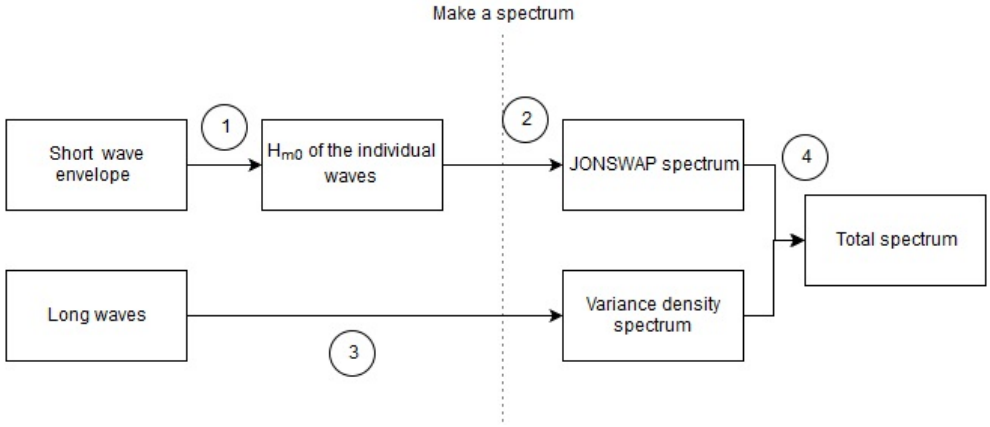

Figure 3.6: Steps for a spectral analysis of a Surf-beat mode

1. The root-mean-squared wave height (H_{rms}) of the incident waves is computed from the long-term RMS average of the modeled wave groups. With the relation $H_{m0} = H_{rms} * \sqrt{2}$, the significant incident wave height (H_{m0}) can be calculated
2. A JONSWAP spectrum, Hasselmann *et al.* [39], is then made based on $T_{p,offshore}$ and the calculated H_{m0}
3. From the long wave signal a spectrum can be made analogous to section 3.3.2
4. These spectra then need to be added, as they can contain energy at the same frequencies. This results in a final complete spectrum of the Surf-beat mode, which can then be further analysed in the same way as the Non-Hydrostatic spectra.

It can be argued how physically correct it is to use a JONSWAP spectrum at the toe. However, the Surf-beat mode bases the HF motions on a delta function at the offshore peak frequency. Using a JONSWAP or a delta function will yield the same $H_{m0,hf}$, as the total energy is the same. Therefore, a JONSWAP spectrum is chosen to make a visual comprehensible spectrum, and because this is the type of spectrum imposed at the offshore boundary. This means that no change in the spectral shape is assumed. From the Surf-beat spectra, it is visible that some long wave energy lies in the HF band, although negligible. Little overlap from the JONSWAP spectrum occurs only for the largest 5 storm conditions of $s_0 = 1\%$. This overlap causes a maximum 6% difference in $H_{m0,hf}$ and a maximum 4% difference $H_{m0,lf}$ for those 5 conditions, which can therefore be seen as negligible. Lastly, it has to be noted that using a JONSWAP spectrum for the HF motions *does* affect the determination of $T_{m-1,0hf}$. As a result, the differences in $T_{m-1,0hf}$ between the Surf-beat and Non-hydrostatic mode are not analysed.

3.4.2. SPLITTING OF TOTAL SIGNAL OF A SURF-BEAT MODE

The signals of Surf-beat can also be separated in an incoming and outgoing part. It has to be noted that the mode is based on the assumption that the short wave energy is dissipated at the shoreline. The incoming signal is thus composed of the short wave variance (for which no phase information is available) and a water

level elevation signal on the wave-group (long wave) scale, whereas the outgoing signal is only composed of the latter of these two, as shown in figure 3.7. Therefore, any outgoing HF motions are a result of LF energy that shifted up in frequency.

The incoming signal is then further analysed according to section 3.4.1, while the outgoing signal is analysed according to section 3.3.2.

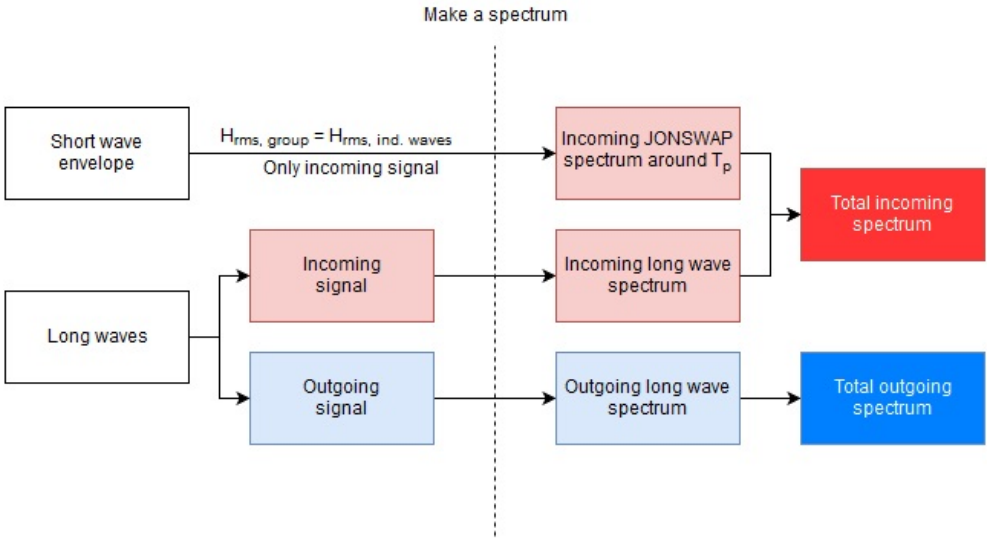

Figure 3.7: Steps to be taken before the incoming and outgoing signal of a Surf-beat mode can be analysed

3.5. OVERVIEW CHANGED PARAMETERS

In order to be able to correctly compare the results of the Non-Hydrostatic and the Surf-beat mode, some parameters have to be changed from their default settings:

- *Maxbrsteep*: The maximum wave steepness criterium for Non-hydrostatic computations. It determines when the Non-hydrostatic correction will be turned off. A value of 0.4 has been found as an optimal solution [33] and will therefore also be used throughout this research.
- *Sprdthr*: This is the threshold ratio to the maximum value of the spectrum, above which the spectrum densities are read in. These values vary in default for Surf-beat and Non-Hydrostatic. Therefore, they are both set to 0.08, the default value of the Surf-beat mode.
- *Random*: When the parameter random is set to 0, the same random wave spectrum is used if the input boundary conditions are equal.
- *Break* The breaker formulation of the Surf-beat mode. The used options are listed in section 2.7.
- *Gamma*: Both γ and γ_2 form the breaker conditions for the breaker formulations. Only for the *Roelvink-Daly, adapted* formulation these two parameters are changed to $\gamma = 0.6$ and $\gamma_2 = 0.25$.
- *Morphology*: When put to 0, the morphology update is excluded in the model.
- *Sedtrans*: When put to 0, the sediment transport is excluded in the model.

The last two parameters, morphology and sedtrans are excluded since the first focus of this research lies on the hydrodynamics that generate the run-up. Directional spreading for the 1D model is turned off, by using only one directional bin.

3.6. EVALUATION METHOD

In order to evaluate the results and how well they agree with each other, an unbiased method is needed. This will be done with an assessment of the measure of accuracy. Important to note is that only linear regressions are assessed in this report.

- **Bias**: This represents the mean error between the computed values (X) and observations (Y), as can be

seen in formula 3.6. In the case of this report, it means that the differences between the *observations* (Non-hydrostatic mode) and the *computed values* (Surf-beat mode) are assessed. It is also used for answering hypothesis 1.2.2.

$$Bias = \frac{1}{N}\sum_{i=1}^{N}(Y_i - X_i) \tag{3.6}$$

- **Coefficient of determination (R^2)**: This parameter is a measure of the degree of predictiveness of a fit (f) in the sample of data (y). The higher the value of this coefficient is, the better the fit follows the data set. Equation 3.7 shows the formula, where SS_{res} is the residual sum of squares, SS_{tot} is the total sum of squares and $\bar{y}$ is the mean of the (observed) data set.

$$\begin{aligned} &R^2 = 1 - \frac{SS_{res}}{SS_{tot}}, \qquad where \\ &SS_{res} = \sum_{i=1}^{N}\left(y_i - f_i\right)^2 \qquad and \\ &SS_{tot} = \sum_{i=1}^{N}\left(y_i - \bar{y}\right)^2 \end{aligned} \tag{3.7}$$

- **Root-mean-squared-error (RMSE)**: The RMSE estimates the variance of the residuals between the observed and computed data, or the data and its fit. Whereas the R^2 coefficient is a dimensionless parameter, the RMSE has the dimension of the data it assesses. Therefore this parameter is often used in papers as well to say something about the magnitude of error variance. The formula for the determination of RMSE is given in formula 3.8

$$RMSE = \sqrt{\frac{1}{N}\sum_{i=1}^{N}(Y_i - X_i)^2} \tag{3.8}$$

4

ANALYSES OF 1D RESULTS

This chapter consists of the analysis of both 1D models, and their differences. At the end of this chapter, both research subquestions 1 and 2 will be answered, with the help of the graphs in Appendix A.

4.1. NON-HYDROSTATIC 1D RESULTS

In order to answer the first 2 research sub-questions, a realistic model is necessary, as there are no available data. The Non-hydrostatic model behaves closest to reality, thus forms a foundation to answer research sub-question (1) and forms the basis for comparing how well surf-beat performs, research sub-question (2). The Non-hydrostatic 1D model is however a simplification of the 2DH model, thus the final conclusion regarding research sub-question 2 can be found in chapter 7. It has to be noted that even though the Non-hydrostatic model behaves close to reality (McCall *et al.* [35]), it is still only a model. Any statements are therefore conclusions about the behaviour of XBeach, not a true conclusion about reality, as data are required to validate any statement.

4.1.1. NON-HYDROSTATIC 1D RESULTS AT TOE

The results at the toe consist of the hydrodynamic parameters H_{m0} and $T_{m-1,0}$ of the total, incoming and outgoing wave signal. Based on figures 4.1 and 4.2, the following can be said:

- The total wave heights of the total, incoming and outgoing signal, increase with offshore wave height, and decrease with offshore wave steepness.
- Where the LF wave heights are roughly the same for both bathymetries for all signals, the total and HF wave height are highest for the cusp embayment.
- The outgoing HF and total motions are lower than the incoming wave heights, due to partial reflection, as shown in figures A.2c and A.2a.
- The LF motions are equal for both the outgoing and incoming waves, due to a full reflection for (almost) all conditions, as shown in figure A.2e.
- The graph of the mean energy wave period of the total signal (figure 4.2), flattens out from about $H_0 = 6m$ (CH) and $H_0 = 7m$ (CE). This indicates that from $H_0 = 6m$ (CH) and $H_0 = 7m$ (CE), the waves at the toe are of similar length. This is mainly due to the LF wave period; instead of determining $T_{m-1,0}$ over the entire spectrum, it is determined using the LF part of the spectrum. The $T_{m-1,0,lf}$ shows a similar flattening of the graph, but then from approximately $H_0 = 5m$ for both bathymetries.
- In the incoming and outgoing graph of $T_{m-1,0}$, it is visible that the LF in and outgoing period are roughly equal, hence concluding that the LF waves are fully reflected and do not undergo a frequency shift. In the same graph, it is also visible that the outgoing period of the HF and total wave motions, is larger than the incoming wave. Also, in the same graphs it is visible that the lines that represent the different offshore wave steepness, are less spread out in the outgoing wave signal than those of the incoming wave signal. Hence, the outgoing HF motions have roughly the same period. The same can be said for

the total wave motions at the toe. Combining the information from the wave heights and wave periods, shows that the outgoing HF and total waves are lower and longer than their incoming counterparts.

- It can also be concluded that in terms of wave height, the CH has lower HF motions and total motions, but equal LF motions compared to CE. In terms of wave period, the CH has similar HF and total periods but higher LF periods compared to CE. This shows that the LF motions at CH are not only more prominent, they are also longer. Vice versa, at CE, the LF motions are shorter and HF/total motions are higher, resulting in an overall higher steepness at CE. This difference can most likely be explained by the presence of the more prominent bar at CH, breaking the waves that are too steep.

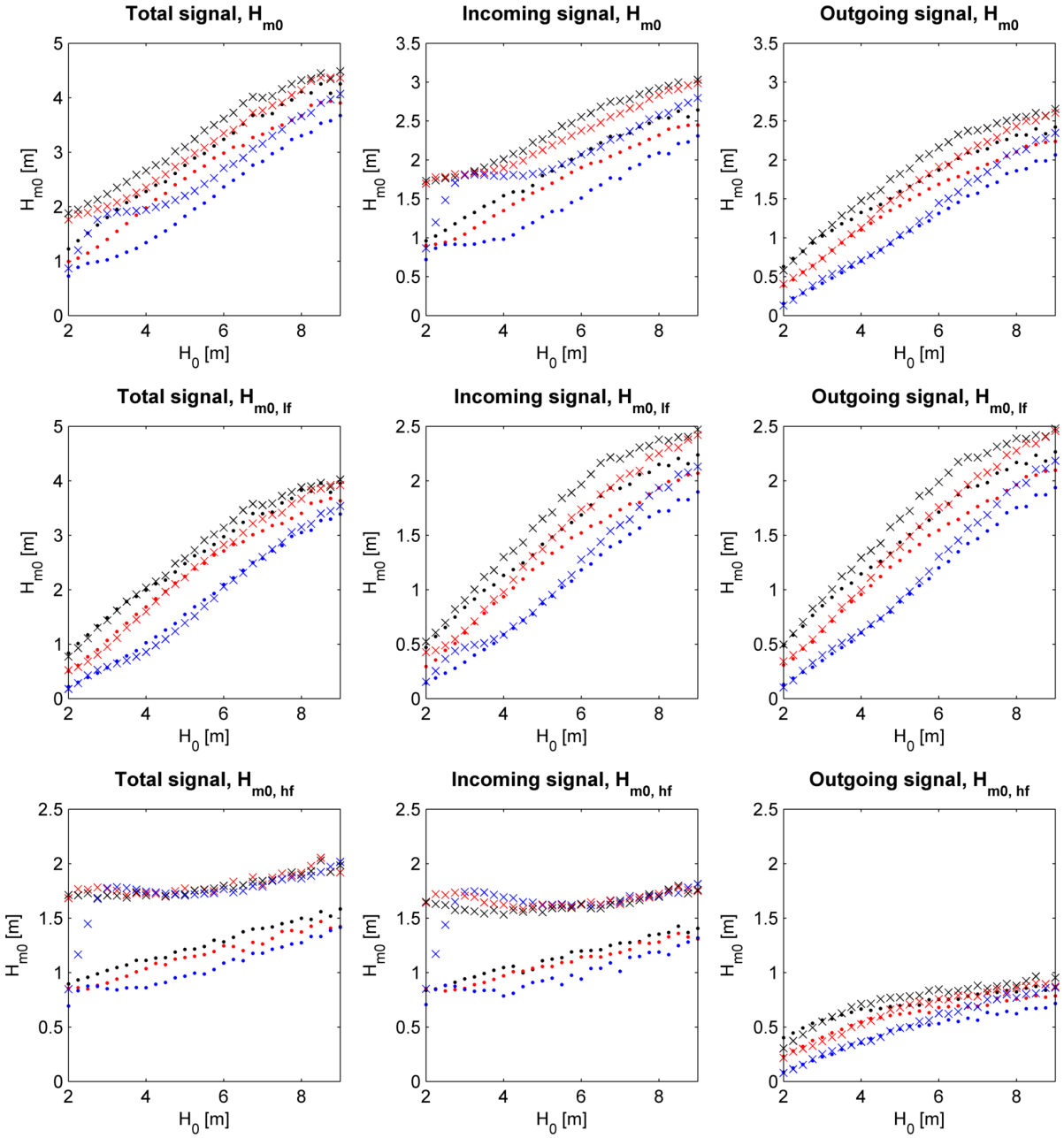

Figure 4.1: Wave heights, H_{m0}, at the toe against the offshore wave height, H_0. Top row: total wave height, middle row: LF wave height, bottom row: HF wave height. Left column: total wave signal, middle column: incoming wave signal, right column: outgoing wave signal. Black markers for $s_0 = 0.01$, red markers for $s_0 = 0.02$ and blue markers for $s_0 = 0.04$, $\cdot = CH$, $\times = CE$.

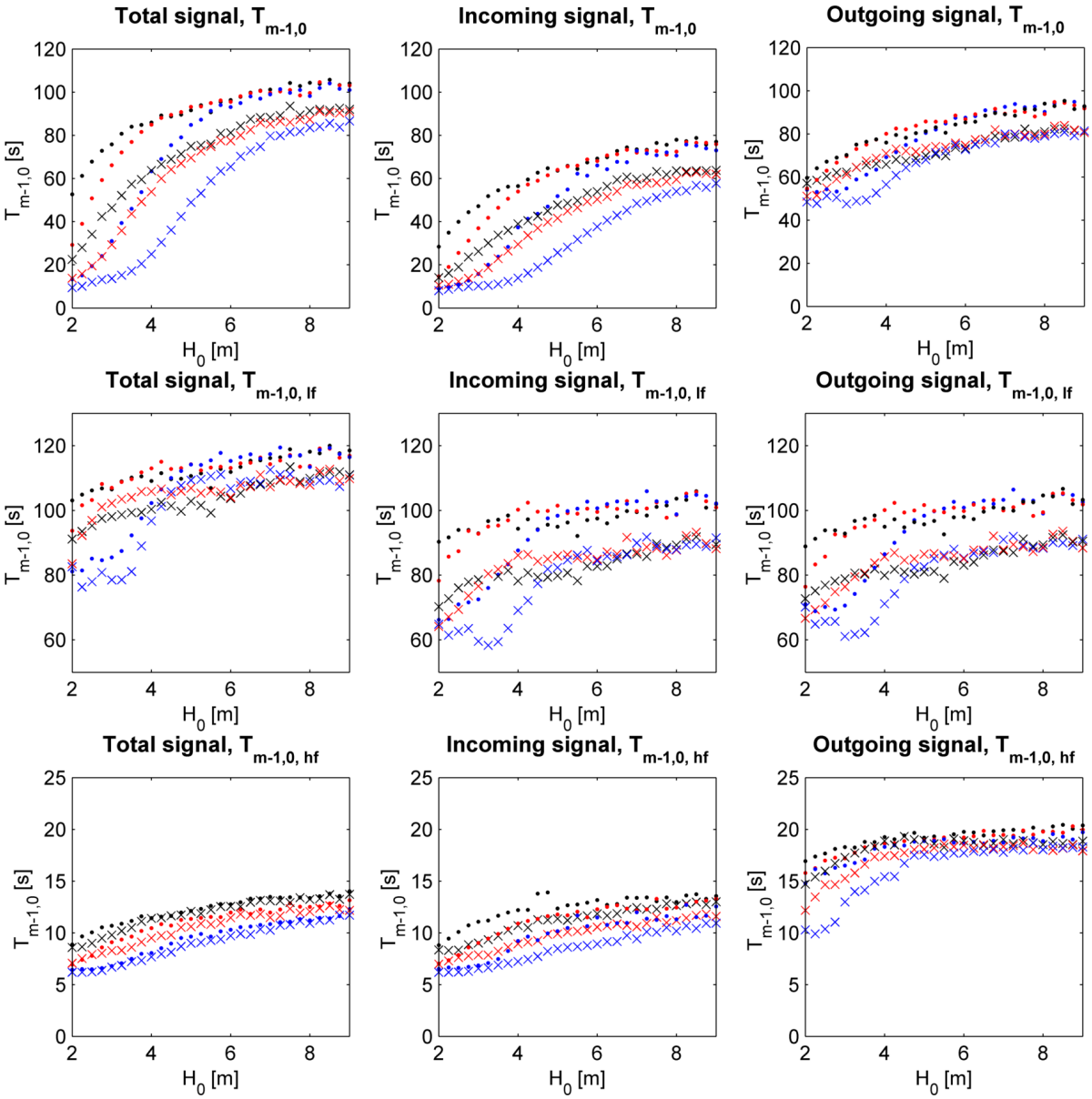

Figure 4.2: Mean energy wave periods, $T_{m-1,0}$, at the toe against the offshore wave height, H_0. Top row: total wave period, middle row: LF wave period, bottom row: HF wave period. Left column: total wave signal, middle column: incoming wave signal, right column: outgoing wave signal. Black markers for $s_0 = 0.01$, red markers for $s_0 = 0.02$ and blue markers for $s_0 = 0.04$, $\cdot = CH$, $\times = CE$.

4.1.2. NON-HYDROSTATIC 1D RESULTS IN SWASH ZONE

The results in the swash zone consist of: $R_{2\%}$, $<\eta>$, S, and the high and low frequency components of S; S_{inc} and S_{IG}.

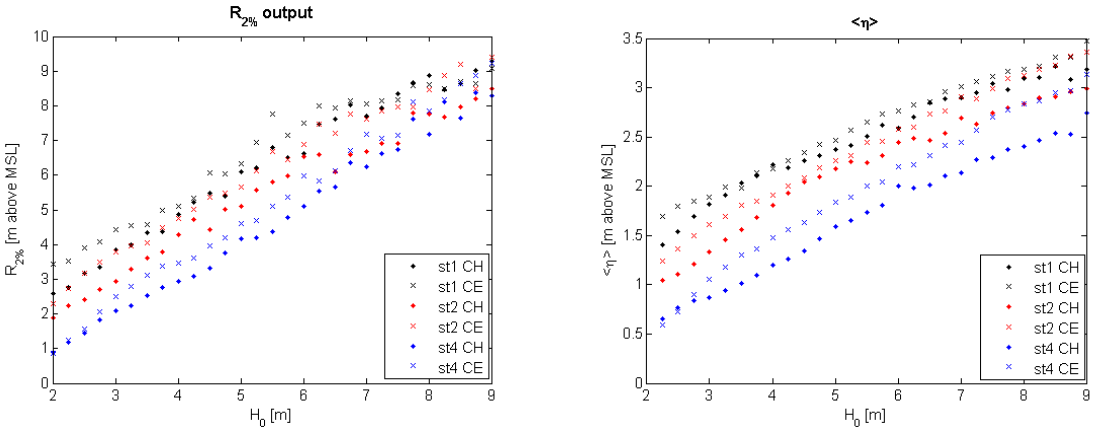

(a) $R_{2\%}$ against H_0 (b) $<\eta>$ against H_0

Figure 4.3: $R_{2\%}$ and $<\eta>$ against H_0. Black markers for $s_0 = 0.01$, red markers for $s_0 = 0.02$ and blue markers for $s_0 = 0.04$, $\cdot = CH$, $\times = CE$

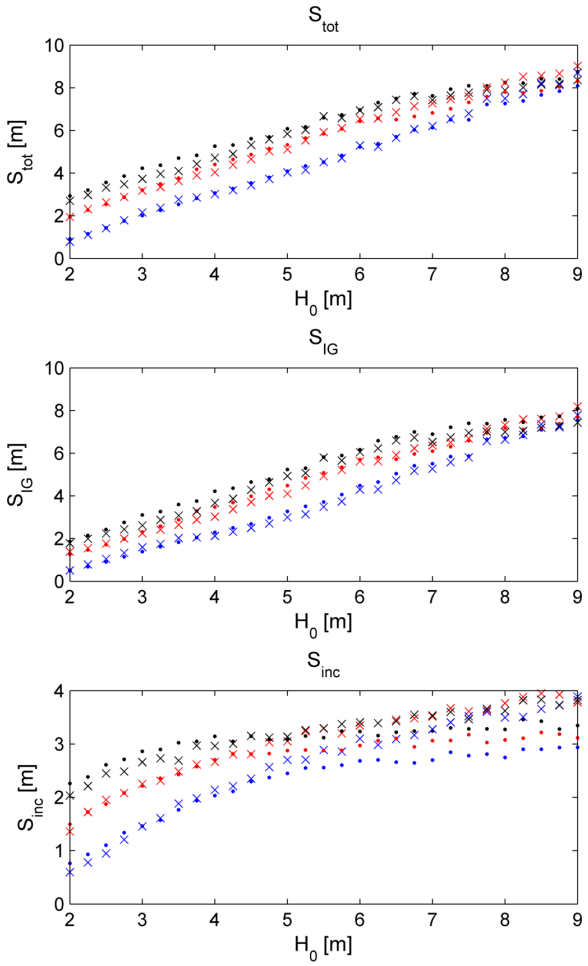

Figure 4.4: S and its components S_{inc} and S_{IG}, against H_0. Black markers for $s_0 = 0.01$, red markers for $s_0 = 0.02$ and blue markers for $s_0 = 0.04$, $\cdot = CH$, $\times = CE$

From figures 4.3 and 4.4, the following can be said:

- As is also visible in the results at the toe, the swash parameters increase with increasing offshore wave height and decreasing wave steepness.
- Comparing the two bathymetries shows that the CE has a slightly higher $<\eta>$ (figure 4.3), but almost the same S (figure 4.4) as the CH. For the $R_{2\%}$ the differences between the two bathymetries vary significantly per H_0. What can be seen for the run-up is that for $H_0 < 5m$ the run-up at CE is larger than at CH. This could be due to the fact that the total wave heights at the toe of the CE are higher, resulting in more energy that is available for the run-up.
- It is also visible from figure 4.4 that the LF swash motions, S_{IG}, are slightly higher or equal at the CH compared to the CE. The HF motions, S_{inc}, are higher at CE for storm conditions with $H_0 > 4-5m$. For storm conditions lower than this offshore wave height, the opposite can be seen.

4.1.3. QUALITATIVE ANALYSIS OF THE NON-HYDROSTATIC 1D RESULTS

This section looks at the behaviour, or qualitative analysis, of the hydrodynamics in the Non-hydrostatic models. Figure 4.5 looks at the percentage of total wave energy that accounts for the LF motions, for the total, incoming and outgoing wave signal. From top to bottom it shows the total, incoming and outgoing wave signal at the toe. The latter two are obtained by splitting the total wave signal by using Guza's theory as explained in section 3.3.3.

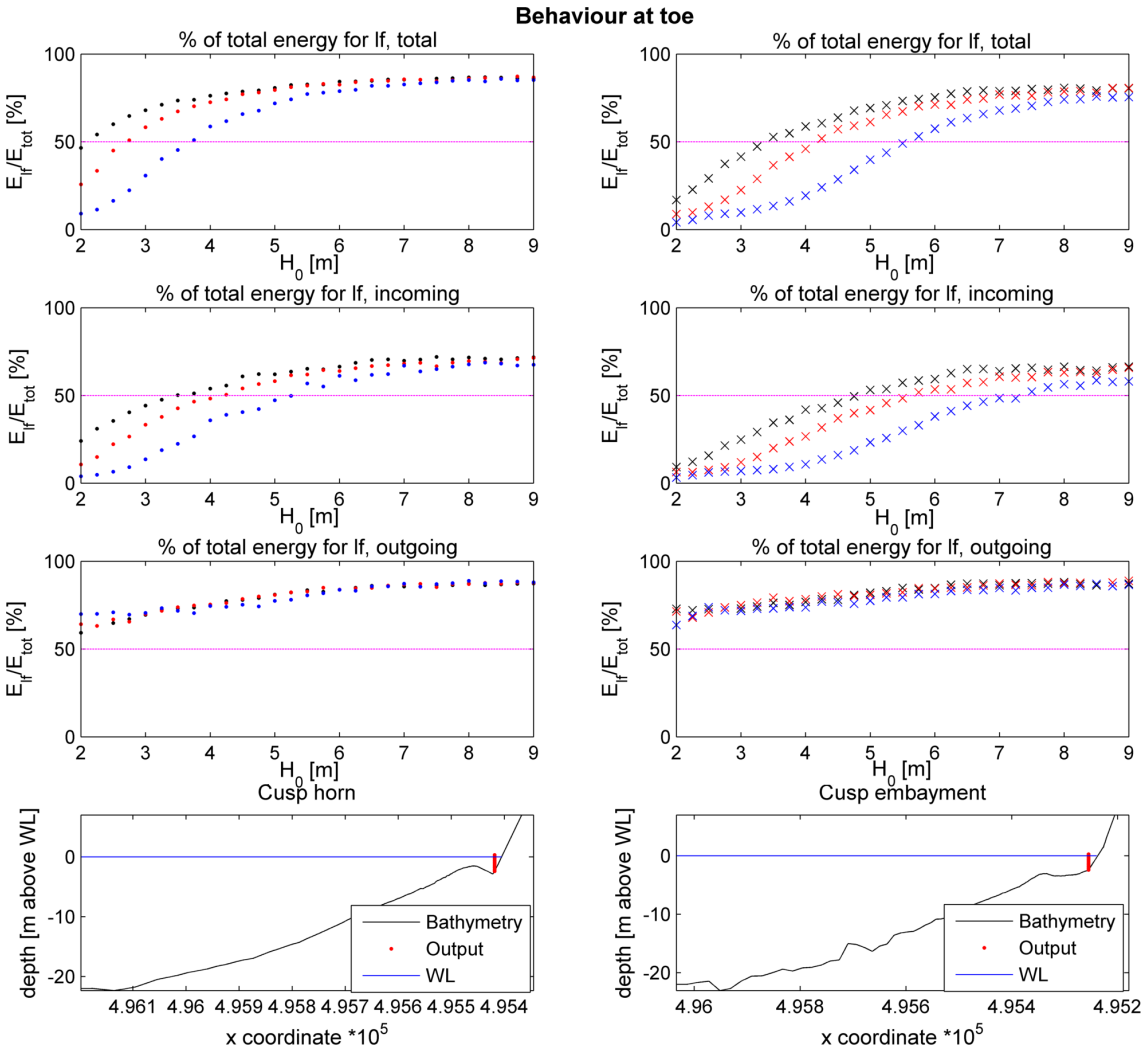

Figure 4.5: Behaviour at the toe, where the different colours indicate the different offshore steepnesses: Black markers for $s_0 = 0.01$, red markers for $s_0 = 0.02$ and blue markers for $s_0 = 0.04$, $\cdot = CH$, $\times = CE$.

From figure 4.5, it can be seen that the point of dominance of LF energy, where the graphs pass the 50% line, depends on multiple variables:

1. **Bathymetry:** The point of dominance for the 3 graphs in CE occur at a higher offshore wave height than at CH. This could be explained by the role of the more prominent nearshore bar in the CH bathymetry, which breaks more waves. Therefore, more HF motions are dissipated, resulting in a relative higher percentage of LF motions for the total wave per condition. This process also results in a higher maximum limit for the percentage of LF motions of the total wave for CH. Figure 4.1 shows this clearly: while the $H_{m0,lf}$ is roughly the same for both 1D bathymetries, there is a clear difference between the $H_{m0,hf}$, where the latter is lower for CH than for CE. This complies with the theory in section 2.6: the longshore variability is mainly due to differences in HF motions.
2. **Offshore wave steepness, s_0:** From the same figures it can be seen that a lower offshore wave steepness results in a higher percentage of LF motions of the total motions. Shoaling and groupiness of the short waves are important to explain the differences between the three offshore wave steepnesses. A higher offshore wave steepness causes waves to break further offshore. As Battjes [21] explains as well, this shortens the distance over which energy transfer can occur towards the LF motions. This is because the transfer is significantly reduced as waves start to break, as both groupiness and short wave height are reduced, leading to less enhancement of the forced LF motions. Thus, higher offshore wave steepness leads to lower HF and LF wave heights at the toe.
3. **Type of signal**: which signal is regarded clearly affects the point of dominance. At the incoming signal, the point of dominance occurs later than that of the total wave signal. This is due to the fact that the outgoing signal is completely LF dominant.

The reason for the higher amount of LF energy in the outgoing signal is reflection. From figures 4.1 and A.2, it can be seen that in almost all cases there is a full reflection of the LF waves, whereas the reflection of the HF waves is only partial (but increasing with an increasing H_0). This is further discussed in section 4.1.5. It also results in an overall higher $T_{m-1,0}$ as it is composed of longer waves.

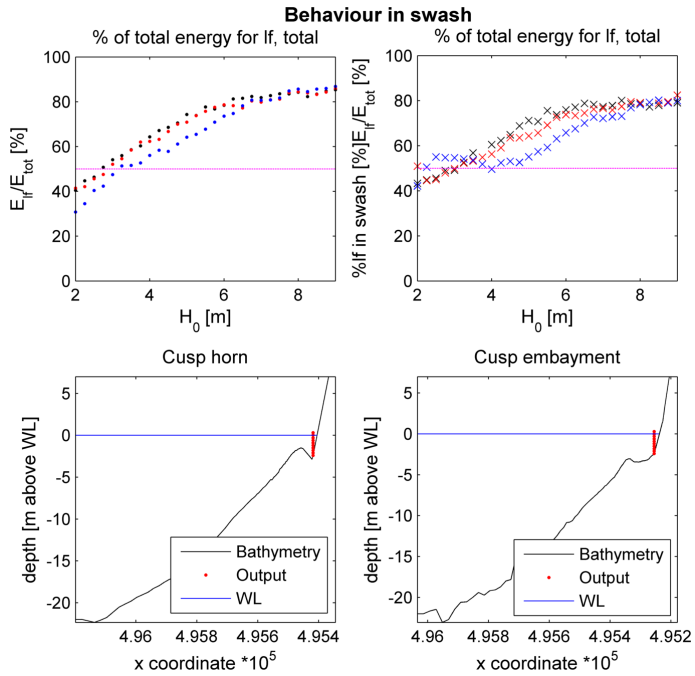

Figure 4.6: Behaviour in the swash zone, where the different colours indicate the different offshore steepnesses: Black markers for $s_0 = 0.01$, red markers for $s_0 = 0.02$ and blue markers for $s_0 = 0.04$, $\cdot = CH$, $\times = CE$.

The same qualitative analysis has been conducted for the swash zone, with again a spectral analysis as explained in section 3.3.2. Figure 4.6 looks at $\frac{E_{lf}}{E_{tot}}$ of both bathymetries. As can be seen, figure 4.6 looks quite similar to figure 4.5, with again different points of dominance and a relative difference between the two bathymetries.

This visual indication alone cannot be used to conclude if hypothesis 1 and 2 are correct. To be able to clearly say something about whether the behaviour at the toe can be linked to the behaviour in the swash zone, the two are plotted against each other as shown in figure 4.7. The best direc relation between the toe and the swash behaviour is reached with total wave signal graph.

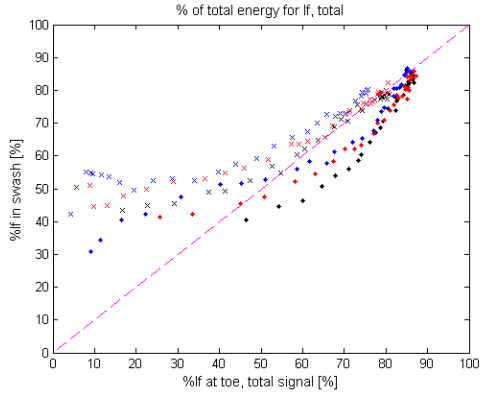

(a) Comparison of the behaviour at the toe of the total wave signal and in the swash zone, where the different colours indicate the different offshore steepnesses: Black markers for $s_0 = 0.01$, red markers for $s_0 = 0.02$ and blue markers for $s_0 = 0.04$, $\cdot = CH$, $\times = CE$.

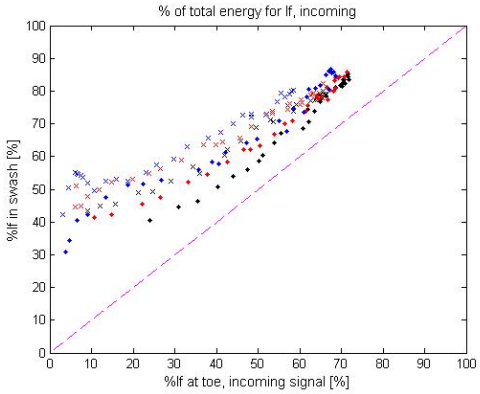

(b) Comparison of the behaviour at the toe of the incoming wave signal and in the swash zone, where the different colours indicate the different offshore steepnesses: Black markers for $s_0 = 0.01$, red markers for $s_0 = 0.02$ and blue markers for $s_0 = 0.04$, $\cdot = CH$, $\times = CE$.

Figure 4.7: Comparison of the behaviour at the toe and in the swash zone

Clear trends are visible in figure 4.7, with a transition from the lowest to the highest $\frac{E_{lf}}{E_{tot}}$, but also a difference between the bathymetries. The following can be said:

1. At the CE and CH of figure 4.7b and at the CE of figure 4.6 a relatively larger amount of LF motions occurs in the swash zone than at the toe. However, with increasing LF dominance at the toe, this difference becomes less and less.
2. At the CH of figure 4.6 the opposite happens; in the swash zone, relatively less LF motions occur that at the toe, except for the low values of LF contribution at the toe of $s_0 = 2\%$ and 4%.
3. From figure 4.7, it can be seen that the minimum of the graphs is significantly higher for the swash zone.

The differences between the results of the two bathymetries is mainly due to large differences in behaviour at the toe, as figure 4.6 shows only little difference in behaviour in the swash zone.

Based on this section, it can be said that firstly, LF motions are dominant in the swash zone in almost all cases. At the toe, they dominate the outgoing signal, as most HF energy dissipates in the swash zone. They are less dominant in the incoming signal, as the HF motions are dominant for the smaller storms (until $H_0 = 3.5 - 5.5m$ (CH) and $H_0 = 4.5 - 7m$ (CE)). The reason for the longer dominance of HF motions at the toe of CE, is most likely due to the less prominent nearshore bar. In the swash zone, a relative higher dominance of LF motions can be seen in the CE than in the CH for $H_0 < 5m$. This is where the CH has a steeper beach face slope, and a higher S_{inc} than the CE. However, a change in beach face slope can be seen for the CE (figure 3.2b) as waves can run-up farther on the beach. As a beach slope becomes steeper, less interaction between swash cycles occurs [10]. This leads to less saturation of HF motions in the swash: the HF swash motions can continue to grow. This could be the reason why S_{inc} becomes larger at the CE than at the CH for $H_0 > 4 - 5m$, which results in a lower LF dominance in the swash zone of the CE, as S_{IG} remains similar for both bathymetries. This supports the statements of Guedes *et al.* [14] and Ciriano *et al.* [40] that the beach slope is a dominant factor for changes in swash behaviour as it affects S_{inc}.

Secondly, the behaviour in the swash zone can be linked to the behaviour at the toe, but only from the point where both the toe and the swash zone experience a dominance of LF motions and differently for the two bathymetries. A small separation between the results of the two bathymetries is visible in figure 4.6, mainly

due to the significant difference in behaviour at the toe. This gap is smaller in figure 4.7b, but there are still differences between the two bathymetries. It can be seen in figure 4.7 that both the incoming and total wave signal show a correlation with the behaviour at the toe, but figure 4.6 shows a smaller difference in $\frac{E_{lf}}{E_{tot}}$ between the swash and the toe. So, qualitatively, the conditions at the toe can be related to the conditions in the swash zone, but this relation changes with changing bathymetry, offshore wave energy and which type of signal is regarded.

4.1.4. QUANTITATIVE ANALYSIS OF THE NON-HYDROSTATIC 1D RESULTS

Besides a qualitative analysis, a quantitative analysis is done in order to analyse the second hypothesis of the first research sub-question. This has been done by investigating multiple parameterizations that normally consist of a relationship between the offshore wave height and the wave run-up, but now with the hydrodynamics at the toe. The investigated options are:

1. A direct relationship with either the total wave signal or the incoming wave signal hydrodynamic parameters with the maximum run-up ($R_{2\%}$), the mean run-up ($<\eta>$), the swash height amplitude (S_{tot}) and its HF and LF components (S_{inc} and S_{IG} respectively).
2. A relationship similar to Hunt's formula [26] between the run-up components and the hydrodynamic parameters at the toe, as modified by Battjes [23] and as shown in formula 2.3.
3. A direct relationship with the waveheight times the inverse of the square-root of the wave steepness, which is basically Hunt's relationship but without the beach face slope.

How well the parameterizations fit is then checked based on the coefficient of determination, R^2, the bias and the root-mean-square error, rsme. Important to note is that only linear relationships have been checked. More information about these three means of quantifying the error of the fit, can be found in section 3.6. The best fits were found to be the following five graphs.

These graphs are chosen as they show the lowest bias, a high R^2 value and a low(er) RMSE, which indicates that their parameterization fits the data well. Therefore, it can be concluded that hypothesis 2 is not entirely correct: the data at the toe and in the swash zone cannot be related to each other. Both the qualitative and quantitative analysis show that the two bathymetries have a different relationship, and that the lowest storm conditions deviate from these relationships. The HF motions at the toe cannot be related directly to the HF swash motions, not even with a Hunt's like relationship. An exception is the parameterization of the S_{IG}, where all data points follow the fit quite well. A further discussion of some of these parameterizations can be found in section 4.1.5.

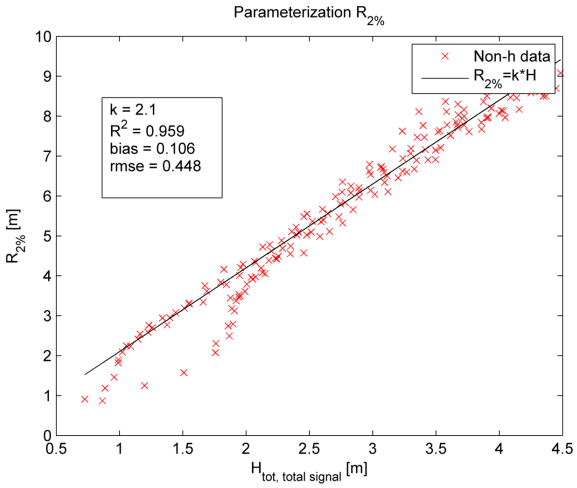

(a) Parameterization of $R_2\%$ with H_{m0} of total signal at the toe

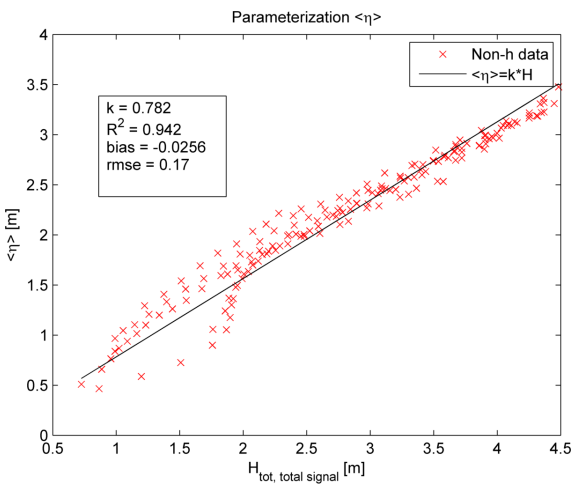

(b) Parameterization of $\langle\eta\rangle$ with H_{m0} of total signal at the toe

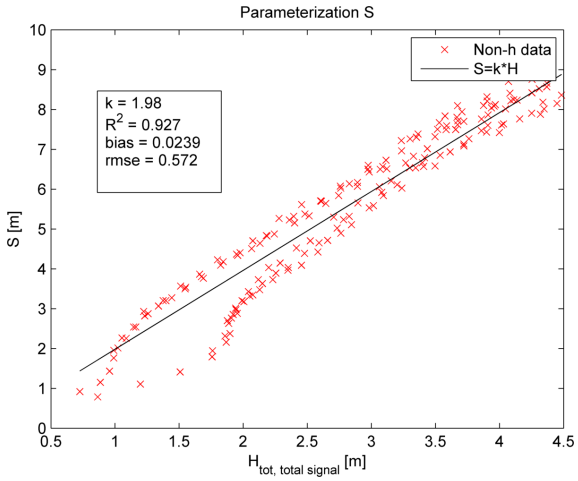

(c) Parameterization of S with H_{m0} of total signal at the toe

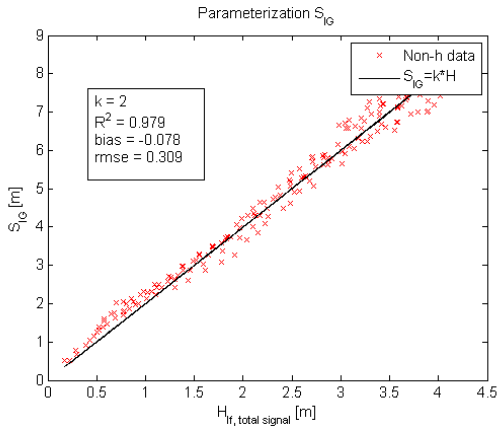

(d) Parameterization of S_{IG} with $H_{m0,lf}$ of total signal at the toe

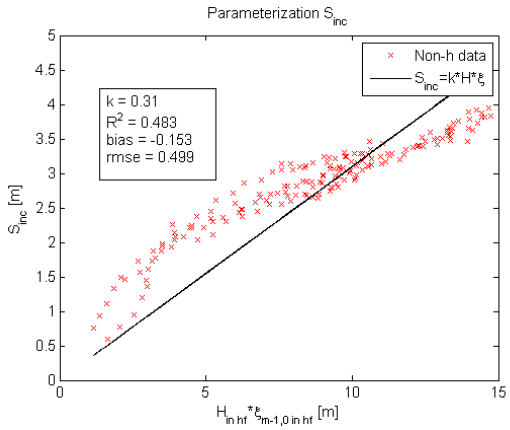

(e) Parameterization of S_{inc} with an Hunt's like relationship of the incoming HF motions at the toe

Figure 4.8: The parameterisation of the swash parameters $R_2\%$,$\langle\eta\rangle$, S, S_{IG} and S_{inc} with wave parameters at the toe

4.1.5. DISCUSSION

As the thesis revolves around a model alone, it is important to check whether the obtained results comply with theories and conclusions from others, based on real data.

SWASH SPECTRA

The Non-hydrostatic swash spectra of the two 1D bathymetries, as shown in figure 4.9, follow the same shape and roll-off as suggested by Hughes *et al.* [5] for intermediate beaches with rhythmic bar and beach state: both graphs in figure 4.9 show a f^{-4} roll-off of the HF motions: an increase in frequency by a $factor$, leads to a decrease in swash variance of $factor^{-4}$. As was stated by them, the spectra evolve towards a more dominant LF behaviour with increasing offshore conditions. This is because higher offshore conditions generate larger LF motions and experience more breaking of the HF motions. This can be seen in figure 2.4: the grey graph resembles a more reflective behaviour, whereas the black graph resembles a more dissipative behaviour.

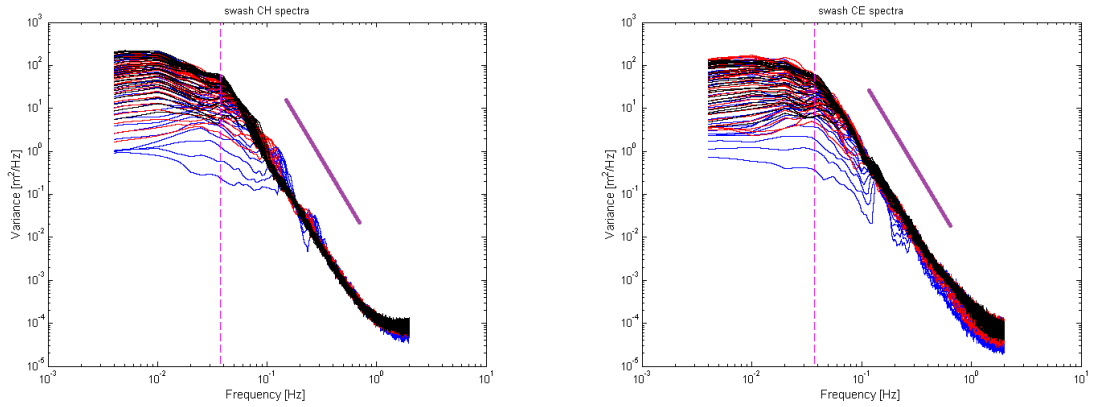

(a) Swash spectrum of cusp horn bathymetry

(b) Swash spectrum of cusp embayment bathymetry

Figure 4.9: Logarithmic graph with both swash spectra. Black lines for $s_0 = 0.01$, red lines for $s_0 = 0.02$ and blue lines for $s_0 = 0.04$. The magenta vertical line represents the f_{split}. The bold purple line represents the HF roll-off of f^{-4}.

DISCUSSION OF THE QUALITATIVE ANALYSIS

In terms of behaviour, after analysing both the LF and HF motions, little to no energy lies in the very low frequency area ($< 0.004Hz$ [36]), as the LF and HF energies add up to 99.9 - 100%. As mentioned before, differences in %LF of total energy between the two bathymetries, are mainly due to the changing amount of HF energy. The HF motions at the toe of the CE are generally larger than at the CH, which could be the reason for higher S_{inc} in the swash zone of the CE as well. However, in this report it is suggested that these (small) variations are most likely due to the (small) difference in beachface slope. This can be explained by the fact that a change in beach face slope can only be seen for the CE further on the beach, while the slope for the CH remains constant. As a beach slope becomes steeper, less interaction between swash cycles occurs [10]. This leads to less saturation of HF motions in the swash: the HF swash motions can continue to grow. The longer growth of HF swash motions causes a transition: where S_{inc} is firstly larger at the CH, it later becomes larger at the CE. As this is the only parameter that changes dissimilarly between the two bathymetries, it is most likely the reason why S_{inc} becomes larger at the CE than at the CH from $H_0 > 4-5m$, which results in a lower LF dominance in the swash zone of the CE, as S_{IG} remains similar for both bathymetries. At the toe, this can be explained by the more dominant presence of a nearshore bar at the CH, where the minimum water depth on the bar crest equals 1.53 m. At the CE this is 3.05 m. Therefore, the CH bathymetry induces more breaking before the toe of the beach, resulting in a lower HF wave height. The LF wave heights are similar for both bathymetries, as their generation is similar: both foreshore slopes are fairly equal, with a slope of 0.025-0.028 before their bars. Therefore shoaling and groupiness of the short waves are similar, thus generating similar low frequency motions as explained in section 2.2.2.

The increasing importance of LF motions with increasing offshore wave height can be explained as follows. As the incoming waves increase in height and length, larger variations in radiation stresses occur thus generating larger LF motions. These LF motions receive a continuous transfer of energy from the HF motions over the cross shore distance (until breaking) and experience shoaling as well. Increasing the incident wave height also results in relatively more breaking of the HF motions, than for lower incident wave heights. Lastly, whereas the HF motions break, the LF motions remain as they are much longer. This all combined leads to dominance of HF motions for low incident waves, as little LF motions are generated and most HF motions survive. On the contrary, a dominance of LF motions occurs with increasing wave height as larger LF motions are generated and more HF motions break.

When looking at swash behaviour graphs, figure 4.6, the graph of $s_0 = 4\%$ of CE, goes first up, then down again before it increases in relative percentage of LF energy of the total swash motions. This is the opposite of the behaviour seen at the toe and in the behaviour of the swash zone of CH, where only an increase is seen with increasing H_0, and could be due to a small model error. It has also to be noted that the conditions where the behaviour at the toe and in the swash do not coincide, are the same conditions which deflect from the parameterization fits.

DISCUSSION OF THE QUANTITATIVE ANALYSIS

In figures 4.8a, 4.8b and 4.8c, a significant deviation from the parameterization can be seen. This could be due to the fact that a linear parameterization is not optimal, due to computational errors, or due to differences in near shore bathymetry. The largest differences with the parameterization occur for the smallest storm conditions of CE, $s_0 = 4\%$. These are the same conditions that show a different behaviour in HF motions at the toe, as can be seen in figure 4.1. The lowest 6 storm conditions show a different trend in $H_{m0,hf}$ than the other s_0 graphs. As the deviations occur for the smallest and shortest offshore wave conditions, it is suggested that the large difference in behaviour are not as well represented by the model. However, caution has to be taken with this suggestion, as no data is available for validation of the model.

The next two paragraphs go more into detail about the parameterizations of S_{IG} and S_{inc} as these parameters are part of the main focus of this report.

Parameterization of S_{IG} It can be seen from figure 4.8d, that S_{IG} does not depend on the bathymetry directly. This same feature was used by Stockdon *et al.* [7]. It can be quantified best with the LF wave height of the total signal. This could be logical, as the total signal is composed of the incoming and outgoing signal, and the outgoing signal contains information about the processes at the beach, such as reflection. Therefore, the $H_{m0,lf}$ of the total signal can have a better fit than the $H_{m0,lf}$ of the incoming signal.

Parameterization of S_{inc} As mentioned in section 4.1.3, the differences in behaviour between the two bathymetries are mainly due to the bathymetry differences and the relative differences between the offshore steepness graphs, which change with increasing offshore wave height. This is mostly due to the effect they have on the HF motions, as figure 4.1 in appendix A shows that the LF wave heights are almost exactly the same. Therefore, the behaviour graph already gave a clue that the parameterization of S_{inc} depends on a wave height and steepness, as well as on the bathymetry, resulting in a Hunt's like relationship.

It can be seen that the difference between the swash motions for the smaller storms and the parameterization of S_{inc} is large. This could be due to the difference in behaviour for those storms between the swash zone results and the results at the toe of the beach: the LF dominance in the swash zone is then larger than at the toe . Finally, the parameterization can be regarded as insufficient, as a low value for R^2 and a high value for the bias is found. Therefore, this parameterization can not be used as a means to improve the S_{inc} of the Surf-beat model, which has been assumed to be represented incorrectly by that mode. However, it has to be kept in mind that only linear parameterizations are regarded. Therefore, another type of parameterization could result in a lower bias and a higher accuracy. Lastly, it has to be mentioned that another reason for the non-fit of the linear parameterization, could simply be the fact that the parameters at the toe are used. The Hunt's parameterization was namely first made with the use of offshore conditions.

4.2. NON-HYDROSTATIC 1D CONCLUSIONS

From the Non-hydrostatic results, it can be concluded that the respective roles of HF and LF motions depend on the bathymetry but also on the offshore storm conditions; both wave height and wave steepness. At the toe of CH, the prominent bar functions as a filter, breaking most of the HF motions coming in. At the CE the bar is less prominent, resulting in more HF motions and higher total motions. The LF motions are similar for the two bathymetries, as the foreshore slopes are similar as well.

In the swash zone, a difference between the two bathymetries is still visible, although small. With the exception for the lowest 5-10 storm conditions, the CE shows larger HF swash motions than the CH. This is most likely due to the fact that as waves become larger, they can run further up on the beach, where they start to experience a steeper beach face slope above the WL only at the CE, whereas the slope of the CH remains constant. As a beach slope becomes steeper, less interaction between swash cycles occurs [10]. This leads to less saturation of HF motions in the swash: the HF swash motions can continue to grow. The LF swash motions are similar for the two bathymetries. Therefore, the behaviour follows Guedes *et al.* [14], who state that alongshore differences in swash motions are due to differences in beach face slope, which only affects the HF energy in the swash. The final differences in total swash height remain small however, as the LF motions are similar between the two bathymetries and dominant. Some difference in maximum run-up can be seen the two bathymetries, where the majority of the CE results for $H_0 < 6$ to $7m$ are larger than the run-up results of the CH. For storms with a wave height higher than this value, this clear difference between the two bathymetries goes away.

An LF dominance in the total wave signal at the toe is found for all storm conditions greater than $H_0 = 4m$ (CH) and $H_0 = 5.5m$ (CE). For the lower wave steepnesses, this dominance of LF motions starts at a lower H_0. With increasing conditions, more energy can be transferred to LF motions, by the processes explained by Longuet-Higgins and Stewart [19]. Longer incoming waves also show larger HF motions. According to Battjes [21] this can be explained with shoaling and groupiness of the incoming waves. Shoaling and groupiness of the short waves are important to explain the differences between the three offshore wave steepnesses. Higher offshore wave steepness waves break further offshore. This shortens the distance over which energy transfer can occur for the generation of LF motions. This is because the transfer is significantly reduced as waves start to break, as both groupiness and short wave height are reduced, leading to less enhancement of the forced LF motions. Therefore, higher offshore wave steepness leads to lower HF and LF wave height at the toe.

The outgoing waves show an overall dominance of LF motions. This is due to the fact that the reflection of the LF motions is larger than the reflection for the HF motions,(figure A.2), resulting in a relative higher percentage of LF energy in the outgoing and thus the total wave. The reflection of LF motions follows the results of Van Dongeren *et al.* [22].

Besides the qualitative relation between the parameters at the toe and in the swash zone, a quantitative relation was made. They mostly show a direct relation with the wave height of the total signal at the toe (of the total spectrum or only LF part of the spectrum), except for the incident-band swash motions. These motions related best with the incoming HF motions, in a Hunt's like relationship. However, the linear fit for S_{inc} has a high bias and a low R^2, thus showing it is not a good fit. Therefore, it can not be used as a substitute for the incident-band swash motions of the Surf-beat model, if that proves to be necessary.

As the working hypothesis in this report, as mentioned in chapter 1, assumes that the 1D Surf-beat mode cannot compute the HF (swash) motions correctly, it is expected to see quite some differences between the Surf-beat and Non-hydrostatic results. This is especially the case for the smaller storm conditions, where the HF motions remain important and even dominant at the toe and in the swash zone. Furthermore, as the CE experiences higher and more dominant HF motions at the toe, it is expected to see a larger difference between the two modes for that bathymetry, compared to the CH bathymetry. In the swash zone however, the smallest conditions actually show higher HF motions for the CH than for the CE. It is therefore expected that for those conditions, the difference between the Non-hydrostatic and Surf-beat results will be larger for the CH than for the CE bathymetry.

4.3. SURF-BEAT 1D RESULTS

This section discusses the results of the same storm conditions for the Surf-beat model. It forms the basis for section 4.4. As mentioned in section 2.7, three different breaker formulations have been used. The wave parameter results of these three different modes can be found in Appendix A.

Based on the figures A.3 until A.14, the following general remarks can be made:

- Overall, the wave heights at the toe increase with an increasing offshore wave height and with a decreasing offshore wave steepness. This is not the same for the outgoing HF motions, which show no variation with offshore wave steepness, but still increase with increasing storm conditions. The outgoing HF motions are based on the outgoing long wave spectrum as shown in figure 3.7, where a similar amount of energy in the HF band of those spectra can be found for all wave steepnesses around the same location. The incoming $T_{m-1,0,lf}$ and $H_{m0,lf}$ show differences between the different wave steepnesses, thus showing that the incoming LF motions are all frequency down-shifted in the swash-zone to the same frequency band. Based on the shape of this spectrum, it can be argued how correct it is to use a split frequency. The little amount of energy in the HF part can be seen as the 'tail' of the LF part of the spectrum. For this report, it will be assumed that the use of the f_{split} is correct for consistency in the analysis.
- In the Non-hydrostatic results, differences between the two bathymetries are visible. In all Surf-beat results, larger wave heights for the CE bathymetry are found as well. The HF motions at the toe of the CE bathymetry are significantly larger than those of the CH bathymetry (up to 70cm), similar to what was found in the Non-Hydrostatic model.
- When looked at the total and incoming $T_{m-1,0,hf}$ in for example figure A.4, the effect of the JONSWAP spectrum is clearly visible. The $T_{m-1,0,hf}$ mainly depends on the offshore wave steepness, and wave height. As this is an incorrect representation of reality, no further analysis will be made of this parameter.
- For the run-up parameters, an increase is seen with decreasing s_0 and increasing H_0, as well as an increase that depends on the bathymetry. The CE shows larger values for $R_{2\%}$, $< \eta >$ and S and its components.
- Interestingly, it is visible in the swash motions figures such as A.5a and A.5b, that the graphs of $s_0 = 4\%$ deviate from the other results. In terms of swash height (due to its deviating behaviour in S_{IG}) and maximum run-up, it is visible that their values are significantly lower than for the other two offshore steepnesses. This is in contrast with the Non-hydrostatic results, where differences between the wave steepnesses can be seen, but not to the same extent.

The details behind these remarks will be discussed in section 4.4. Even though the general remarks are consistent for all three breaker formulations, this does not mean that the obtained results are the same. Generally for the modes it can be concluded that:

1. At the toe, the different breaker formulations cause different ratios of LF and HF energy, as can be seen in figure 4.10. By changing from the *default* breaker formulation to the *Roelvink-Daly* formulation, a **small increase in** $H_{m0,lf}$ (5-10cm) and a **significant decrease in** $H_{m0,hf}$ $(20-50cm)$ are found. This is because the latter formulation lowers the incoming HF wave height significantly. The difference between the *Roelvink-Daly* and the *Roelvink-Daly, adapted* formulation, lies in the **increase of** $H_{m0,lf}$ (maximum $20cm$) by the latter, as **barely any difference in HF motions** occur.
2. In the swash zone, changing from the *default* breaker formulation to the *Roelvink-Daly* formulation, results in: An **increase of** S_{IG}, which increases with increasing storm conditions. And an **increase of** S_{inc}, which decreases with increasing storm conditions. The same effects are obtained by changing from the *Roelvink-Daly* to the the *Roelvink-Daly, adapted* breaker. formulation

It can be concluded that some general remarks seem to be consistent with the conclusions from the Non-hydrostatic results, but some completely are different, based on the above mentioned remarks. Therefore, graphs have been made to evaluate the behaviour of these LF motions in the Surf-beat mode. These graphs can be found in figures 4.10 and 4.11.

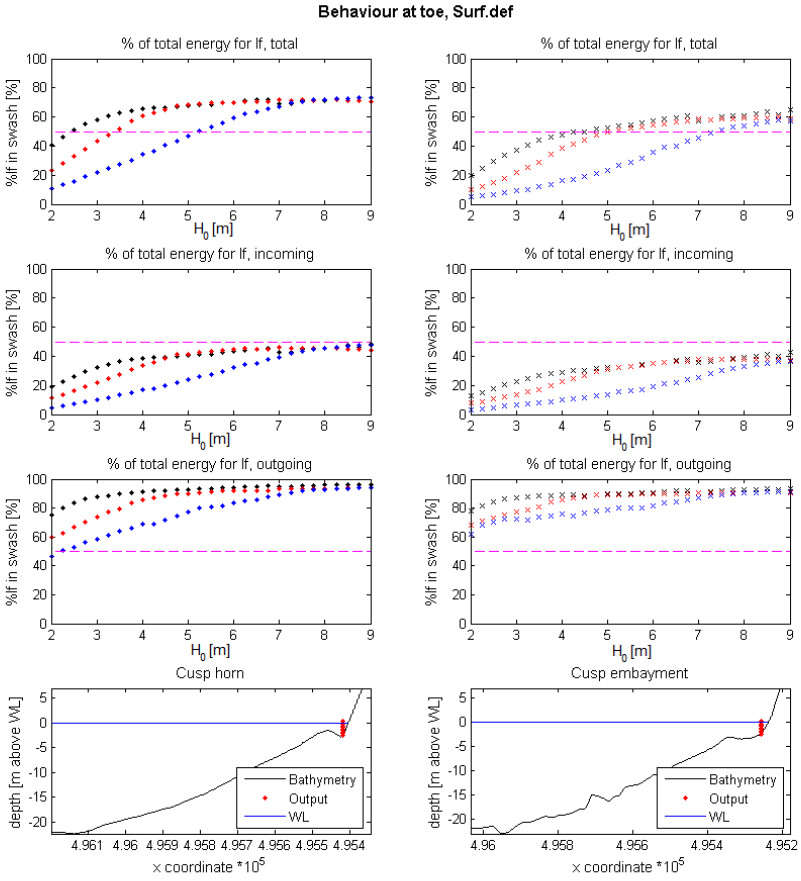

Figure 4.10: Behaviour at the toe of the Surf-beat default mode, where the different colours indicate the different offshore steepnesses: Black markers for $s_0 = 0.01$, red markers for $s_0 = 0.02$ and blue markers for $s_0 = 0.04$, $\cdot = CH$, $\times = CE$. The magenta dashed line represents the 50% line.

By comparing figures 4.10, 4.11 and 4.12 and the graphs in section A.1, the following can be said.

- Due to the high $H_{m0,hf}$ in the incoming signal, only a bare dominance of LF energy is found for the largest storm conditions alone. The swash zone experiences an overall dominance, as can be seen in the graphs of figure 4.11. Combined, this results in the graphs in figure 4.12, where there is clearly a higher relative amount of LF energy in the swash zone than at the incoming signal at the toe. This is more so the case for the CE.
- In those same figures, it can be seen that there is a clear difference between the two bathymetries, as well as the fact that the smaller storm conditions follow the same trend as the larger conditions. The latter is in contrast to the Non-hydrostatic results, where the smaller storm conditions show relatively a higher $\frac{E_{lf}}{E_{tot}}$ in the swash zone than at the toe[1]. Another difference with the Non-hydrostatic mode, is that now both bathymetries experience an overall higher dominance of LF motions in the swash than at the toe, whereas in the Non-hydrostatic mode this was only the case for the CE.
- Lastly, the outgoing wave behaviour graphs in figure 4.10, as well as the swash zone behaviour graphs in figure 4.11, show a generally more spread out behaviour between the graphs of the different offshore wave steepnesses when compared to the same graphs of the Non-hydrostatic mode.

[1] the smaller conditions show 30-55% of the total energy is for LF motions in the swash zone, and 5-10% at toe. The larger storm conditions show a 15-20% relative difference maximum between the swash zone and the toe

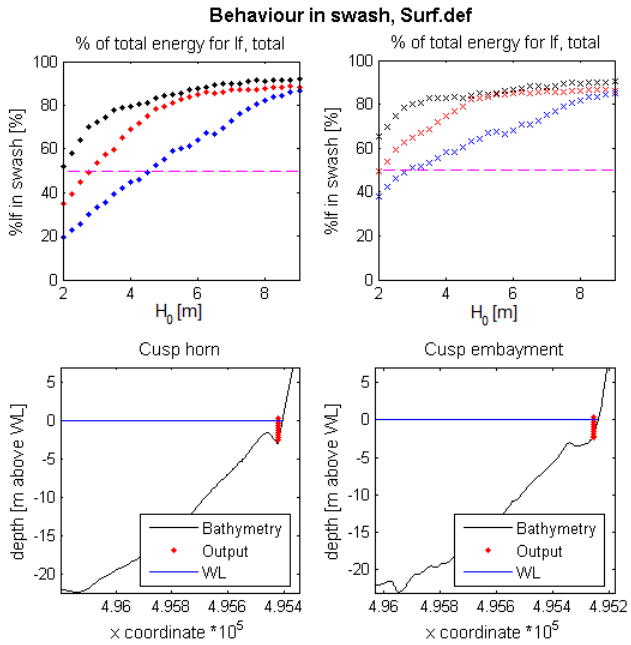

Figure 4.11: Behaviour of the swash zone of the Surf-beat default mode. The magenta dashed line represents the 50% line. The different colours indicate the different offshore steepnesses: Black markers for $s_0 = 0.01$, red markers for $s_0 = 0.02$ and blue markers for $s_0 = 0.04$, $\cdot = CH$, $\times = CE$.

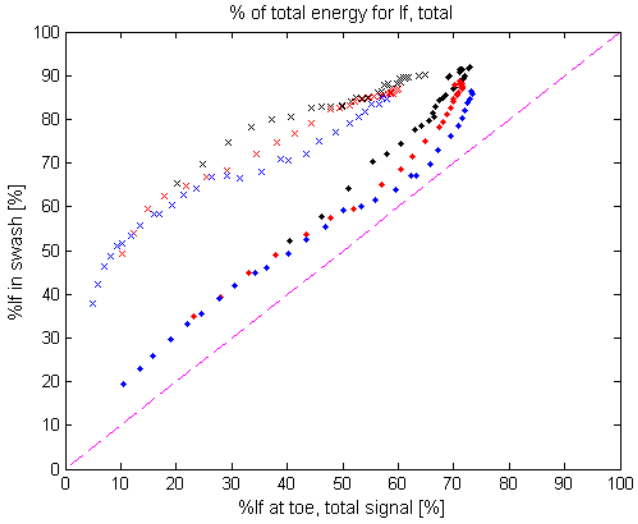

Figure 4.12: The qualitative comparison between the swash zone and the toe of the Surf-beat default mode. The magenta dashed line represents the 50% line. The different colours indicate the different offshore steepnesses: Black markers for $s_0 = 0.01$, red markers for $s_0 = 0.02$ and blue markers for $s_0 = 0.04$, $\cdot = CH$, $\times = CE$.

4.4. SURF-BEAT AND NON-HYDROSTATIC COMPARISON

As mentioned before, the figures with the results of both the Non-hydrostatic and Surf-beat model can be found in Appendix A. This section will only contain the most important graphs for the comparison of the two models. When figures 4.10 and 4.11 are compared with the Non-hydrostatic behaviour graphs, some differences can be seen. These differences involve more spreading between the wave steepness graphs of the Surf-beat modes, as well as differences in the relative amount of energy that is taken by LF motions. In order to explain these differences, scatterplots of the Surf-beat results against the Non-hydrostatic results have been made. This section only shows the scatterplots of the *default* breaker formulation. The other formulations are textually described by comparing them to the *default* scatterplots. Their scatterplots can be found in Appendix A.2.

4.4.1. AT THE TOE

This section focuses on the qualitative graphs of the wave heights at the toe. Firstly the total signal is analysed, after which the incoming and outgoing signal follow. As mentioned before, the comparison here focuses on the differences between the *default* breaker formulation of the Surf-beat model and the Non-hydrostatic model.

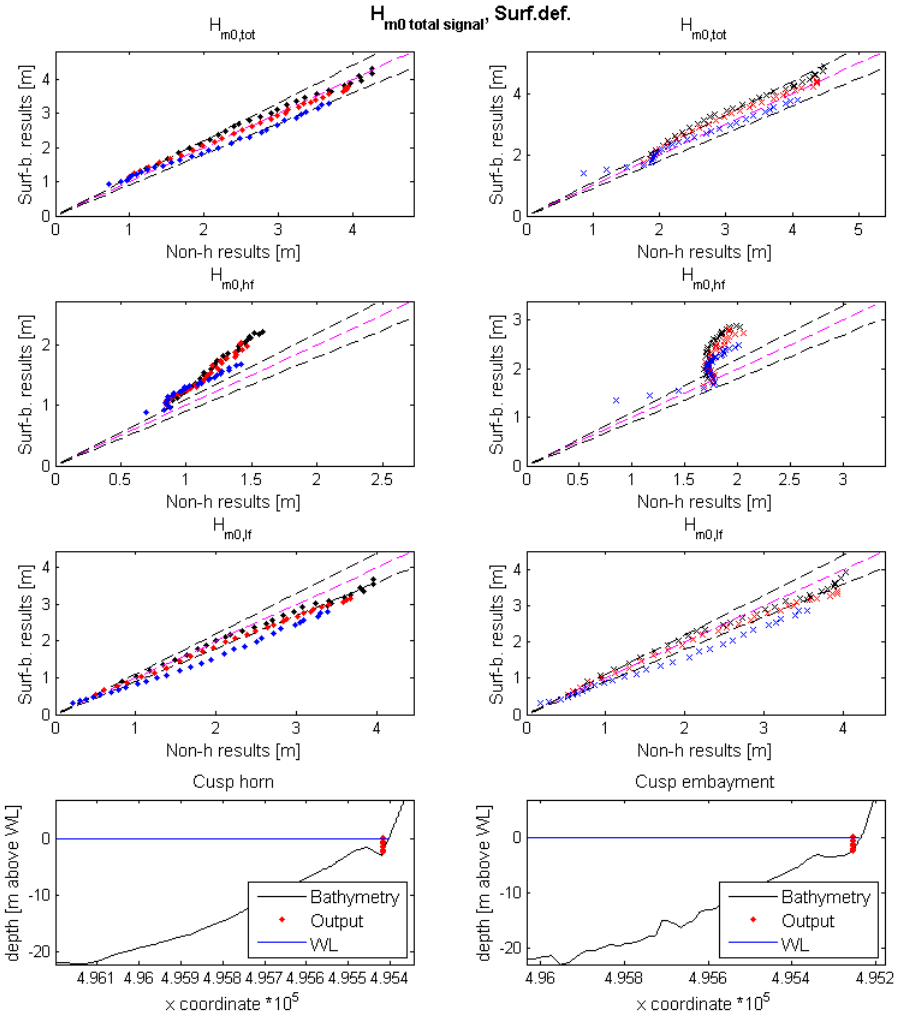

Figure 4.13: Surf-beat and Non-hydrostatic scatterplots of the total wave signal at the toe. The black dashed lines (- -) represent a 10% difference between the two modes. The magenta dashed line (- -) represents a 0% difference. Black markers for $s_0 = 0.01$, red markers for $s_0 = 0.02$ and blue markers for $s_0 = 0.04$, $\cdot = CH$, $\times = CE$.

Table 4.1: RMSE of total wave signal, Surf.def.

	CH				CE			
Total signal	**All**	$s_0 = 1\%$	$s_0 = 2\%$	$s_0 = 4\%$	**All**	$s_0 = 1\%$	$s_0 = 2\%$	$s_0 = 4\%$
$H_{m0,tot}$	**0,172**	0,079	0,069	0,136	**0,245**	0,197	0,109	0,097
$H_{m0,lf}$	**0,311**	0,137	0,163	0,227	**0,300**	0,116	0,158	0,227
$H_{m0,hf}$	**0,385**	0,278	0,221	0,149	**0,560**	0,411	0,316	0,210

The total signal behaviour graphs of the Non-hydrostatic (figure 4.5) and Surf-beat mode (figure 4.10) show a similar behaviour at first glance. When examined more in detail, the Surf-beat graph shows a lower maximum limit of $\frac{E_{lf}}{E_{tot}}$, as well as a later point of dominance (where the 50% line is crossed). This can be explained by evaluating the scatterplots of figure 4.13 of the total signal. In this figure, it can be seen that the Surf-beat model *overestimates the HF energy with more than 10%.* This overestimation increases with decreasing offshore steepness. Also a difference between the two bathymetries can be seen; the results at the CE are more compactly scattered than at the CH. This is because the Surf-beat mode of CE shows a larger increase in HF motions with increasing offshore conditions than the Non-hydrostatic mode does: the Non-hydrostatic $H_{m0,hf}$ results range between 1 and 2 m, whereas the Surf-beat results range between 1 and 3 m.

The LF motions are both under and overestimated, but the differences lie in a 10% range with the Non-Hydrostatic results. Hence, the severe over estimation of the HF motions, combined with the smaller differences for the LF motions, result in a lower $\frac{E_{lf}}{E_{tot}}$ for the Surf-beat model compared to the Non-hydrostatic model. It has to be noted however, that significant more underestimation of LF motions occurs for $s_0 = 4\%$ than for $s_0 = 1\%$ and $s_0 = 2\%$. This can be seen in figure 4.14, where an example of the total RMSE of all Surf-beat results compared to the Non-hydrostatic results can be found, as well as the individual contribution of the different offshore wave steepnesses to this total RMSE. In that figure it is clear that $s_0 = 4\%$ contributes the most to the RMSE of LF motions, and $s_0 = 1\%$ contributes most to the RMSE of the HF motions. This explains the relative larger difference in behaviour for $s_0 = 4\%$ between the Surf-beat and Non-hydrostatic model, especially where LF motions are dominant.

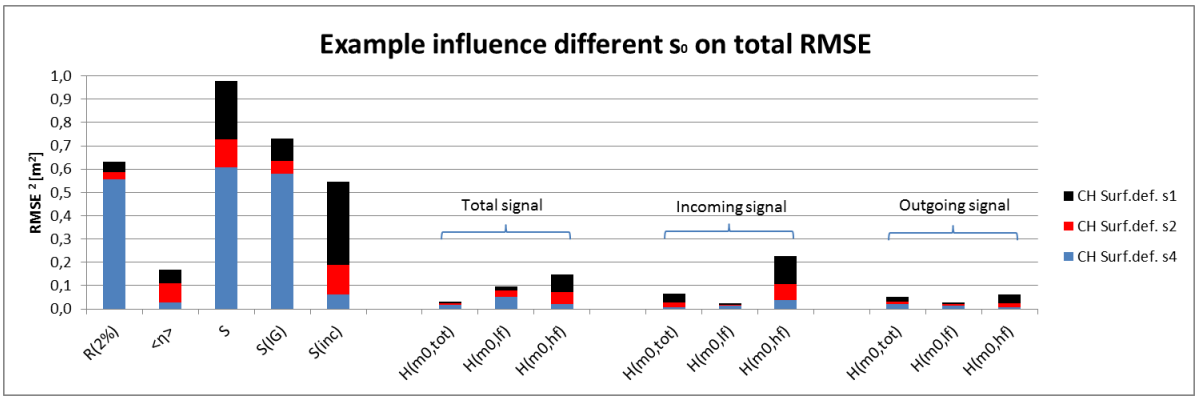

Figure 4.14: Contribution to total RMSE by the different offshore wave steepnesses for the Surf-beat default breaker formulation. It is a cumulative graph, where the summation of the squares of the RMSE of the different s_0 form the squared total RMSE. The different colours indicate the different offshore steepnesses, s_0: Black for $s_0 = 0.01$, red for $s_0 = 0.02$ and blue for $s_0 = 0.04$

The incoming signal behaviour graphs of the Surf-beat (figure 4.10) mode show large differences with those of the Non-hydrostatic mode (figure 4.5). This can be explained by the scatterplots of the incoming signal, shown in figure 4.15. It shows many similarities to figure 4.13. The main difference is that the HF motions are relatively even more overestimated by the Surf-beat model. This overestimation is so significant that it results in an overestimation of the total incoming motions as well. This overestimation of the total motions, similarly to the HF motions, increases with decreasing offshore wave-steepness.The LF motions however,

show the same relative amount of over and underestimation as in the scatterplot of the total wave signal, figure 4.13.

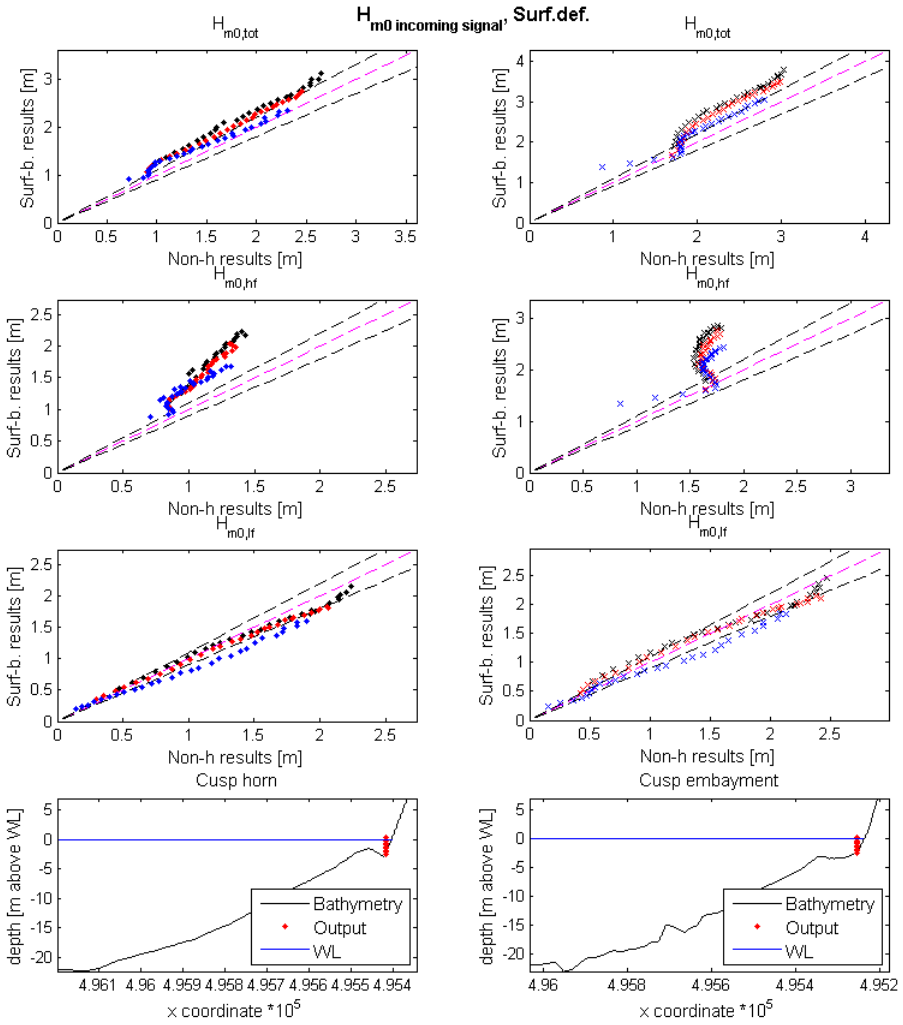

Figure 4.15: Surf-beat and Non-hydrostatic scatterplots of the incoming wave signal at the toe. The black dashed lines (- -) represent a 10% difference between the two modes. The magenta dashed line (- -) represents a 0% difference. Black markers for $s_0 = 0.01$, red markers for $s_0 = 0.02$ and blue markers for $s_0 = 0.04$, $\cdot = CH$, $\times = CE$

Table 4.2: RMSE of incoming wave signal, Surf.def.

	CH				**CE**			
Incoming signal	**All**	$s_0 = 1\%$	$s_0 = 2\%$	$s_0 = 4\%$	**All**	$s_0 = 1\%$	$s_0 = 2\%$	$s_0 = 4\%$
$H_{m0,tot}$	**0,257**	0,197	0,141	0,086	**0,450**	0,339	0,255	0,148
$H_{m0,lf}$	**0,150**	0,067	0,070	0,114	**0,159**	0,081	0,077	0,113
$H_{m0,hf}$	**0,475**	0,343	0,267	0,191	**0,667**	0,486	0,379	0,254

The outgoing signal shows a quite good approximation of the Non-hydrostatic results, when looking at the total and LF wave height in figure 4.16. From this figure, the following can be seen:

- The LF motions are again under and over estimated by 10% for $s_0 = 1\%$ and $s_0 = 2\%$. The underestimation is more significant for $s_0 = 4\%$. Overestimation occurs only for the lowest few conditions.
- The HF energy is mainly severely underestimated, with the exception of the lowest 4 (CE) and 8 (CH) conditions of $s_0 = 4\%$, where the HF motions are overestimated by the Surf-beat model.

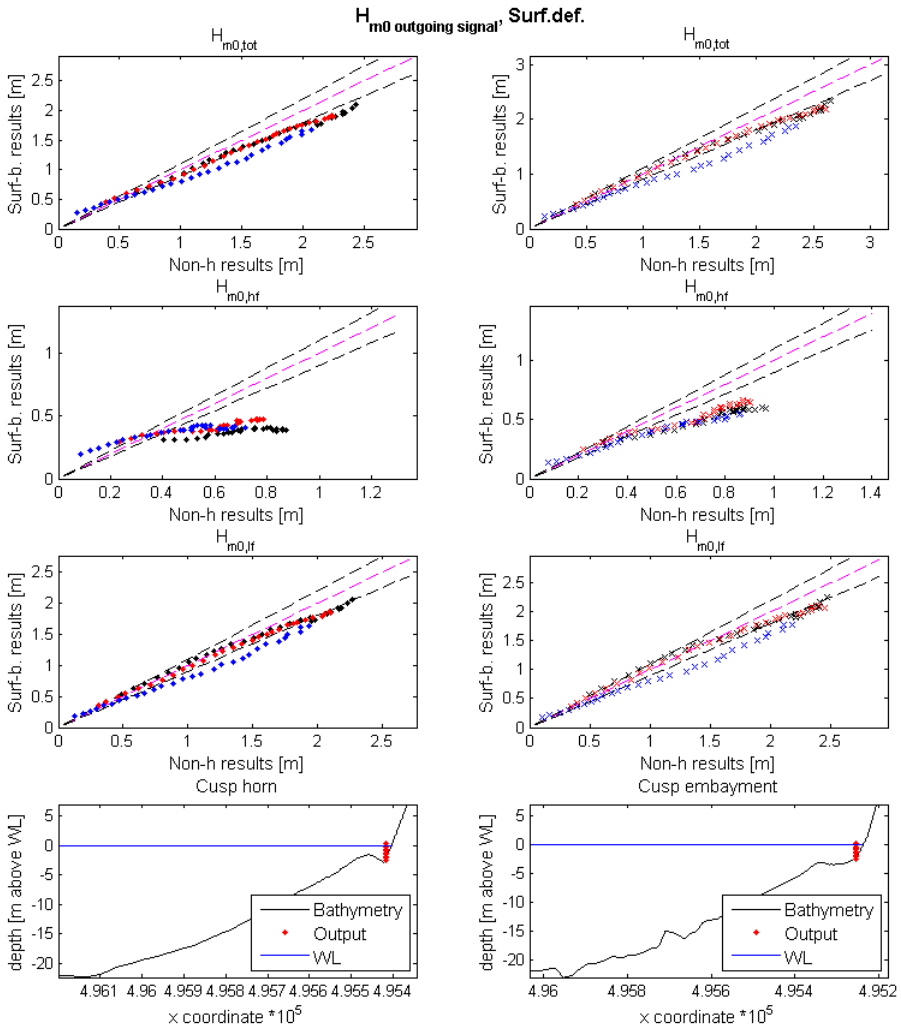

Figure 4.16: Surf-beat and Non-hydrostatic scatterplots of the outgoing wave signal at the toe. The black dashed lines (- -) represent a 10% difference between the two modes. The magenta dashed line (- -) represents a 0% difference. Black markers for $s_0 = 0.01$, red markers for $s_0 = 0.02$ and blue markers for $s_0 = 0.04$, $\cdot = CH$, $\times = CE$

Table 4.3: RMSE of outgoing wave signal, Surf.def.

	CH				CE			
Outgoing signal	**All**	$s_0 = 1\%$	$s_0 = 2\%$	$s_0 = 4\%$	**All**	$s_0 = 1\%$	$s_0 = 2\%$	$s_0 = 4\%$
$H_{m0,tot}$	**0,224**	0,135	0,107	0,144	**0,250**	0,142	0,111	0,174
$H_{m0,lf}$	**0,166**	0,086	0,071	0,123	**0,206**	0,111	0,088	0,149
$H_{m0,hf}$	**0,251**	0,198	0,125	0,091	**0,197**	0,142	0,095	0,100

Overall it can be concluded that at the toe, the LF motions are well approximated by the Surf-beat model, as the results lie in a 10% range from the Non-hydrostatic results, with the exception of the $s_0 = 4\%$ graph. This can also be seen from tables 4.1 to 4.3 and figure 4.14, as $s_0 = 4\%$ has the largest contribution to the total RMSE. Excluding this offshore wave steepness significantly lowers the total RMSE. The HF motions are overestimated in the incoming and total wave signal, with the highest overestimation by $s_0 = 1\%$. Underestimation occurs for most outgoing results as well.

4.4.2. IN THE SWASH ZONE

This section focuses on the results in the swash zone. Again, the comparison between the two models is made, but this section only focuses on the comparison with the Surf-beat model with the *default* breaker formulation. The other two breaker formulations are discussed in section 4.4.3.

The total swash motions are a direct result of the incoming waves at the toe, which are then partially affected by the beach face slope. The total swash height amplitude consists also of a HF and LF part. These are discussed in the next paragraphs.

The S_{inc} is, as expected, an important reason for the differences between the results of the Non-hydrostatic and Surf-beat mode. From figure A.6, it can be seen that the Surf-beat S_{inc} increases little with increasing wave height and decreasing wave steepness. This is more apparent for the CH bathymetry than for CE bathymetry. Interestingly, the results show that the Surf-beat mode still simulates HF swash motions, despite the fact that the model assumes that all incoming HF energy dissipates at the shoreline. In the Non-hydrostatic results however, figure 4.4, the overall increase in S_{inc} is far larger and more spread out. It is also visible in these Non-hydrostatic results, that the HF motions stop growing significantly after an offshore condition of $H_0 = 5-6m$.

It can also be noted that the HF swash scatterplots show similarities to the outgoing $H_{m0,hf}$ scatterplots, displaying that the outgoing motions are, as by definition, a result of the processes in the swash zone. In the scatterplot in figure 4.17, it can be seen that an underestimation of most HF swash motions occurs. An overestimation occurs for the smallest 3 (CE) to 6 (CH) storm conditions of $s_0 = 4\%$. The same conditions result in a under and overestimation of 10% for $s_0 = 2\%$, and a severe underestimation for $s_0 = 1\%$. These differences are also visible in figure 4.14; $s_0 = 1\%$ contributes the most to the total RMSE of the HF swash height. These under and overestimations can be explained by looking at the differences in the swash spectra, as shown in figure 4.18. When looking at the energy around the f_{split}, it can be noticed that the lowest conditions experience more energy in the HF band, whereas the highest conditions experience less energy in the HF band, compared to the Non-hydrostatic swash spectra. This can be explained as the Surf-beat assumptions are based on dissipative conditions. It results in a more dissipative shape of the swash spectra, compared to the Non-hydrostatic swash spectra in 4.1.5. Another reason can be the overestimation of the incoming LF motions for the lowest few storm conditions. They could be frequency down-shifted in the swash zone, resulting in an overestimation of the HF motions there as well. Despite the more dissipative shape of the swash spectra, which would result in a LF dominance [5], $s_0 = 4\%$ still shows a lower E_{lf}/E_{tot} compared to the Non-hydrostatic mode. This is mainly due to the severe underestimation of the LF motions (S_{IG}). The other two offshore wave steepnesses lie in a 10% difference range with the Non-hydrostatic results. The smallest few conditions show again an overestimation compared to the Non-hydrostatic model.

By combining the results of S_{inc} and S_{IG}, the spreading in behaviour between the different offshore wave steepnesses (figure 4.11) can be explained. The different offshore wave steepnesses are handled differently by the Surf-beat model. It results in relatively more or less, under and overestimation of both the HF and LF swash motions, especially for the lowest few storm conditions. This results in a varying behaviour in the swash zone of the Surf-beat mode, in contrast to the almost constant behaviour in the swash zone results of the Non-hydrostatic mode.

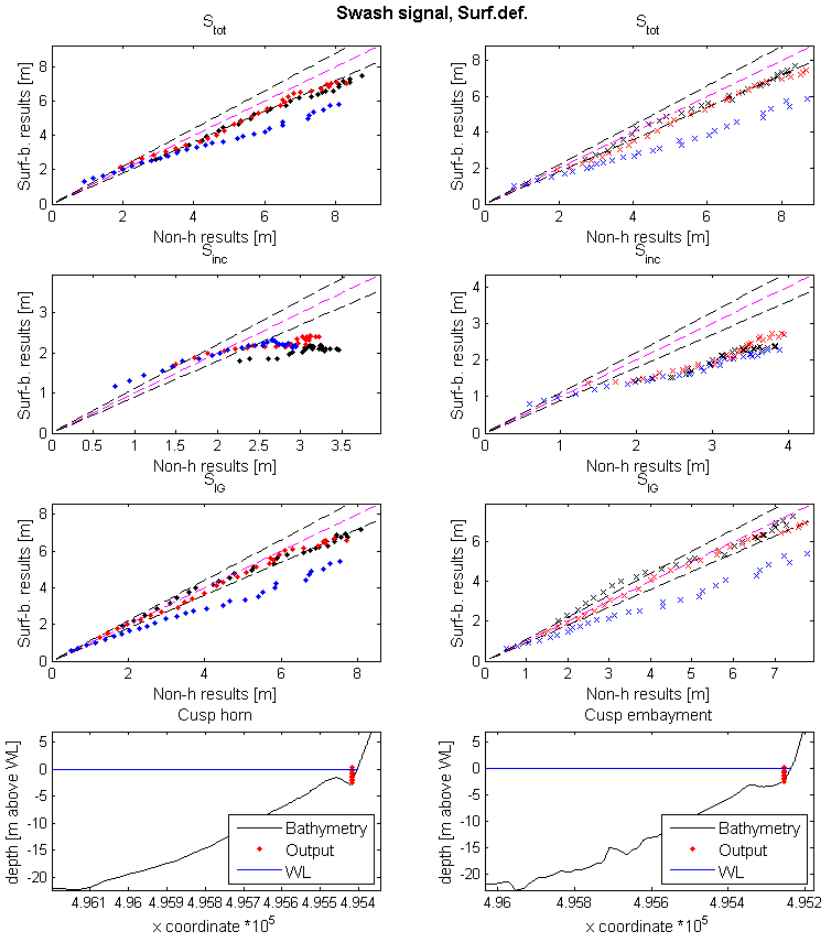

Figure 4.17: Surf-beat and Non-hydrostatic scatterplots of the swash height amplitude in the swash zone. The black dashed lines (- -) represent a 10% difference between the two modes. The magenta dashed line (- -) represents a 0% difference. Black markers for $s_0 = 0.01$, red markers for $s_0 = 0.02$ and blue markers for $s_0 = 0.04$, $\cdot = CH$, $\times = CE$

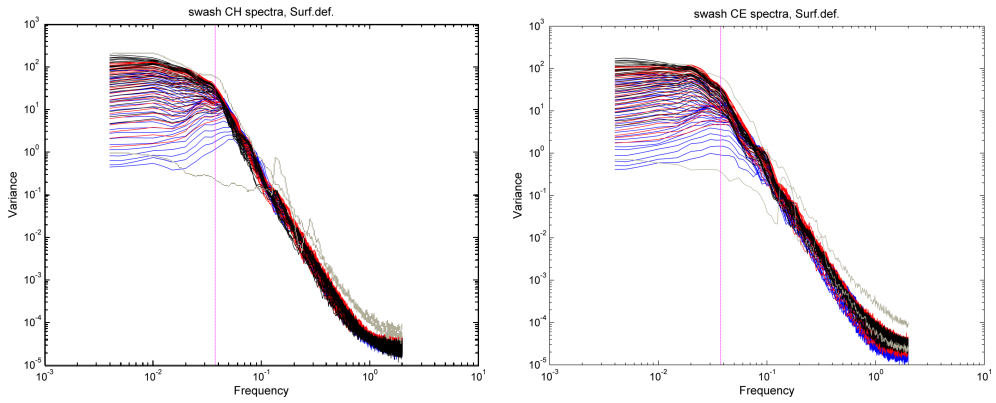

(a) Swash spectrum of the CH bathymetry, Surf-beat default

(b) Swash spectrum of the CE bathymetry, Surf-beat default

Figure 4.18: Logarithmic graph with both swash spectra. Black lines for $s_0 = 0.01$, red lines for $s_0 = 0.02$ and blue lines for $s_0 = 0.04$. The magenta vertical line represents the f_{split}. The grey lines represent the minimum and maximum of the Non-hydrostatic results for comparison.

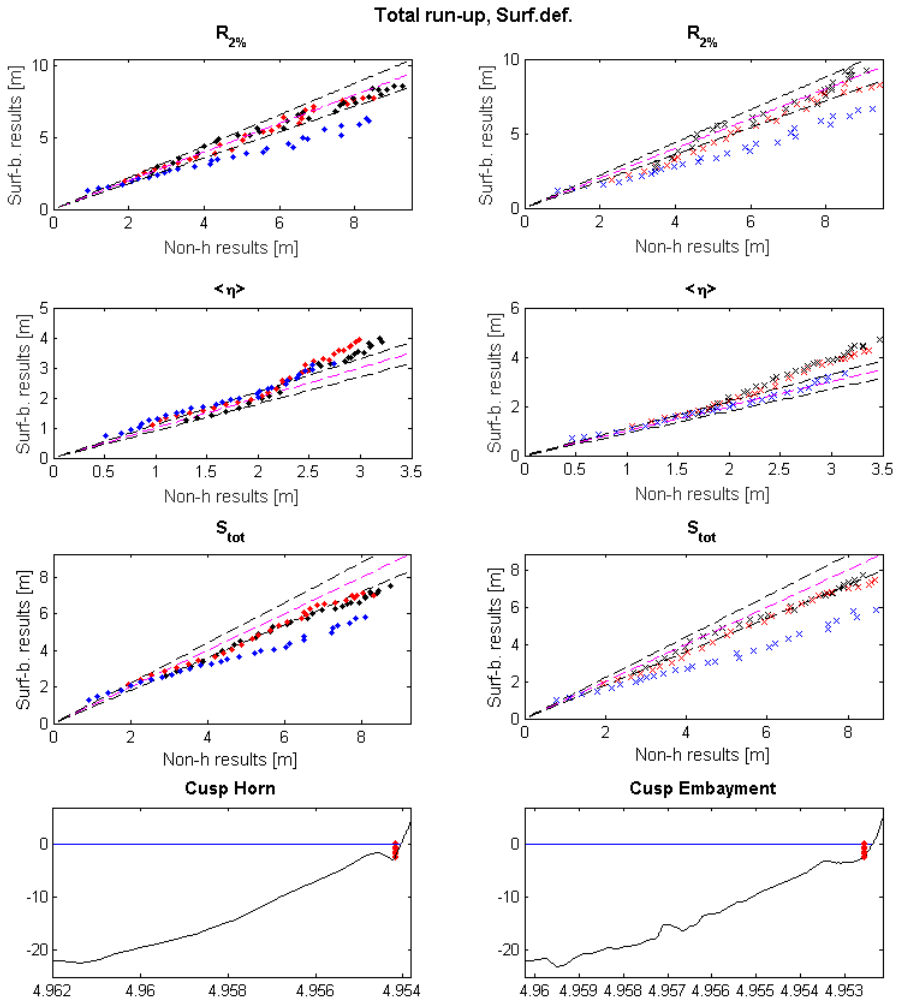

Figure 4.19: Surf-beat and Non-hydrostatic scatterplots of the run-up and its components. The black dashed lines (- -) represent a 10% difference between the two modes. The magenta dashed line (- -) represents a 0% difference. Black markers for $s_0 = 0.01$, red markers for $s_0 = 0.02$ and blue markers for $s_0 = 0.04$, $\cdot = CH$, $\times = CE$

Table 4.4: RMSE of run-up parameters, Surf.def

	CH				**CE**			
Swash signal	**All**	$s_0 = 1\%$	$s_0 = 2\%$	$s_0 = 4\%$	**All**	$s_0 = 1\%$	$s_0 = 2\%$	$s_0 = 4\%$
$R_{2\%}$	**0,795**	0,213	0,170	0,747	**1,057**	0,217	0,376	0,964
$<\eta>$	**0,411**	0,242	0,291	0,162	**0,558**	0,448	0,327	0,061
S	**0,988**	0,499	0,346	0,780	**1,129**	0,326	0,447	0,984
S_{IG}	**0,855**	0,310	0,230	0,762	**0,859**	0,226	0,249	0,790
S_{inc}	**0,740**	0,600	0,352	0,252	**1,056**	0,653	0,570	0,604

The mean run-up, $<\eta>$, in the Surf-beat mode shows an *overestimation* of more than 10% compared to the Non-hydrostatic results, for the majority of the storm conditions. This has been found before by Stockdon *et al.* [13]. Combined with the *underestimation* of the total swash height, it results in a total run-up close to

the Non-hydrostatic one. It has to be noted that this statement is correct for the offshore wave steepnesses of 1 and 2%. At the cusp embayment, the offshore wave height also has to be larger than 3m ($s_0 = 0.01$) and 4m ($s_0 = 0.02$)

Overall, the following general statements can be made. Firstly, for most conditions, a (severe) underestimation of S_{inc} is made by the *default* Surf-beat model. Secondly, the results of S_{IG} lie in a 10% difference range, which has been stated as sufficiently well for engineering purposes. This is with the exception of the results of $s_0 = 4\%$. As LF motions are dominant in the swash zone, the scatterplots of S_{tot} turn out quite similar to the scatterplots of S_{IG}. However, for S_{tot}, the underestimation is slightly larger than 10%, due to the severe underestimation of S_{inc}. $< \eta >$ is overestimated in most cases and combined with the general underestimation of S_{tot}, this leads to a generally good approximation of $R_{2\%}$. Again, with the exception of the $s_0 = 4\%$ results.

4.4.3. OTHER BREAKER PARAMETERS

In this section, the two other breaker parameters are described. The results of the *Roelvink-Daly* formulation are compared to the *default* results. Hereafter, the *Roelvink-Daly, adapted* is compared to the *Roelvink Daly*, as only small differences occured between the two. The scatterplots and their analysis can be found in Appendix A.2. They result in figure 4.20. Based on this appendix, it can be said that calibrating the *Roelvink-Daly* breaker formulation proves to have the largest positive effect for $s_0 = 4\%$. Overall, the smallest difference with the Non-hydrostatic mode for both the toe and swash zone combined, is found for $s_0 = 2\%$ by the *Roelvink-Daly, default* breaker formulation.

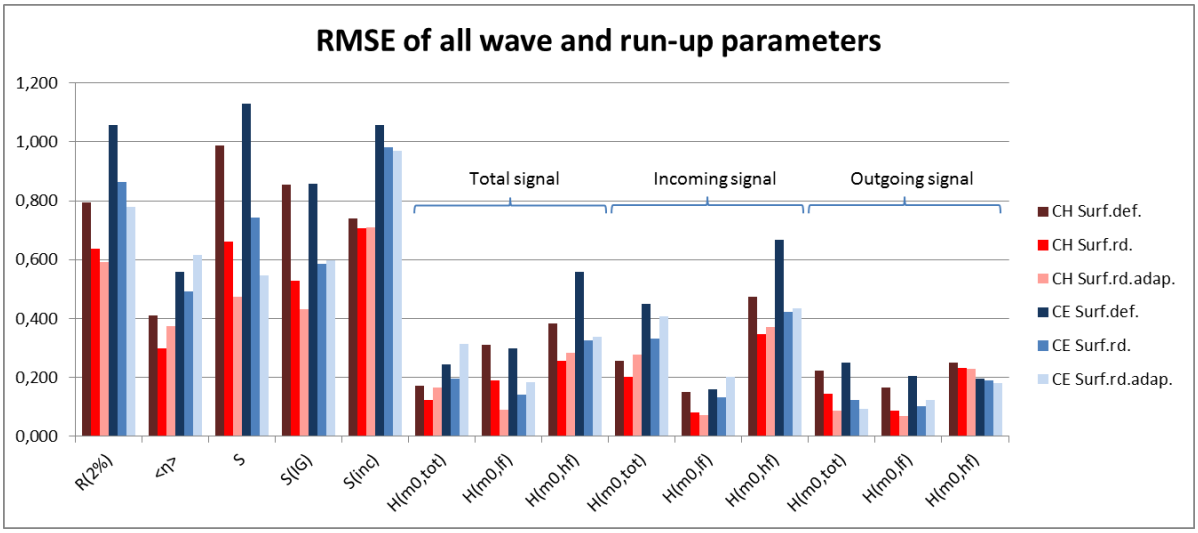

Figure 4.20: Total RMSE of the different wave and swash motions for the different breaker formulations, where the different colours indicate the two bathymetries: Red = CH and blue = CE.

4.5. 1D MODE COMPARISON CONCLUSIONS

In the swash zone, the Surf-beat mode both underestimates the HF and LF swash motions. The first is severe, the latter falls in the range of 10% approximation for s_0 = 1 and 2%. Combined, this also leads to a general underestimation of the total swash height by the Surf-beat mode. However, as the LF motions proved to be dominant, also in the Non-hydrostatic mode, the underestimation of S_{tot} also falls in the range of about 10% approximation for s_0 = 1 and 2%. The mean run-up or setup is generally overestimated, more than 10%. Combined with the swash height amplitude, which experienced a general underestimation, this leads to a good approximation within the range of a 10% difference of the maximum run-up height, $R_{2\%}$, for s_0 = 1% and 2%.

In the incoming wave signal scatterplots, it can be seen that an overestimation of HF motions leads to an overestimation of total wave height as well. This overestimation of the total incoming wave motions can be the reason for the overestimation in mean run-up or setup by the Surf-beat mode, as higher incoming waves lead to a higher set-up [17].

The outgoing wave signal is by definition a result of the processes at the beach. This becomes visual when looking at the $H_{m0,hf}$ scatterplots and comparing them to the swash zone scatterplots in figures 4.17 and 4.16. However, again, since LF motions are mostly dominant and approximated within a 10% range in both the outgoing and swash signal, the over and underestimations of the HF motions do not impact the estimations of the total motions significantly.

No comparison of the wave period has been made for the Surf-beat model, nor a quantitative analysis between the toe and the swash zone. This is because of the fact that the $T_{m-1,0}$ is not well represented in the analysis of the Surf-beat model, as a JONSWAP spectrum is enforced at the location of $T_{p,offshore}$. This is the general approach, but is not a physically correct spectrum for nearshore processes. However, this does not mean that the wave heights are not well represented as well. The wave heights are based on the energy in the spectrum, which does not change by using a JONSWAP shape.

By changing the breaker formulation, these effects change. Changing from the *default* to *Roelvink-Daly* formulation leads to a decrease in HF motions at the toe, but an increase in LF motions. In the swash zone, however, it leads initially to in increase in S_{inc}, but this decreases with increasing storm conditions. The S_{IG} increases for all conditions. These effects lead to an overall better approximation, as can be concluded from the lower RMSE in figure 4.20. However, this RMSE value is based on the total set of results. It has to be noted that some conditions that first fell within the range of 'acceptable for engineering purposes' fall outside of this range, after changing towards *Roelvink-Daly*. This is mostly the case for the lowest few conditions, where HF motions are more important. Adapting this breaker formulation to generate more LF motions, is advised when a severe underestimation occurs. For s_0 = 4% this is the case, however using this adapted breaker formulation still is not enough for an approximation within a range of 10%. It is also visible in the LF scatter plot of the CE bathymetry, that using the breaker formulation *Roelvink-Daly, adapted*, actually leads to an overestimation for the s_0 = 1% and s_0 = 2% results, which first showed an underestimation.

5

1D CONCLUSIONS AND RECOMMENDATIONS

5.1. CONCLUSIONS

This section answers the first two research questions, based on the 1D model results of chapter 4. The first research question is answered based on the Non-hydrostatic results in section 4.1. The second question is based on the results in section 4.4.

1. How do the contributions of setup, incident (HF) and infragravity (LF) band swash vary under the aforementioned conditions?

The first hypothesis for this research question is:

With increasing offshore wave height and decreasing offshore wave steepness, the role of LF motions in the swash zone is mainly dominant

The higher storm conditions show indeed a higher LF dominance, especially in the outgoing wave signal. With increasing conditions, more energy can be transferred to LF motions, by the processes explained by Longuet-Higgins and Stewart [19]. Longer incoming waves also show larger HF motions. According to Battjes [21] this can be explained with shoaling and groupiness of the incoming waves. Shoaling and groupiness of the short waves are important to explain the differences between the three offshore wave steepnesses. Higher offshore wave steepness waves break further offshore. This shortens the distance over which energy transfer can occur for the generation of LF motions. This is because the transfer is significantly reduced as waves start to break, as both groupiness and short wave height are reduced, leading to less enhancement of the forced LF motions. Therefore, higher offshore wave steepness leads to lower HF and LF wave height at the toe, thus a larger LF dominance.

It can be concluded that the respective roles of HF and LF motions at the toe and in the swash zone, depend on the bathymetry but also on the offshore storm conditions; both wave height and wave steepness. At the toe of CH, the prominent bar functions as a filter, breaking most of the HF motions coming in. At the CE the bar is less prominent, resulting in more HF motions and higher total motions. The LF motions are similar for the two bathymetries, as the foreshore slopes are similar as well. To conclude, a dominance in the total wave signal at the toe is found for all storm conditions from $H_0 = 4m$ (CH) and $H_0 = 5.5m$ (CE). For the lower wave steepnesses, a this dominance of LF motions starts at a lower H_0. In the swash zone, with the exception for $H_0 < 3m$, all storm conditions show an dominance of LF motions, thus confirming the first hypothesis.

The first hypothesis lead to a second one, which is as follows:

The respective roles of incident and infragravity band swash are determined by the respective significant high frequency and low frequency wave-height at the toe of the beach.

From section 4.1.3, it can be concluded that this is not entirely the case, both qualitatively and quantitatively. Qualitatively, the following can be said: the behaviour at the toe is affected by the incoming waves and the nearshore bar and the behaviour in the swash zone is affected by incoming waves and the beach face slope. This is explained in section 4.1.5. There is also a large difference in behaviour at the toe between the two

bathymetries, which is mainly due to differences in HF motions, as LF motions are similar. In the swash zone, the difference in behaviour between the two bathymetries becomes small, as the difference in incident band swash is not as significant as at the toe. This shows again that the degree of LF dominance at the toe does not result in the same degree of dominance in the swash zone: at the toe a significant difference between the bathymetries is found, but in the swash zone this difference remains small. Quantitatively it is seen that some parameters in the swash can be directly and linearly linked to the total wave signal at the toe, such as the total and LF swash height. The HF swash however shows no clear linear relationship with any wave parameters at the toe, not even with an Hunt's like relationship.

2. What are the differences in the predictions of the swash motions between the Non-hydrostatic and the Surf-beat mode, and are these differences a function of the aforementioned conditions?

In the swash zone, the Surf-beat mode both underestimates the HF and LF swash motions. The underestimation of all HF and LF ($s_0 = 4\%$) swash motions is severe. The other LF swash motions of $s_0 = 1$ and 2% fall in the range of 10% approximation. Combined, this also leads to a general underestimation of the total swash height by the Surf-beat mode. However, as the LF motions proved to be dominant, also in the Non-hydrostatic mode, the underestimation of S_{tot} also falls in the range of about 10% approximation for $s_0 = 1$ and 2%.

The mean run-up or setup is generally overestimated, more than 10%. Combined with the swash height amplitude, which experienced a general underestimation, this leads to a good approximation within the range of a 10% difference of the maximum run-up height, $R_{2\%}$, for $s_0 = 1$ and 2%. Again, for $s_0 = 4\%$ this approximation lies outside of the 10% range of difference.

From the above, it can be concluded that there are clear differences between the three different offshore wave steepnesses, for both the HF and LF motions in the swash.This shows that the approximation of the Non-hydrostatic mode by the Surf-beat mode is a function of the offshore wave steepness. A high s_0 (4%) shows a better approximation of the HF motions, at both the toe and in the swash zone, but a worse approxmimation of the LF motions, at both the toe and in the swash zone, when compared to the other s_0.

By examining all LF graphs of all scatter plots, as well as the HF graphs of the outgoing and swash signal, a transition from overestimations to underestimations can be seen with an increase of the regarded parameter. Both the swash and toe wave parameters show an increase with an increase in offshore wave height. Therefore, the approximation of the Non-hydrostatic results by the Surf-beat mode is also a function of the offshore wave height.

Finally, a difference in the total RMSE of the HF motions between the two bathymetries can be seen, whereas the total RMSE of the LF motions is similar for both bathymetries. This shows that the overall accuracy in the estimation of LF motions by the Surf-beat model does not depend on the bathymetry, but the accuracy in the estimation of HF motions does. This affects the total wave height at the toe and the total swash height in the swash zone, thus having an effect on the run-up as well. Therefore, it can also be concluded that the differences between the two modes are a function of the bathymetry.

5.2. RECOMMENDATIONS

This section lists the recommendations regarding the 1D model.

- First of all, a verification and validation of the results is advised. This will enhance the validity of the statements and the Non-hydrostatic model.
- Secondly, it is advised to check if non-linear parameterizations improve the results in section 4.1.4. If this is the case, a parameterization of HF swash motions can be used in the Surf-beat estimation of $R_{2\%}$. However, since the Surf-beat estimation is mostly sufficient for engineering purposes, it is advised to only look into this if a good estimation of HF motions proves necessary.
- According to Guedes *et al.* [14], the beach face slope is the main reason for alongshore variations in run-up. The conclusions of the Non-hydrostatic 1D model show that both the bar and the slope are important for variations. It is therefore advised to further investigate the individual roles of the beach face slope and the bar. This could be done by using only one bathymetry and vary its slope or bar configuration.
- This report has focused on the nearshore processes, mostly within the swash zone. A full analysis of the cross-shore behaviour is advised if the role of the bars is investigated.
- Only run-up is regarded in this report. However, since the crest height of the dune is only 5 m high, in reality overtopping will occur for the larger offshore storm conditions. It is therefore advised to look into the ability of the Non-hydrostatic model (and the Surf-beat model) to estimate this, as well as to perform an analysis between the two models.
- Lastly, as figure 1.5 shows as well, the hydrodynamics and sediment dynamics affect each other. This has been shown in for example Masselink and Puleo [3], Puleo [41] and Masselink and Hughes [42]. The sediment transport is very complex in the swash zone, hence a good estimation of the hydrodynamics is important.
- It is advised to use a coarser grid for the Surf-beat model to utilise the computational advantage that it does not require a fine grid. This will also speed up any further research. However, a quick check has to be done in order to quantify if any significant differences arise when a coarser grid is used.
- It is also recommended to look into the near shore spectrum, and if it is possible to change the JONSWAP spectrum of the HF motions in order to perform a correct analysis of $T_{m-1,0}$.
- Adapting the Roelvink-Daly breaker formulation proved to have a positive effect where the underestimation of LF motions is the main reason for significant differences with the Non-hydrostatic model. A more detailed analysis is advised to see if other calibrated values for γ and γ_2 could work for other s_0, hence improving the Surf-beat results.

6

2D Model, methodology and results

This chapter consists of the methodology and analysis of the results of the 2D model of Gangneung, South Korea. It involves 2DH modeling of the swash processes and the role the alongshore varying bathymetry and topography have on it.

6.1. Methodology

The focus in the 2D model lies in answering research sub-question 3. In order to be able to answer this question, more cusp horns and embayments are modeled, as can be seen in figure 6.1.

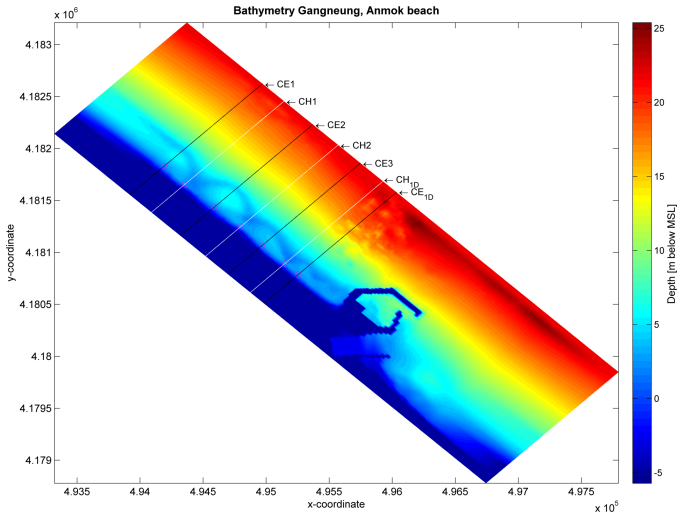

Figure 6.1: The locations of the 1D bathymetries within the 2D model

In total, 3 extra cusp embayments and 2 extra cusp horns are analysed in this chapter. Again, similarly to the 1D model, output is generated at the shoreline, as well as at the toe of the beach. The 2D model is, however, much coarser than the 1D model: where the 1D model has about 2900 cells in the cross shore direction, the 2D model has 215 (Surf-beat) and 613 (Non-hydrostatic) as shown in table 6.2. This results in also difference in gridsize in the cross-shore direction: the 1D model had a minimal gridsize of 0.20m, the 2DH Non-hydrostatic model has a minimal gridsize of 0.57m and the 2DH Surf-beat model a minimal gridsize of 1.7m in the nearshore. Therefore, in the 2DH model of both the Surf-beat and Non-hydrostatic mode, the output locations at the toe could not be taken at exactly 2.4 m depth. The final depth at the toe is shown in table 6.1.

Table 6.1: Depth at toe locations

	CE_1	CH_1	CE_2	CH_2	CE_3	CH_{1D}	CE_{1D}
Depth	2.397	2.339	2.414	2.347	2.452	2.476	2.407

Most of the methodology is similar to the 1D model. Both a Surf-beat and Non-hydrostatic model will be used, and their results undergo a spectral analysis as explained in chapter 3. The difference is that no in and outgoing signal analysis is made, as the method by Guza *et al.* [38] is made for a 1D model.

6.1.1. STORM CONDITION

Based on the results of chapter 4, and due to time-constraints, it is chosen to model only one storm condition. This storm condition has to:

- Have a $R_{2\%}$ lower than 5 m, in order to use the current bathymetry
- Have a breaker formulation in the Surf-beat model, with the smallest error with the Non-hydrostatic model in chapter 4

Therefore, storm condition 10 of $s_0 = 2\%$ has been chosen to be modeled. This condition has a $H_0 = 4.25m$ and a $T_{p,offshore} = 11.67s$. The run-up of this condition reaches about 5 m in the 1D model, but this is expected to be lower in the 2D model due to wave spreading. This wave spreading is defined in the wave boundary condition as seen in equation 6.1.

$$\sigma = \sqrt{\frac{2}{s+1}} \tag{6.1}$$

Similarly to the 1D wave boundary condition, a value of 5 is chosen for s. This results in a spreading of 0.577 radians, or 33 degrees. As this results in the spreading of the wave energy, lower values for wave run-up and wave height can be expected, compared to the 1D model.

6.1.2. MODEL

As the 2D model requires more computational demand, the Non-hydrostatic and Surf-beat model do not run with the same grid. They both run on their required (minimal) size, to minimize the computational time. This results in the sizes as shown in table 6.2. Here, the *M-direction* represents the cross-shore direction, and the *N-direction* the alongshore direction.

Table 6.2: Grid size of the 2D model for the two modes.

	M-direction	**N-direction**	**Minimal gridsize [m]**
Non-hydrostatic	613	235	0.57
Surf-beat	215	235	1.7

Finally, a cyclic lateral boundary condition is used for both models. As explained in the XBeach manual [6], this boundary condition considers the two lateral boundaries as physically connected.

6.2. ANALYSIS OF RESULTS

The first part of the analysis is based on the Non-hydrostatic mode. Analogous to the 1D analysis, firstly the results at the toe are analysed, after which the swash zone is regarded. After the Non-hydrostatic analysis, another comparison with the Surf-beat mode is made to answer research sub-question 4.

6.2.1. NON-HYDROSTATIC

This section analysis the Non-hydrostatic computation of the 2D model, in order to answer research sub-question 3. The results can be found in figure 6.3 and in table 6.3.

Table 6.3: Non-hydrostatic results

Location	H_{m0}	$H_{m0,lf}$	$H_{m0,hf}$	**S**	S_{IG}	S_{inc}	$<\eta>$	$R_{2\%}$
CE1	2,24	0,92	2,03	2,72	2,25	1,45	1,53	2,92
CH1	1,67	1,04	1,29	2,93	1,82	2,27	1,26	2,64
CE2	2,17	0,81	2,00	2,95	1,80	2,07	1,80	2,55
CH2	1,74	1,09	1,34	3,11	2,12	2,22	1,50	2,85
CE3	1,83	0,91	1,57	2,63	1,85	1,77	1,49	2,84
CH1D, 2D model	1,43	0,98	1,02	2,92	1,84	2,23	1,29	2,63
CE1D, 2D model	1,68	1,00	1,34	2,40	1,82	1,52	1,45	2,92
CH1D, 1D model	2,13	1,83	1,08	4,64	3,69	2,81	1,93	4,72
CE1D, 1D model	2,48	1,78	1,72	4,39	3,37	2,81	2,00	5,02

AT THE TOE

From the graphs and the table, it can be seen that that the behaviour at the toe depends on the bathymetry. First of all, the $H_{m0,hf}$ is higher for all CEs whereas the $H_{m0,lf}$ is relatively constant for all locations. This result suggest that the LF waves are not so much affected by the 2D processes, as their generation mechanism (the foreshore slope) is similar over the entire bathymetry. When figure 6.3a is compared to the bar depth in table B.1, it can be seen that the relative importance of the LF motions at the toe depends on the depth of the top of the nearshore bar. Figure 6.2 shows that this bar depth mostly affect the HF motions, whereas the LF motions barely vary with the bar depth. The deeper the bar is located, the less HF motions break over the bar, thus reducing the importance of the LF motions. This indicates that the nearshore bar is an important component for the amount of HF motions that remain at the toe.

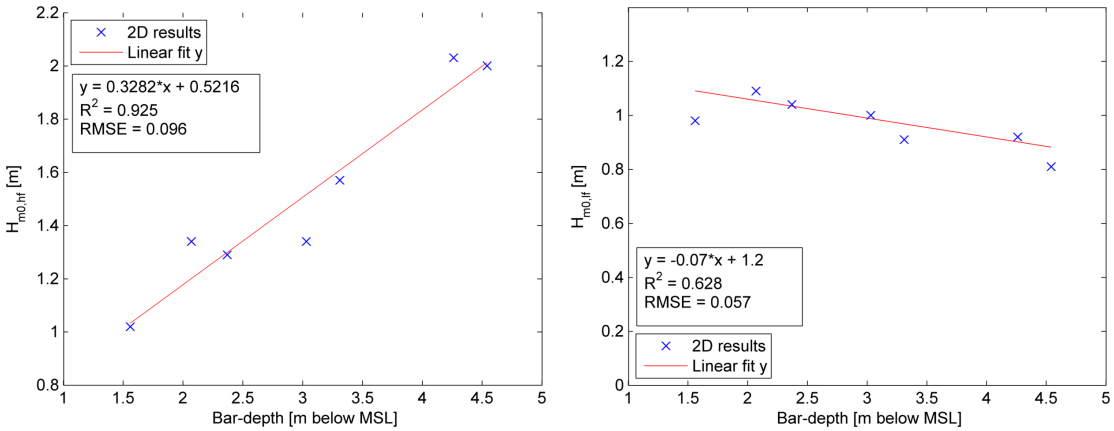

(a) Bar depth vs HF wave height at the toe.

(b) Bar depth vs LF wave height at the toe.

Figure 6.2: Bar depth vs the HF and LF wave heights at the toe.

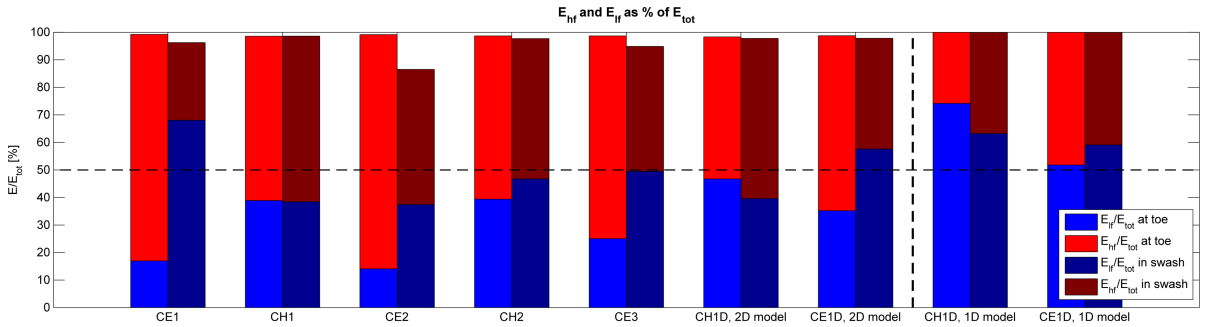

(a) Behaviour graph of both the motions at the toe and in the swash zone

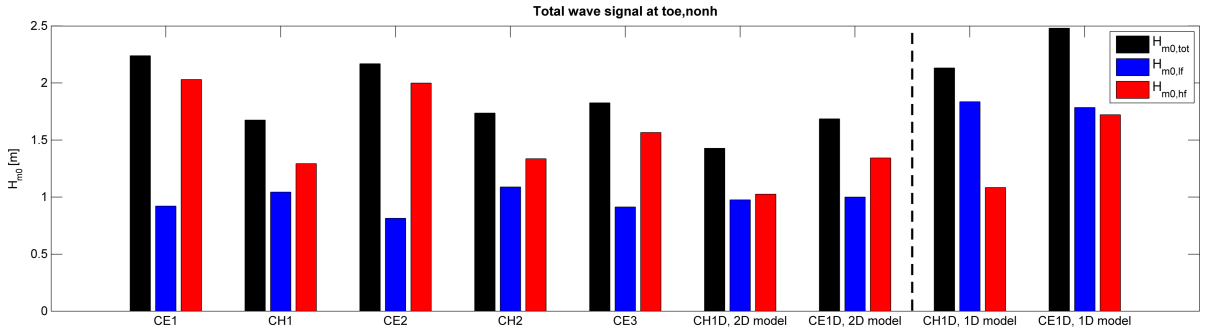

(b) 2D Non-hydrostatic wave heights at the toe, compared to the 1D results

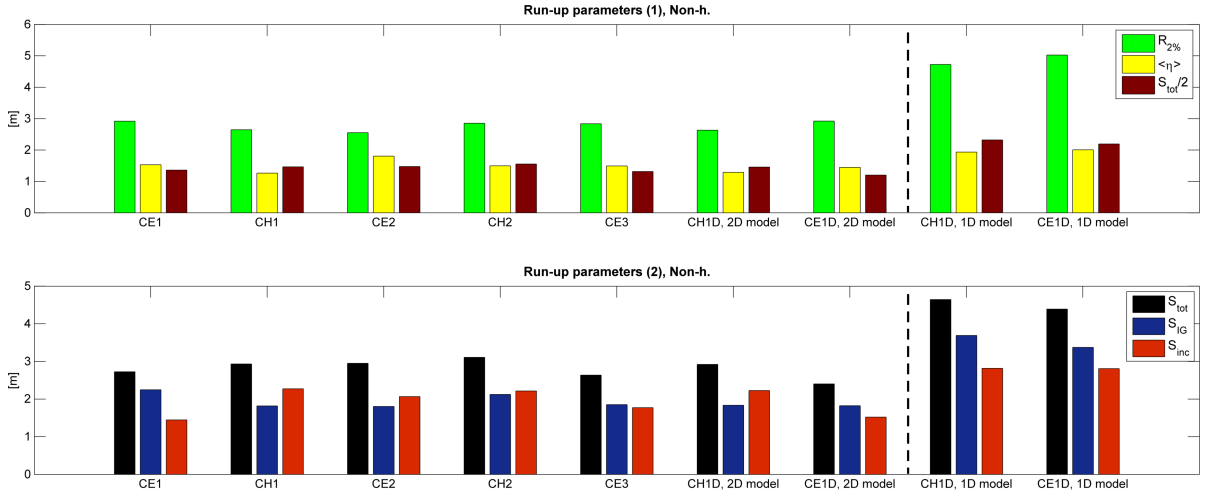

(c) 2D Non-hydrostatic swash heights at the toe, compared to the 1D results

Figure 6.3: Non-hydrostatic results, FTTB: (6.3a) Behaviour in at the toe and in the swash zone, (6.3b) Total, LF and HF wave height at the selected locations, (6.3c) Swash parameters such as the total, LF and HF swash height, as well as the maximum and mean run-up. All graphs show the 1D values for the same storm condition at location $CH_{1Dmodel}$ and $CE_{1Dmodel}$. Details of all graphs can be found in table 6.3

The figures also show a main difference with the 1D model. The $H_{m0,lf}$ for the 2DH model is much lower than for the 1D model. This means that, contrary to the 1D model, there is no LF dominance at the toe for the 2DH model. Although the same offshore boundary condition has been used, with the same spreading, this spreading is suspected to be the main reason behind the difference in $H_{m0,lf}$. In the 1D model, the lateral boundaries limit the amount of spreading which is possible, resulting in a more uniform wave front. In the 2DH model, the spreading is not limited, resulting in a more dispersed wave front. This dispersion induces a less efficient energy transfer from the wave groups to the bound long (LF) wave, resulting in a lower $H_{m0,lf}$. Hence, when looking at the results at the toe, not refraction but spreading seems to be the main reason for differences between the 1D and 2DH model. This can stated with greater certainty by carrying out a run without any spreading and compare it to the 1D results. However, due to lack of time, this has not been done

for this report.

Besides the LF motions, also the HF wave height of the CE1D is a little bit lower in the 2DH model than in the 1D model. It is suggested this could be due to some differences in reflection, but since no incoming and outgoing wave signal are determined, more research has to be done to state this with absolute certainty.

IN THE SWASH-ZONE

The results in the swash zone are not as straight forward as at the toe. In general it is visible that:

- S_{IG} seems to be relatively stable among the locations, with the exception of *CE1* and *CH2*. A closer look at their spectra shows slightly higher energies at certain frequencies around the VLF separation.
- S_{inc} on first glance does not seem to follow any logical order. However, by comparing it to the beach face slope (table 6.4 and figure 6.4), it is visible that this slope shows a correlation with the height of the S_{inc}. An exception is *CE2*. This complies with the statement of Guedes *et al.* [14] and the formula by Stockdon *et al.* [7] that the beach face slope is the main reason for variability in S_{inc}, however, as there are only a few results, strong conclusions cannot be drawn.
- The total swash height S_{tot} is higher for a certain CH that its neighbouring CE, as was also found for cusping beaches by Masselink *et al.* [11]. Again, *CE2* forms an exception. It has to be noted that this does not imply that the S_{tot} of a certain CH is always larger than S_{tot} of all other CEs in the system.

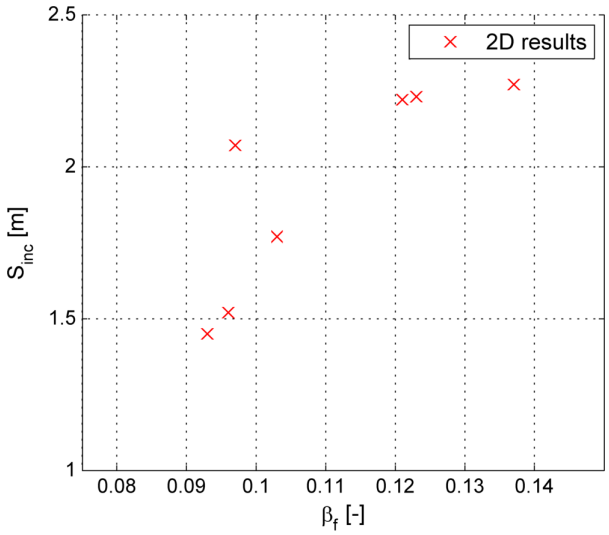

Figure 6.4: HF swash results plotted against the beach face slope

The reason for the deviation of *CE2* to these remarks comes to light when looking at the swash spectra in figure C.1. Here, it is visible that already from 0.1 Hz, the *CE2* spectrum shows a much higher energy for the HF swash. The reason for this cannot be attributed to the wave-height at the toe or the beach face slope. Further research is required to conclude whether this is due to the model or an actual physical feature. A glance at the bathymetry does show a clear transition in beach face slope around the WL; 0.072 below and 0.139 above WL. The last value would then comply with the statement that a steeper slope increases the HF swash height.

In general, it can also be seen that the mean run-up (or wave setup) is higher than the swash amplitude at the *CEs* and vice versa at the *CHs*. This is most likely a result from the HF importance at the toe, and thus due to the nearshore bar depth. The locations where the HF motions are more dominant are also the locations where the total wave height at the toe remains higher. Both the bar and trough depth affect maximum wave height that can be reached at the toe, which can then run-up the beach thus affecting the mean run-up as well.

By combining the statements, a varying $R_{2\%}$ can be expected. However, as S_{tot} and $< \eta >$ vary opposing to each other, it is expected that the variability of $R_{2\%}$ cannot be crudely attributed to a cusp horn or embayment.

This is also visible in table 6.3. Surprisingly, it also does not occur at the highest combination of the swash height amplitude (*S/2*) and the mean run-up ($< \eta >$), as visible in figure 6.5. This contradicts formula 2.6 where the run-up is expected to relate linearly to the summation of the two.

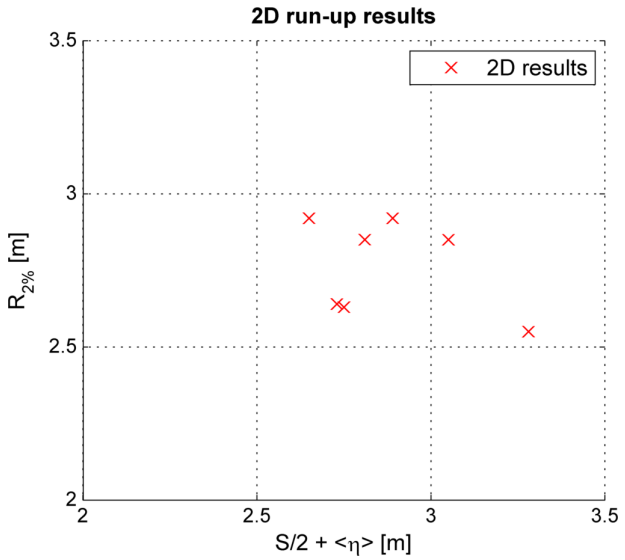

Figure 6.5: $R_{2\%}$ plotted against the combination of swash height amplitude and mean run-up.

One reason for this deviation is thought to be the absence of a cutoff frequency, as wiggles are visible in the run-up signal. Using a cutoff frequency smooths out this run-up signal. The main results of the cutoff frequency can be found in Appendix B. Using the smoothed run-up signal instead of the regular obtained signal, has almost no effect on the spectral analysis, as little to no energy was found in the energy band above this frequency. It has, however, a variable effect on the mean and run-up[1]. However, both using a cutoff frequency or not, $R_{2\%}$ remains to have a variable relation with $S/2$ and $< \eta >$. Overall, it is suggested that this could be due to the significant offshore spreading, smearing out the energy over the longshore distance. Based on the model, it seems that the maximum run-up depends thus on a combination of bar height, beach face slope, wave height and wave steepness, showing it is more complex than simply attributing it to a cusphorn or embayment.

Finally, again a large difference between the 1D and 2DH results can be seen. This differences is most pronounced in the swash height and its components. Combined with also a smaller mean run-up, the $R_{2\%}$ is much lower for the 2DH results. It is suggested to be a result of an underestimation of the LF motions at the toe, lowering the total wave height at the toe and thus the motions which can run up on the beach.

Table 6.4: Non-hydrostatic HF swash and beach face slopes of the different output locations

	CE1	**CH1**	**CE2**	**CH2**	**CE3**	**CH1D**	**CE1D**
β_f	0,093	0,137	0,097	0,121	0,103	0,123	0,096
S_{inc}	1,45	2,27	2,07	2,22	1,77	2,23	1,52

[1] CE2 forms again an exception, however as this location consists of a lot more energy in the HF band, this could have been expected

6.2.2. SURF-BEAT AND NON-HYDROSTATIC COMPARISON

The last part of the 2DH analysis consists of a comparison between the Surf-beat and Non-hydrostatic modes. Figure 6.6 shows the graph with the results, and tables 6.5 to 6.7 show the relative differences of the two modes. Behaviour comparison can be found in Appendix B.

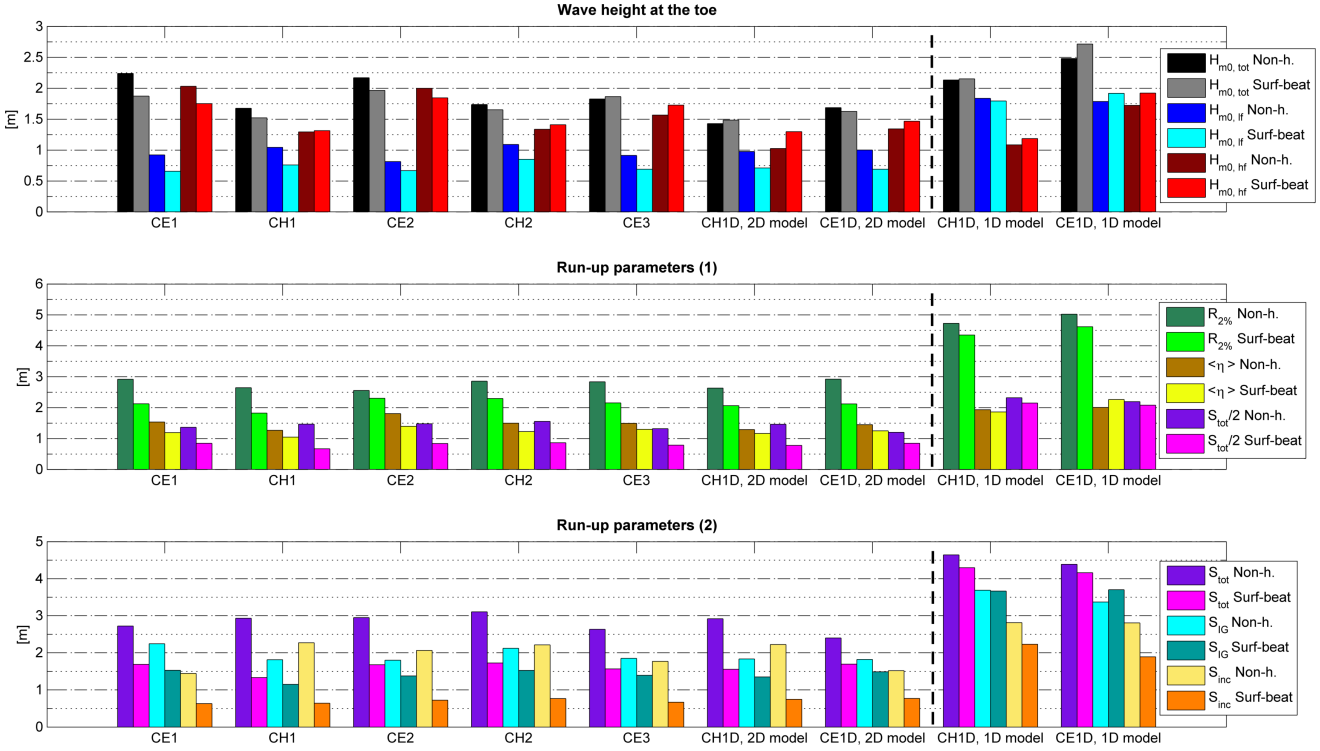

Figure 6.6: Comparison of the wave parameters at the toe and in the swash zone, of both the Non-hydrostatic (1-3-5 in the bargroup) and Surf-beat (2-4-6 in the bargroup)

Table 6.5: Difference between Non-hydrostatic and Surf-beat results for wave-height

	H_{m0}			$H_{m0,lf}$			$H_{m0,hf}$		
Location	**Non-h.**	**Surf-b.**	**difference [%]**	**Non-h.**	**Surf-b.**	**difference [%]**	**Non-h.**	**Surf-b.**	**difference [%]**
CE1	2,24	1,87	**16,4**	0,92	0,66	**28,6**	2,03	1,75	**13,8**
CH1	1,67	1,52	**9,2**	1,04	0,76	**27,4**	1,29	1,31	**-1,6**
CE2	2,17	1,96	**9,4**	0,81	0,67	**18,0**	2,00	1,84	**7,8**
CH2	1,74	1,65	**4,9**	1,09	0,85	**21,9**	1,34	1,41	**-5,5**
CE3	1,83	1,86	**-2,1**	0,91	0,69	**24,5**	1,57	1,73	**-10,3**
CH1D, 2D model	1,43	1,48	**-3,9**	0,98	0,71	**27,2**	1,02	1,30	**-26,5**
CE1D, 2D model	1,68	1,62	**3,6**	1,00	0,69	**31,0**	1,34	1,47	**-9,2**
CH1D, 1D model	2,13	2,15	**-0,9**	1,83	1,79	**2,2**	1,08	1,19	**-9,4**
CE1D, 1D model	2,48	2,71	**-9,4**	1,78	1,92	**-7,4**	1,72	1,92	**-11,5**

Table 6.6: Difference between Non-hydrostatic and Surf-beat results for swash-height

	S			S_{IG}			S_{inc}		
Location	**Non-h.**	**Surf-b.**	**difference [%]**	**Non-h.**	**Surf-b.**	**difference [%]**	**Non-h.**	**Surf-b.**	**difference [%]**
CE1	2,72	1,69	**37,9**	2,25	1,53	**31,8**	1,45	0,63	**56,1**
CH1	2,93	1,33	**54,5**	1,82	1,15	**36,5**	2,27	0,64	**71,6**
CE2	2,95	1,68	**43,0**	1,80	1,38	**23,6**	2,07	0,73	**64,8**
CH2	3,11	1,73	**44,4**	2,12	1,53	**28,0**	2,22	0,77	**65,2**
CE3	2,63	1,57	**40,4**	1,85	1,40	**24,6**	1,77	0,67	**62,1**
CH1D, 2D model	2,92	1,56	**46,6**	1,84	1,35	**26,4**	2,23	0,75	**66,3**
CE1D, 2D model	2,40	1,70	**29,4**	1,82	1,49	**18,2**	1,52	0,77	**49,3**
CH1D, 1D model	4,64	4,29	**7,5**	3,69	3,67	**0,6**	2,81	2,23	**20,6**
CE1D, 1D model	4,39	4,16	**5,2**	3,37	3,70	**-9,8**	2,81	1,90	**32,5**

Table 6.7: Difference between Non-hydrostatic and Surf-beat results for $R_{2\%}$ and $<\eta>$

	$<\eta>$			$R_{2\%}$		
Location	**Non-h.**	**Surf-b.**	**difference [%]**	**Non-h.**	**Surf-b.**	**difference [%]**
CE1	1,53	1,19	**22,1**	2,92	2,12	**27,2**
CH1	1,26	1,05	**17,2**	2,64	1,82	**31,0**
CE2	1,80	1,40	**22,7**	2,55	2,30	**9,9**
CH2	1,50	1,23	**18,1**	2,85	2,29	**19,7**
CE3	1,49	1,30	**12,9**	2,84	2,15	**24,2**
CH1D, 2D model	1,29	1,16	**9,7**	2,63	2,06	**21,6**
CE1D, 2D model	1,45	1,25	**13,8**	2,92	2,12	**27,5**
CH1D, 1D model	1,93	1,86	**3,8**	4,72	4,35	**7,9**
CE1D, 1D model	2,00	2,26	**-12,8**	5,02	4,61	**8,1**

At the toe, the total wave height differences lie around the range of 10% as was found in the 1D model. However, even though the $H_{m0,tot}$ is well represented, its HF and LF components are not. The Surf-beat mode significantly underestimates the LF motions (20-30%), and generally overestimates the HF motions, but mostly within the range of 10%[2]. The severe underestimation of LF motions is dissimilar to what was seen in the 1D model, where they were well approximated.

[2]With the exception of CE1 and CE2, where an underestion of the HF motions occurs

The severe underestimations of the HF and LF swash motions, results in an underestimation of all motions in the swash zone. The underestimation of the HF swash by Surf-beat is part of the working hypothesis. However, contrary to the 1D results, the HF motions are mostly dominant in the 2DH model for this particular wave condition. Therefore, the underestimation of S_{inc} becomes a more important factor in how well the Surf-beat mode represents the Non-hydrostatic mode. In terms of behaviour, the severe underestimation of HF swash leads to a high LF dominance in the swash, completely opposing of what was found in the Non-hydrostatic results.

As all wave motions are underestimated, in the toe and in the swash, so are the mean and maximum run-up. Where the 1D model had a difference between the modes of about 10% for the mean and maximum run-up, this doubles and triples in the 2DH model.

6.3. 2DH CONCLUSIONS

This section answers both the 2DH research subquestions 3 and 4.

3. Are there differences in the predictions of the swash dynamics between the 2DH and 1D model, and are they caused by the alongshore varying bathymetry and topography of the research location?
4. Is the (dis)similarity between simulated swash dynamics in the non-hydrostatic and surf-beat mode different for 1D and 2DH models?

This question can be answered by checking whether the hypotheses are correct.

The wave run-up in a 2DH model will be higher at the cusp horn and lower at the embayment compared to the run-up at these locations in a 1D model, due to non-uniform refraction.

The total run-up variability is not extremely significant, as the maximum difference between the minimum and maximum run-up is only 12% in the 2DH model. The variability of $R_{2\%}$ cannot be assigned to the fact that its height depends if it is at a cusp horn or embayment. However, the variability of its components, $<\eta>$ and $S_{tot}/2$ can be assigned to the location, as a cusp horn shows a general lower $<\eta>$ and higher $S_{tot}/2$ than the cusp embayment. Figure 6.3c shows that a correlation between the importance of HF and LF motions of the incoming signal: A higher importance of LF motions at the toe, results in a lower $<\eta>$. This is most likely due to the fact that for a higher importance of LF motions at the toe, the total wave height at the toe is lower as well. This is due to a lower HF wave height, as the LF wave height is spatially quite constant. Thus, a lower total wave height at the toe, leads to a lower $<\eta>$. A similar result can be seen in figure 4.8b of the 1D results.

The longshore variability in S_{tot} can be attributed to the variability in S_{inc}, as S_{IG} is (almost) constant throughout the system, with the exception of CE1 and CH2. The variability in S_{inc} shows a high correlation with the beach face slope, suggesting that the statement of Guedes *et al.* [14] is correct. However, there are not enough results to make a definite conclusion. It also partially confirms Stockdon *et al.* [7], as the S_{IG} depends on the cross shore generation of LF motions and not on the beach face slope.

Based on formula 2.4, it can be expected that a higher combination of $<\eta>$ and $S_{tot}/2$ leads to a higher $R_{2\%}$, if the relationship has a constant factor. However, this factor varies for all locations within this system. It could be stated that this method is simply unsuitable for this type of beach, but there are not enough result to make a proper conclusion about this.

Spreading of the incoming wave signal has been mentioned several times in this chapter. It is also expected to be main reason for differences between the 1D and 2DH computations, and for the larger differences between the Non-hydrostatic and Surf-beat mode. This confirms the hypothesis of research sub-question 4:

Due to the alongshore uniformity assumption in 1D models, the LF wave growth will be stronger in 1D models than 2DH models. Therefore the difference between the Non-hydrostatic and Surf-beat modes will increase in a 2DH model as the LF contribution to the modeled swash decreases.

As the wave front is more dispersed, less energy can be transferred to the bound long wave. Both the 1D and 2DH model use this input, but the 1D model is limited by its lateral symmetric boundaries. Therefore, a spread wave signal in 1D can still lead to a more uniform wave crest, enhancing the transfer to the LF motions and thus overestimating them compared to the 2DH model. This can be seen in the results for both the Surf-beat and Non-hydrostatic model, but more severely for the Surf-beat mode: where the 1D results showed that the LF swash height was similar for both the Non-hydrostatic and Surf-beat mode, in 2DH the Surf-beat mode severely underestimates them. Combined with already a significant underestimation of HF motions in the swash, this leads to larger differences in the estimations of the run-up and its components between the two modes.

7

Discussion, Conclusions and Recommendations

This final chapter discusses the overall work done in this report, provides the final conclusion to the main research question, as well as some final recommendations.

7.1. Discussion

- An important question that can be asked is if the conclusions that are drawn, are valid for all type of intermediate beaches. Based on the results, it can be stated that this is not the case. Only one case has been studied, and this case showed that the results vary with the bathymetry/topography of the location and the offshore storm conditions. Both can vary for a random intermediate beach, which could lead to different conclusions.
- It has to be noted that all conclusions are based on model results:
  - The 1D model had a large range of results, but the 2DH model was limited to only 1 storm conditions. Therefore, no strong conclusions can be drawn based on the 2DH results, but they do provide a suggestion of what can be expected.
  - Since the focus lay on the hydrodynamics, the results were generated without a morphological update. In reality, the waves affect the bathymetry, and the bathymetry on its own affects the waves again.
  - The Non-hydrostatic model approaches reality the most, but it remains a model and can thus show some differences with reality.
- The analysis mainly focused on the swash zone. An overall cross shore analysis has not been executed. It could provide more insight in the alongshore variability in run-up, as well as into 2D effects such as edge waves and longshore currents
- Finally, it can be said that good approximation of the run-up is necessary for the design of coastal protection measures. This is the foundation of the main research question. However, having its components correct, such as mean and swash amplitude, is just as important, especially for the calculation of overtopping. A combination of a higher and lower amplitude could lead to the same maximum water level, but leads to a higher and more constant amount of overtopping, which is just as important for the design of coastal protection.

7.2. CONCLUSION

To answer the main research question

"Under what conditions can wave run-up be modeled sufficiently well for engineering purposes, by a 1D Surf-beat model of intermediate beaches"

the following can be said:

Firstly, the 2DH Non-hydrostatic model is assumed to be the closest to reality. Therefore, the fact that the 1D results show much higher values is an indication that a 1D models cannot be used for this system. The large differences arise as the two models handle significant spreading differently, thus affecting the low frequency wave generations. It is expected that a smaller spreading in the input signal will improve the estimations of the 1D model.

Secondly, differences are visible along the bathymetry, where the bar and beach face slope are the other governing factors for the amount of HF motions within the system. Using one 1D model for the whole system would neglect the longshore variability which proves to be important for this beach system. So even when less spreading is used in the offshore boundary, the whole system cannot be simplified to one 1D model. It will require multiple 1D models when the alongshore differences in incident and infragravity band swash are going to be regarded.

Lastly, the question involves the use of the Surf-beat model. In the 1D results, Surf-beat proved to be able to estimate the run-up in a 10% difference range in some cases. These cases showed an overall low frequency dominance, reducing the negative effect of the severe differences in high frequency motions. However, as mentioned before, the 2DH model showed much lower low frequency motions and actually a high frequency dominance. The estimation of the total wave height at the toe was still within the 10% range, but the individual high and low frequency components showed differences well outside of this range. In the swash-zone, the incident band swash is significantly underestimated as expected. However, in the 2DH Non-hydrostatic model, these motions proved to be important, hence limiting the estimation capabilities of the Surf-beat mode.

It has to be noted that these conclusions are based on the use of only one offshore storm condition in the 2DH model. It is expected that adjusting the spreading and using other conditions will affect the conclusions significantly. Finally, the effectiveness of the Surf-beat mode is based on its accuracy in estimating the Non-hydrostatic results. Although these are assumed to represent reality the best, both modes need data to validate any statements that have been made. However, based on the Non-hydrostatic results and the input conditions, it can be said that an intermediate beach with a rhythmic bar and beach state is a complex system, which proves to be difficult to simplify.

7.3. RECOMMENDATIONS

This section shows the final recommendations based on the 2DH results. These recommendations are regarded to be more important than the recommendations in section 5.2, as the 2DH model is assumed to approach reality better.

1. The first and foremost recommendation is to compute more storm conditions, with the emphasis on different degrees of spreading. It is expected that a smaller degree of spreading results in more LF generation. This on its own is expected to enhance the accuracy of the predictions of the Surf-beat mode compared to the Non-hydrostatic mode, and the 1D models compared to the 2DH model.
2. Using more alongshore output locations could enhance the validity of the statements in the 2DH chapter, as well as to give more insight in the alongshore variability of run-up.
3. Based on figure 6.3a, it can be seen that some of the energy occurs in the VLF energy band in the swash zone. It is recommended to investigate if this also occurs in reality, as the toe shows little to no VLF energy.
4. Both in the 2DH Surf-beat and Non-hydrostatic mode, the location CE2 showed an overall higher amount of incident energy in the swash spectra. It is recommended to investigate if this is due to the

sensitivity of the spectral analysis of the swash zone, or if there are other mechanisms causing this increased amount of incident band swash.

5. Overall, a further validation of the 2DH model is recommended, with a large variety in storm conditions and energy spreading before looking into the 1D model.

BIBLIOGRAPHY

[1] T. Hedges, *Coastal Zone Terminology,* (2009).

[2] L. D. Wright and A. D. Short, *Morphodynamic variability of surf zones and beaches: A synthesis,* Marine Geology **56**, 93 (1984).

[3] G. Masselink and J. A. Puleo, *Swash-zone morphodynamics,* Continental Shelf Research **26**, 661 (2006).

[4] P. Hawkes, T. Coates, and R. Jones, *Impact of bi-model seas on beaches and control structures,* (1998).

[5] M. Hughes, T. Aagaard, T. Baldock, and H. Power, *Wave runup (Swash) spectra on natural beaches: Morphodynamic controls,* Coasts and Ports 2013 , 412 (2013).

[6] D. Roelvink, A. van Dongeren, R. McCall, B. Hoonhout, A. van Rooijen, P. van Geer, L. de Vet, K. Nederhoff, and E. Quataert, *XBeach Technical Reference: Kingsday Release* (2015).

[7] H. F. Stockdon, R. A. Holman, P. A. Howd, and A. H. Sallenger, *Empirical parameterization of setup, swash, and runup,* Coastal Engineering **53**, 573 (2006).

[8] L. Holthuijsen, N. Booij, and T. Herbers, *A prediction model for stationary, short-crested waves in shallow water with ambient currents,* Coastal Engineering **13**, 23 (1989).

[9] T. Baldock, P. Holmes, and D. Horn, *Low frequency swash motion induced by wave grouping,* Coastal Engineering **32**, 197 (1997).

[10] M. Brocchini and T. E. Baldock, *Recent advances in modeling swash zone dynamics: Influence of surf-swash interaction on nearshore hydrodynamics and morphodynamics,* Reviews of Geophysics **46**, 1 (2008).

[11] G. Masselink, B. J. Hegge, and C. B. Pattiaratchi, *Beach cusp morphodynamics,* Earth Surface Processes and Landforms **22**, 1139 (1997).

[12] C. Swinkels, J. Friedman, W. D. Boer, R. Mccall, and B. Huisman, *CoMIDAS - East Coast Case*, Tech. Rep. (Deltares, 2016).

[13] H. F. Stockdon, D. M. Thompson, N. G. Plant, and J. W. Long, *Evaluation of wave runup predictions from numerical and parametric models,* Coastal Engineering **92**, 1 (2014).

[14] R. M. Guedes, K. R. Bryan, and G. Coco, *Observations of alongshore variability of swash motions on an intermediate beach,* Continental Shelf Research **48**, 61 (2012).

[15] VLIZ, *Swash zone,* (2013).

[16] USACE, *Coastal Engineering Manual,* **1100** (2003).

[17] *Waves in Oceanic and Coastal Waters* (Cambridge University Press, 2007).

[18] W. Munk, *Surf beats,* EOS, Transactions American Geophysical Union **30**, 849 (1949).

[19] M. S. Longuet-Higgins and R. Stewart, *Radiation stresses in water waves; a physical discussion, with applications,* in *Deep Sea Research and Oceanographic Abstracts*, Vol. 11 (Elsevier, 1964) pp. 529–562.

[20] G. Symonds, D. A. Huntley, and A. J. Bowen, *Two-dimensional surf beat: Long wave generation by a time-varying breakpoint,* Journal of Geophysical Research: Oceans **87**, 492 (1982).

[21] J. A. Battjes, *Shoaling of subharmonic gravity waves,* Journal of Geophysical Research **109**, 1 (2004).

[22] A. Van Dongeren, J. Battjes, T. Janssen, J. Van Noorloos, K. Steenhauer, G. Steenbergen, and A. Reniers, *Shoaling and shoreline dissipation of low-frequency waves,* Journal of Geophysical Research: Oceans **112** (2007).

[23] J. Battjes, *Surf similarity,* Coastal Engineering **1**, 466 (1974).

[24] L. Erikson, M. Larson, and H. Hanson, *Prediction of swash motion and run-up including the effects of swash interaction,* Coastal Engineering **52**, 285 (2005).

[25] J. W. van der Meer, *Wave Run-up and Wave Overtopping at Dikes*, Tech. Rep. (Technical Advisory Committee on Flood Defence, 2002).

[26] I. A. Hunt, *Design of seawalls and breakwaters* (U.S. Lake Survey, 1958).

[27] M. I. Vousdoukas, D. Wziatek, and L. P. Almeida, *Coastal vulnerability assessment based on video wave run-up observations at a mesotidal, steep-sloped beach,* Ocean Dynamics **62**, 123 (2012).

[28] T. E. Baldock and P. Holmes, *Simulation and prediction of swash oscillations on a steep beach,* Coastal Engineering **36**, 219 (1999).

[29] M. P. Bradshaw, *Topographic control of run-up variability,* Coastal Engineering Proceedings **1** (1980).

[30] R. A. Holman and A. Sallenger, *Setup and swash on a natural beach,* Journal of Geophysical Research: Oceans **90**, 945 (1985).

[31] D. Roelvink, A. Reniers, A. van Dongeren, J. van Thiel de Vries, R. McCall, and J. Lescinski, *Modelling storm impacts on beaches, dunes and barrier islands,* Coastal Engineering (2009), 10.1016/j.coastaleng.2009.08.006.

[32] C. Daly, D. Roelvink, A. van Dongeren, J. v. T. de Vries, and R. McCall, *Short wave breaking effects on low frequency waves,* Coastal Engineering Proceedings **1**, 20 (2010).

[33] J. A. Roelvink, A. Dastgheib, T. Spencer, I. Moller, E. Christie, M. Berenguer, D. Sempere, J. W. van der Meer, M. Seyyedabdolhossein, K. Nederhoff, and W. Vermin, *Resilience-Increasing Strategies for Coasts - Toolkit - Improvement of physical processes XBeach improvement & validation; wave dissipation over vegetated marshes and flash flood module*, Tech. Rep. (Deltares, UNESCO-IHE, UCAM, UPC-CRAHI,SURFSARA, 2015).

[34] G. Stelling and M. Zijlema, *An accurate and efficient finite-difference algorithm for non-hydrostatic free-surface flow with application to wave propagation,* International Journal for Numerical Methods in Fluids **43**, 1 (2003).

[35] R. McCall, G. Masselink, T. Poate, J. Roelvink, L. Almeida, M. Davidson, and P. Russell, *Modelling storm hydrodynamics on gravel beaches with xbeach-g,* Coastal Engineering **91**, 231 (2014).

[36] M. A. de Schipper, A. Reniers, J. MacMahan, and R. Ranasinghe, *Vortical vlf motions under shore-normal incident waves,* Coastal Engineering Proceedings **1**, 58 (2012).

[37] J. A. Roelvink and M. J. F. Stive, *Bar-generating cross-shore flow mechanisms on a beach,* Journal of Geophysical Research: Oceans **94**, 4785 (1989).

[38] R. T. Guza, E. B. Thornton, and R. A. Holman, *Swash on steep and shallow beaches,* Coastal Engineering , 708 (1984).

[39] K. Hasselmann, T. P. Barnett, E. Bouws, H. Carlson, D. E. Cartwright, K. Enke, J. A. Ewing, H. Gienapp, D. E. Hasselmann, P. Kruseman, A. Meerburg, P. Muller, D. J. Olbers, K. Richter, W. Sell, and H. Walden, *Measurements of Wind-Wave Growth and Swell Decay during the Joint North Sea Wave Project (JONSWAP),* Ergnzungsheft zur Deutschen Hydrographischen Zeitschrift Reihe **A(8)**, p.95 (1973).

[40] Y. Ciriano, G. Coco, K. Bryan, and S. Elgar, *Field observations of swash zone infragravity motions and beach cusp evolution,* Journal of Geophysical Research: Oceans **110** (2005).

[41] J. A. Puleo, *Hydrodynamics and Sediment Transport in the Inner Surf and*, Ph.D. thesis, University of Florida (2004).

[42] G. Masselink and M. Hughes, *Field Investigation of sediment transport in the swash zone,* Continental Shelf Research **18**, 1179 (1998).

A

1D RESULTS

This chapter consists of hydrodynamic results, obtained by the spectral analysis. Firstly, relative contributions to the total run-up by the mean run-up and the swash height amplitude are shown in figure A.1. Next, the Non-hydrostatic reflection results can be found in figure A.2. Hereafter, the Surf-beat results can be found in section A.1. It is split up into three parts, reflecting the three different breaker parameters used in this mode.

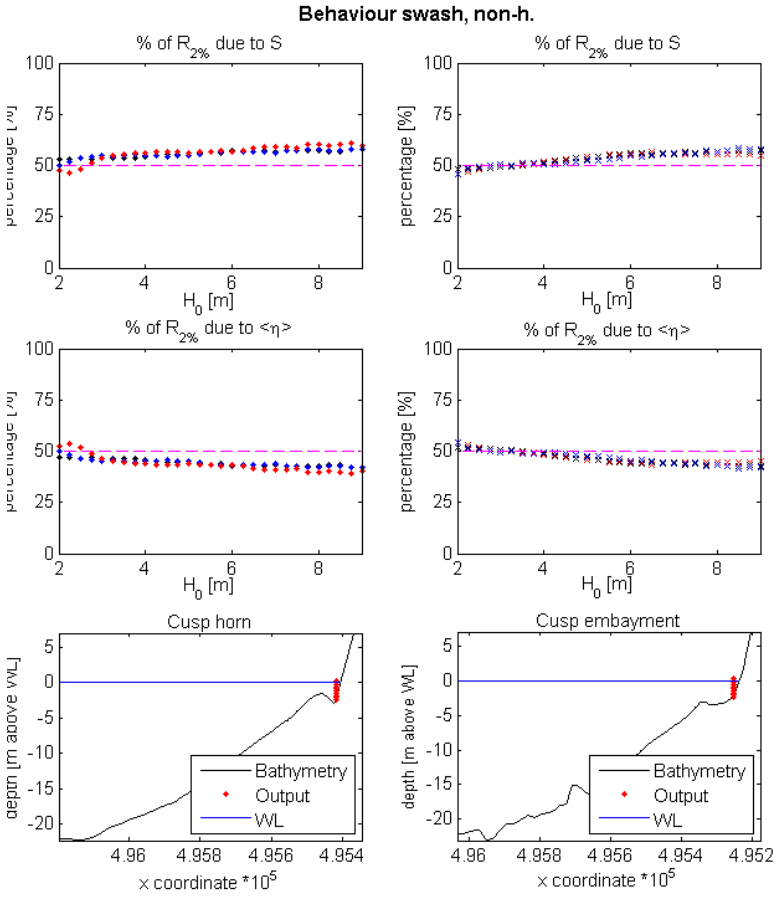

Figure A.1: respective contribution by $<\eta>$ and S to $R_{2\%}$, against H_0. Black markers for $s_0 = 0.01$, red markers for $s_0 = 0.02$ and blue markers for $s_0 = 0.04$, $\cdot = CH$, $\times = CE$

When figure A.1 is compared to the emperical formula (2.6) of Stockdon *et al.* [7], the ratio of contribution

could have been expected. In figure A.1, the maximum ratios of contribution (contribution S : contribution $< \eta >$) of are 42:58% (CH) and 45:55% (CE). By inserting the beach face slope in formula 2.6, a ratio of 44:56% (CH) and 46:54% (CE) is obtained. This shows that the relative contribution by the mean is higher for a more reflective beach slope. A difference between the results of this report and the formula comes to light as the swash amplitude energy is regarded, and its LF and HF components (figure 4.7a). Based on the energy, the formula expects an HF to LF swash energy ratio (% $\frac{E_{hf}}{E_{tot}}$:$\frac{E_{lf}}{E_{tot}}$) of 70:30 (CH) and 82:18 (CE) for all storm conditions. This means that she expects almost negligible LF motions. From figure 4.6, it is clearly visible that this ratio is different and changing with increasing storm conditions.

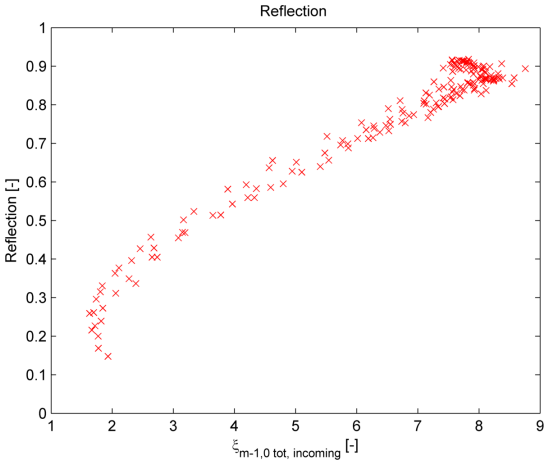

(a) Total wave reflection

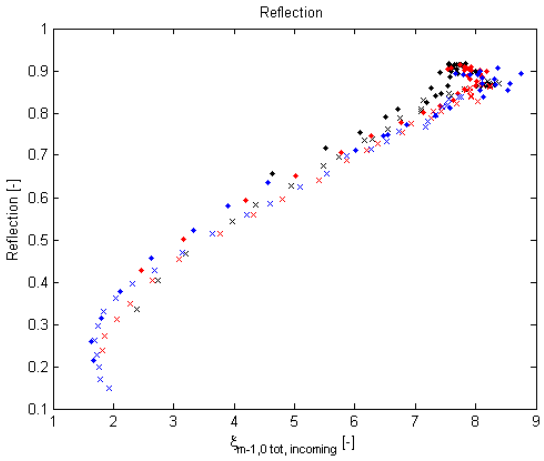

(b) Total wave reflection, colours represent the different s_0, $\cdot = CH$, $\times = CE$

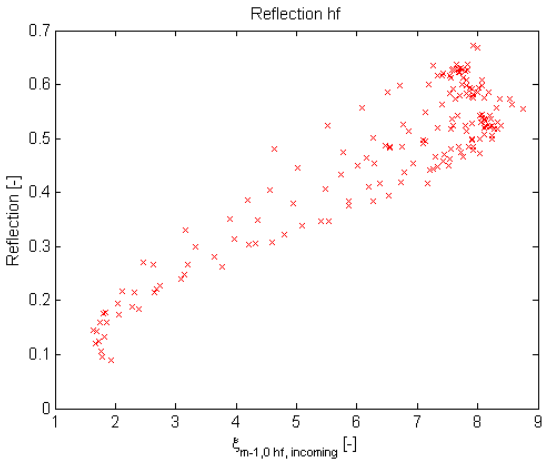

(c) Hf wave reflection

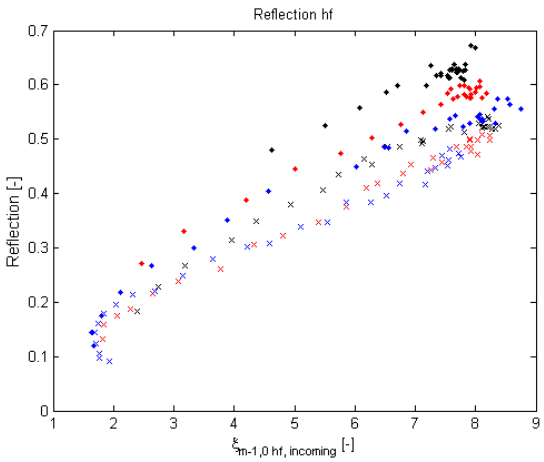

(d) Hf wave reflection, colours represent the different s_0, $\cdot = CH$, $\times = CE$

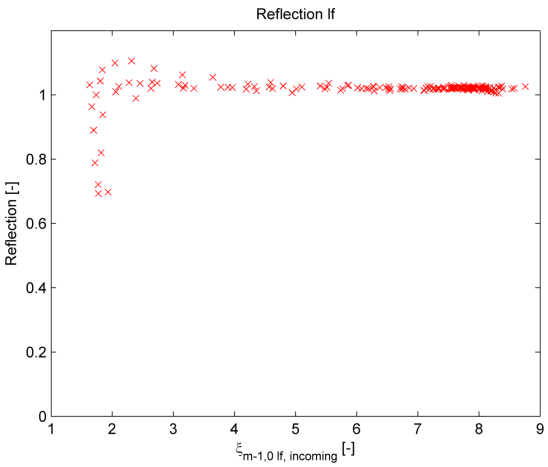

(e) Lf wave reflection

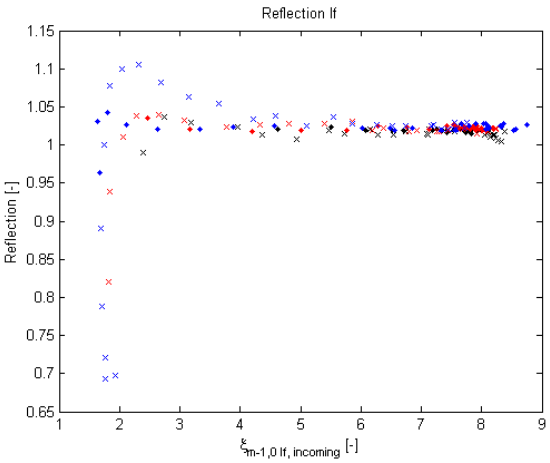

(f) Lf wave reflection, colours represent the different s_0, $\cdot = CH$, $\times = CE$

Figure A.2: Reflection graphs for the total, hf and lf motions

A.1. SURF-BEAT 1D RESULTS

Since 3 different breaker formulations have been used, this section is divided in 3 subsections, according to the breaker formulations. All subsections will provide some general remarks of the figures.

A.1.1. SURF-BEAT DEFAULT

AT THE TOE

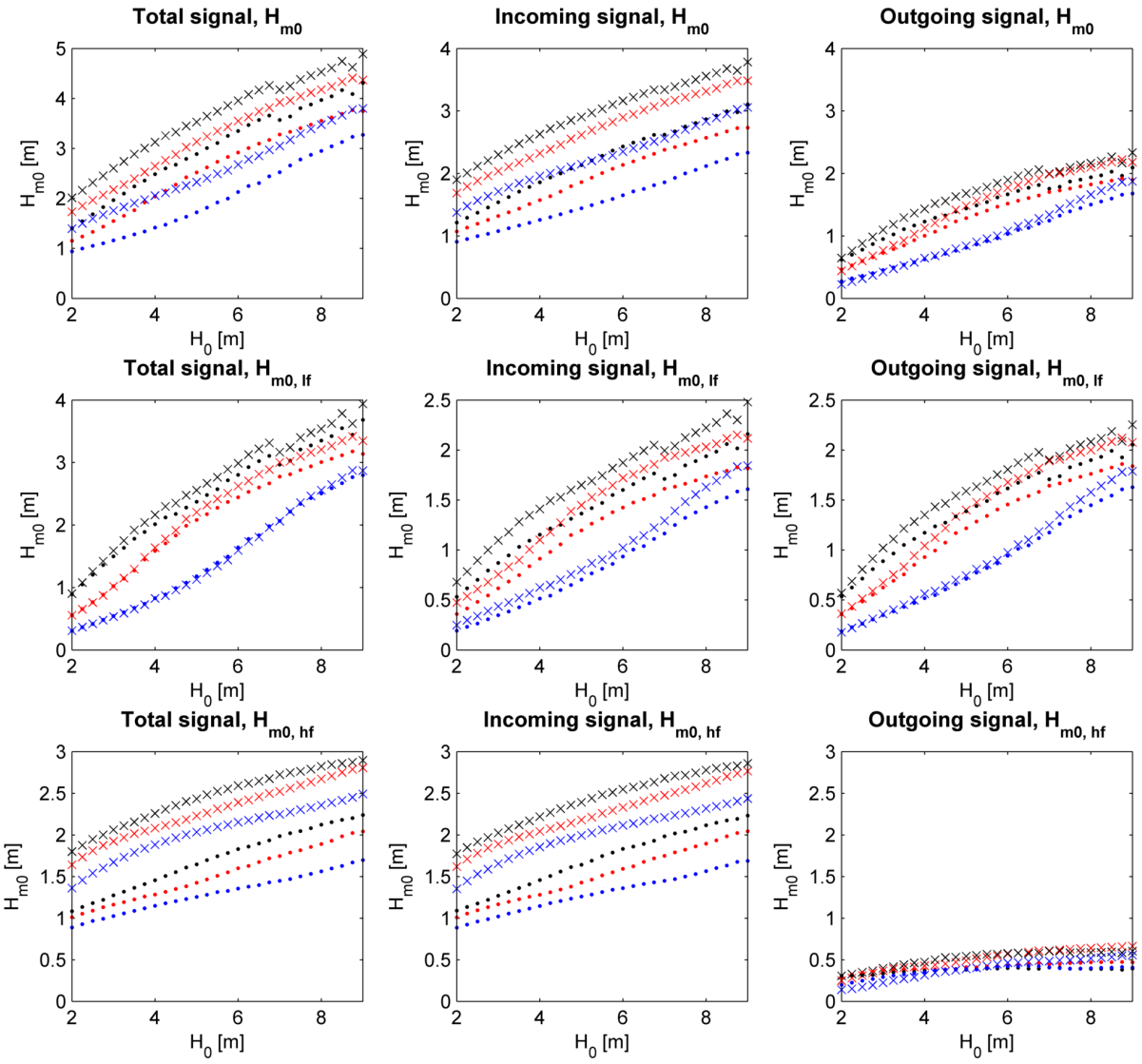

Figure A.3: Wave heights at the toe, Surf.def. Black markers for $s_0 = 0.01$, red markers for $s_0 = 0.02$ and blue markers for $s_0 = 0.04$, $\cdot = CH$, $\times = CE$.

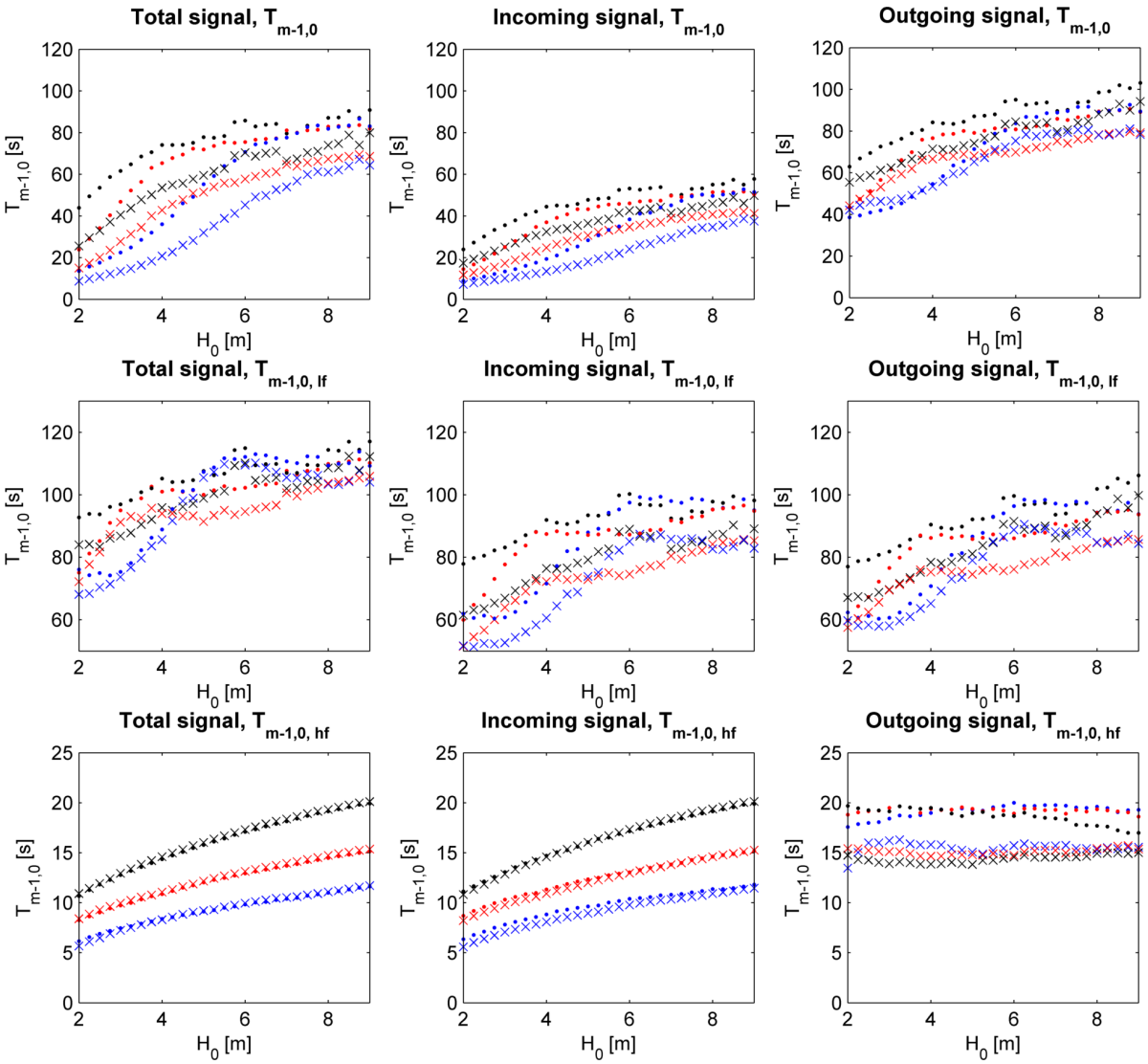

Figure A.4: Mean energy wave periods at the toe, Surf.def. Black markers for $s_0 = 0.01$, red markers for $s_0 = 0.02$ and blue markers for $s_0 = 0.04$. Solid line for incoming signal, dashed line for outgoing signal

IN THE SWASH ZONE

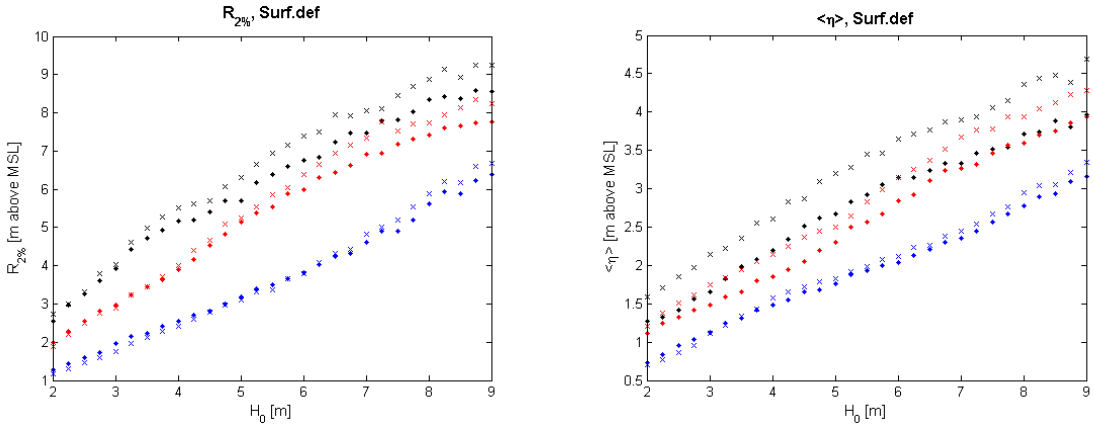

(a) $R_{2\%}$ against H_0, Surf-beat default (b) $<\eta>$ against H_0, Surf-beat default

Figure A.5: $R_{2\%}$ and $<\eta>$ against H_0, Surf-beat default. Black markers for $s_0 = 0.01$, red markers for $s_0 = 0.02$ and blue markers for $s_0 = 0.04$, $\cdot = CH$, $\times = CE$

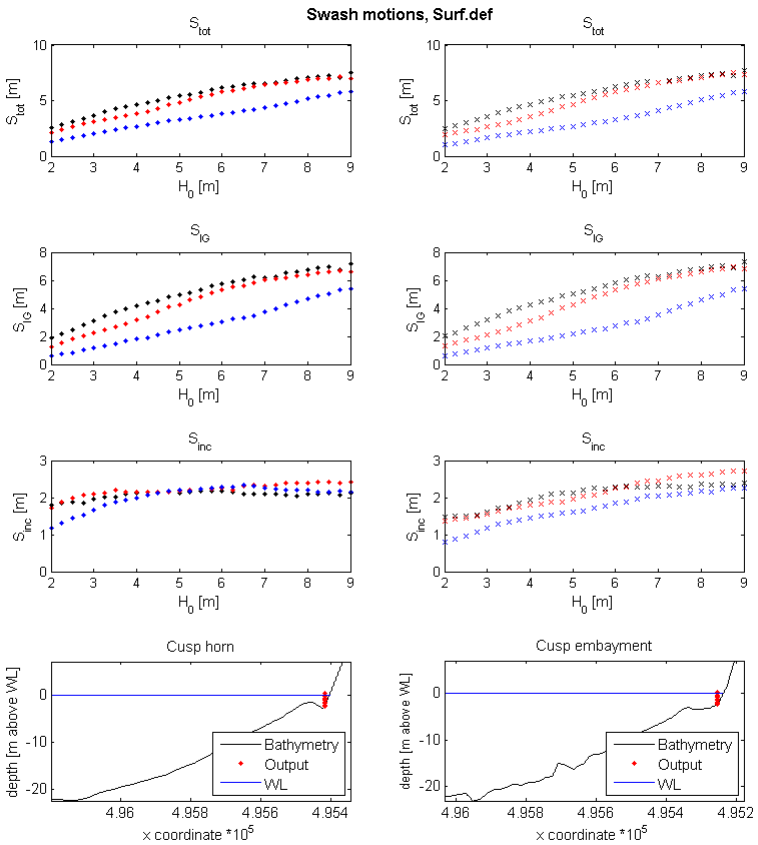

Figure A.6: S and its components S_{inc} and S_{IG}, against H_0, Surf-beat default. Black markers for $s_0 = 0.01$, red markers for $s_0 = 0.02$ and blue markers for $s_0 = 0.04$, $\cdot = CH$, $\times = CE$

A.1.2. SURF-BEAT R.D.

AT THE TOE

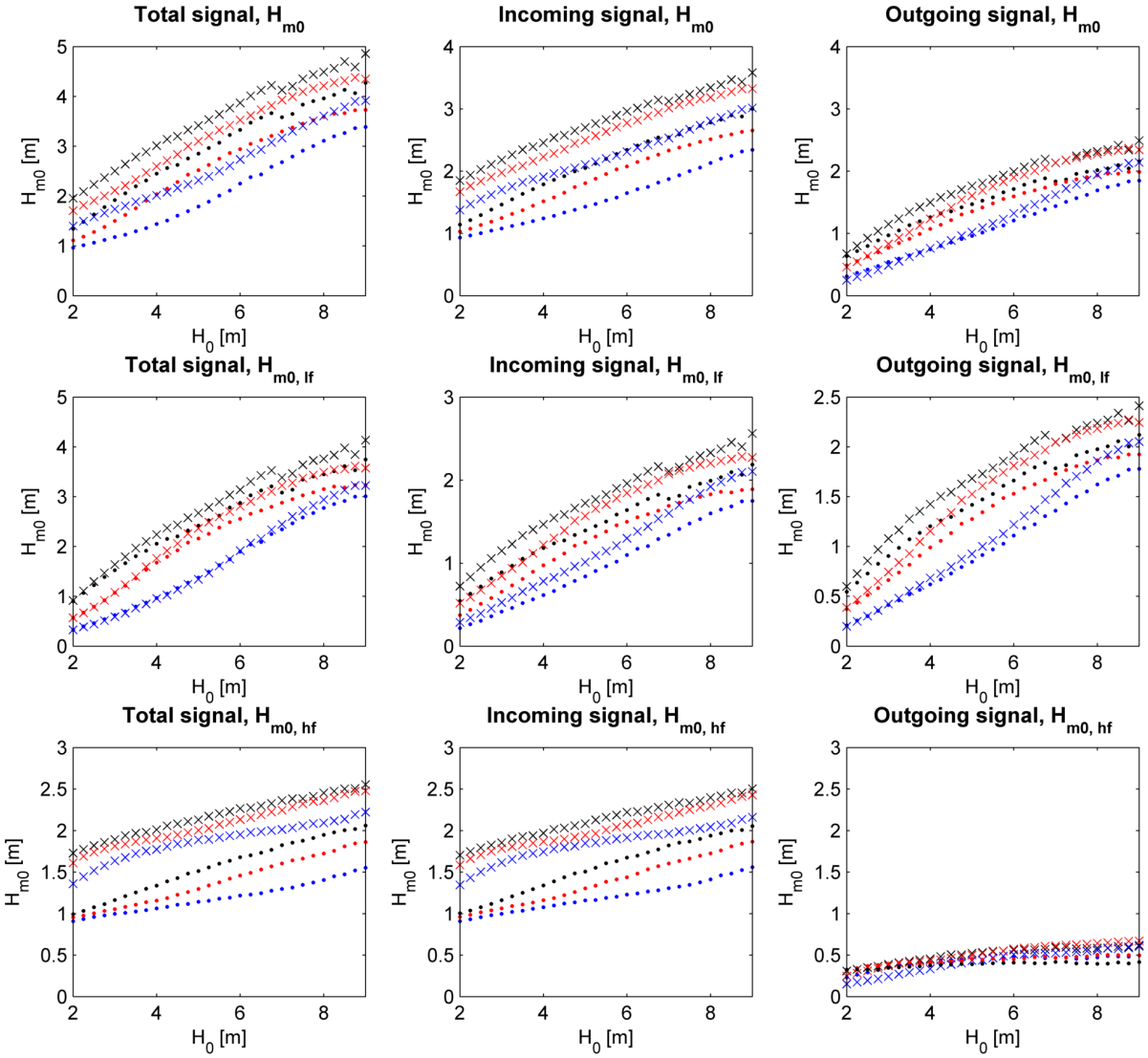

Figure A.7: Wave heights at the toe, Surf.rd. Black markers for $s_0 = 0.01$, red markers for $s_0 = 0.02$ and blue markers for $s_0 = 0.04$, $\cdot = CH$, $\times = CE$.

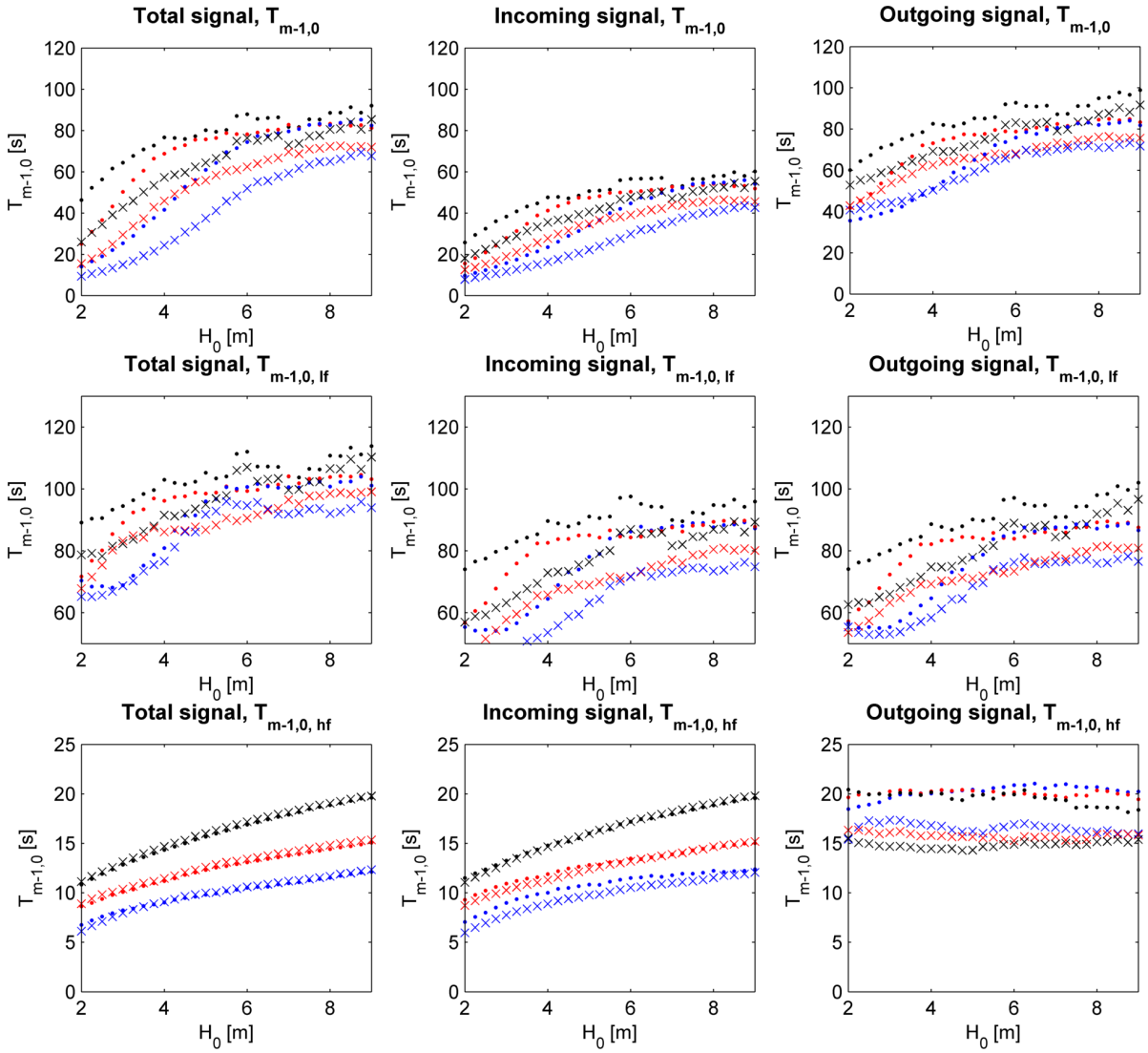

Figure A.8: Mean energy wave periods at the toe, Surf.rd. Black markers for $s_0 = 0.01$, red markers for $s_0 = 0.02$ and blue markers for $s_0 = 0.04$. Solid line for incoming signal, dashed line for outgoing signal

IN THE SWASH ZONE

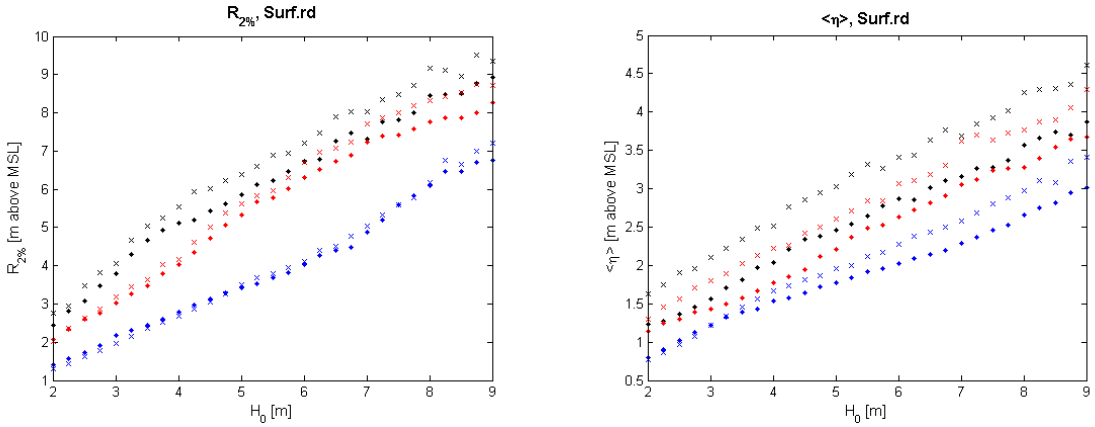

(a) $R_{2\%}$ against H_0, Surf-beat Roelvink-Daly

(b) $< \eta >$ against H_0, Surf-beat Roelvink-Daly

Figure A.9: $R_{2\%}$ and $< \eta >$ against H_0, Surf-beat Roelvink-Daly. Black markers for $s_0 = 0.01$, red markers for $s_0 = 0.02$ and blue markers for $s_0 = 0.04$, $\cdot = CH$, $\times = CE$

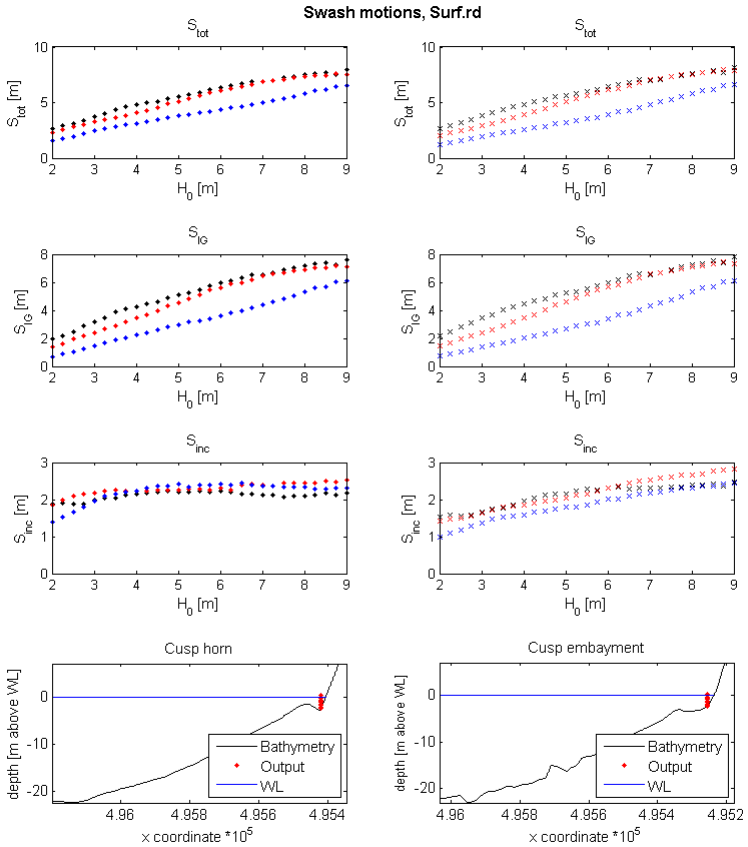

Figure A.10: S and its components S_{inc} and S_{IG}, against H_0, Surf-beat Roelvink-Daly. Black markers for $s_0 = 0.01$, red markers for $s_0 = 0.02$ and blue markers for $s_0 = 0.04$, $\cdot = CH$, $\times = CE$

A.1.3. SURF-BEAT R.D. ADAPTED

AT THE TOE

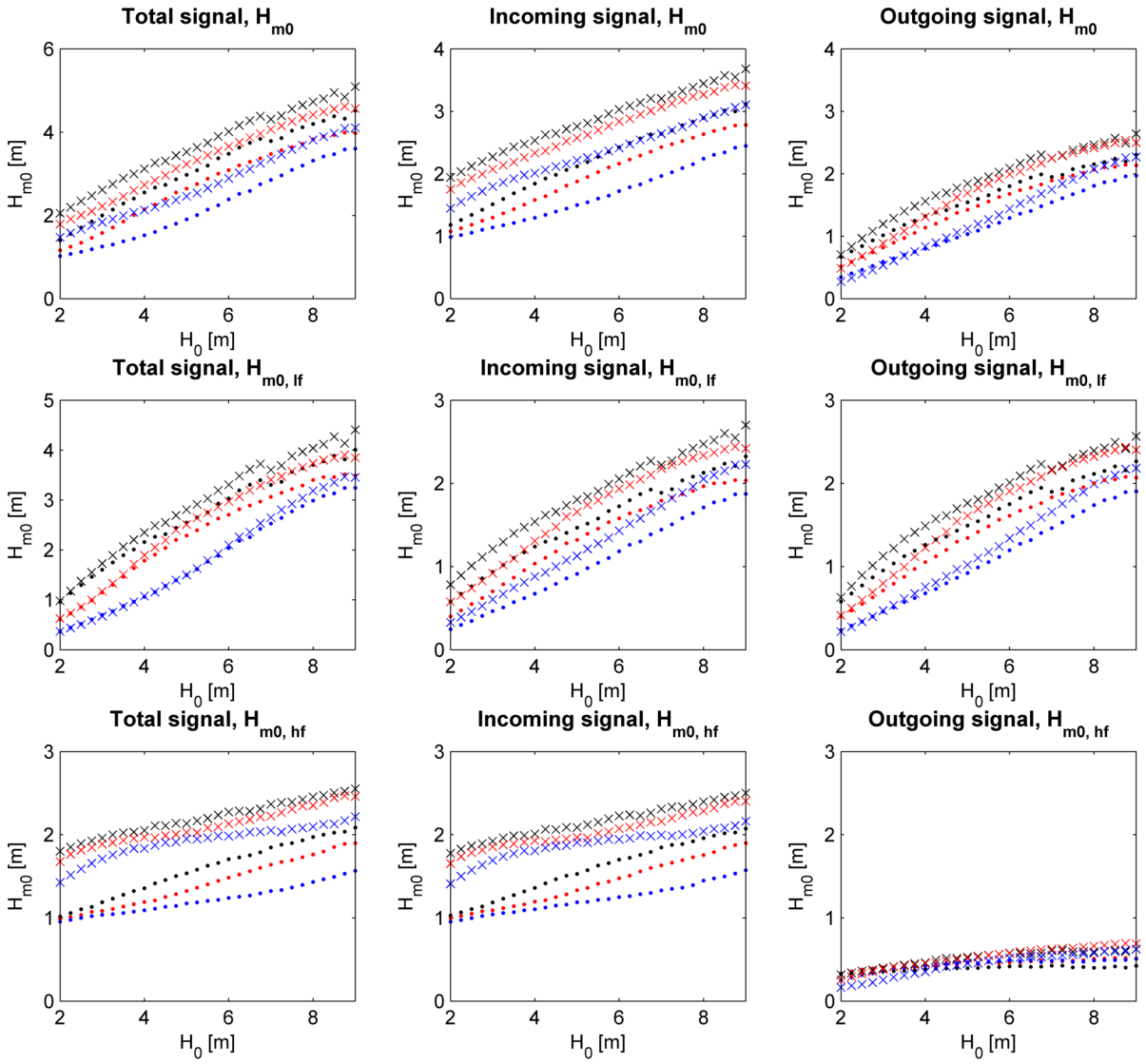

Figure A.11: Wave heights at the toe, Surf.rd. Black markers for $s_0 = 0.01$, red markers for $s_0 = 0.02$ and blue markers for $s_0 = 0.04$, $\cdot = CH$, $\times = CE$.

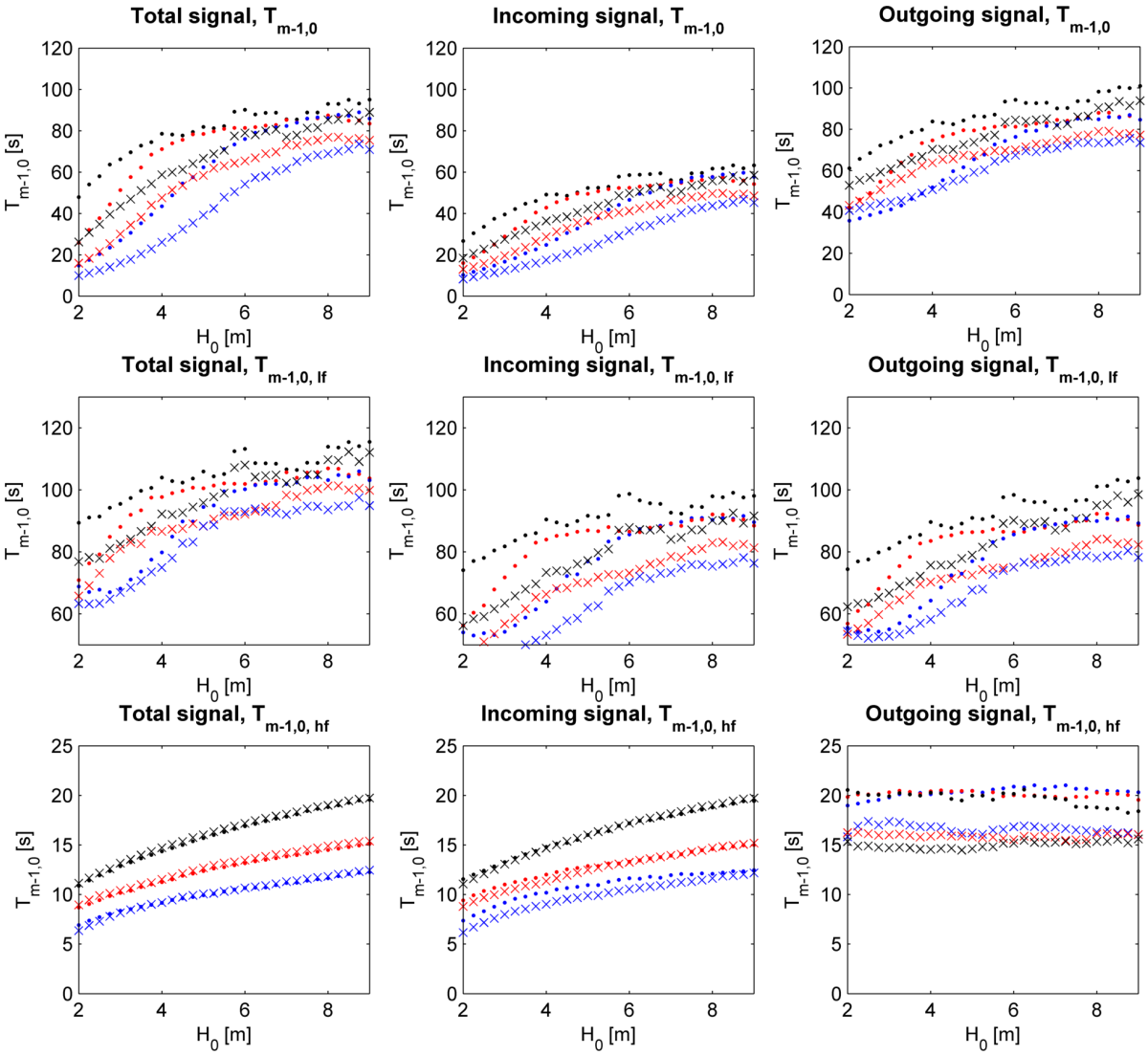

Figure A.12: Mean energy wave periods at the toe, Surf.rd. Black markers for $s_0 = 0.01$, red markers for $s_0 = 0.02$ and blue markers for $s_0 = 0.04$. Solid line for incoming signal, dashed line for outgoing signal

IN THE SWASH ZONE

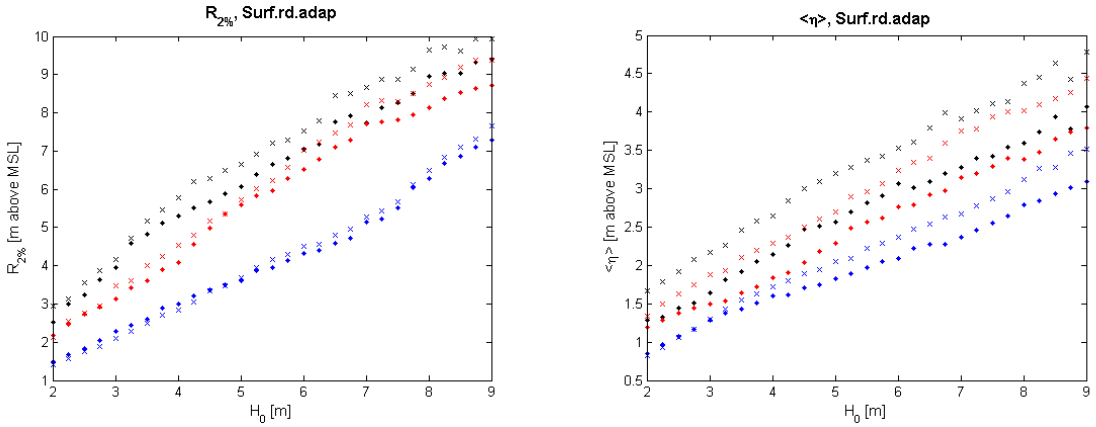

(a) $R_{2\%}$ against H_0, Surf-beat Roelvink-Daly (adapted) (b) $< \eta >$ against H_0, Surf-beat Roelvink-Daly (adapted)

Figure A.13: $R_{2\%}$ and $< \eta >$ against H_0, Surf-beat Roelvink-Daly (adapted). Black markers for $s_0 = 0.01$, red markers for $s_0 = 0.02$ and blue markers for $s_0 = 0.04$, $\cdot = CH$, $\times = CE$

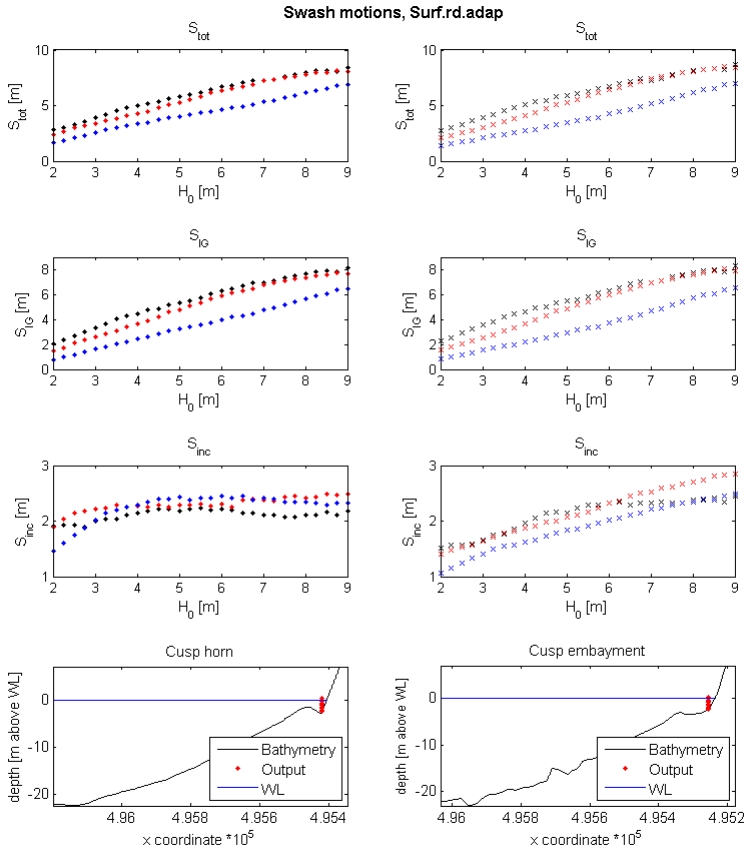

Figure A.14: S and its components S_{inc} and S_{IG}, against H_0, Surf-beat Roelvink-Daly (adapted). Black markers for $s_0 = 0.01$, red markers for $s_0 = 0.02$ and blue markers for $s_0 = 0.04$, $\cdot = CH$, $\times = CE$

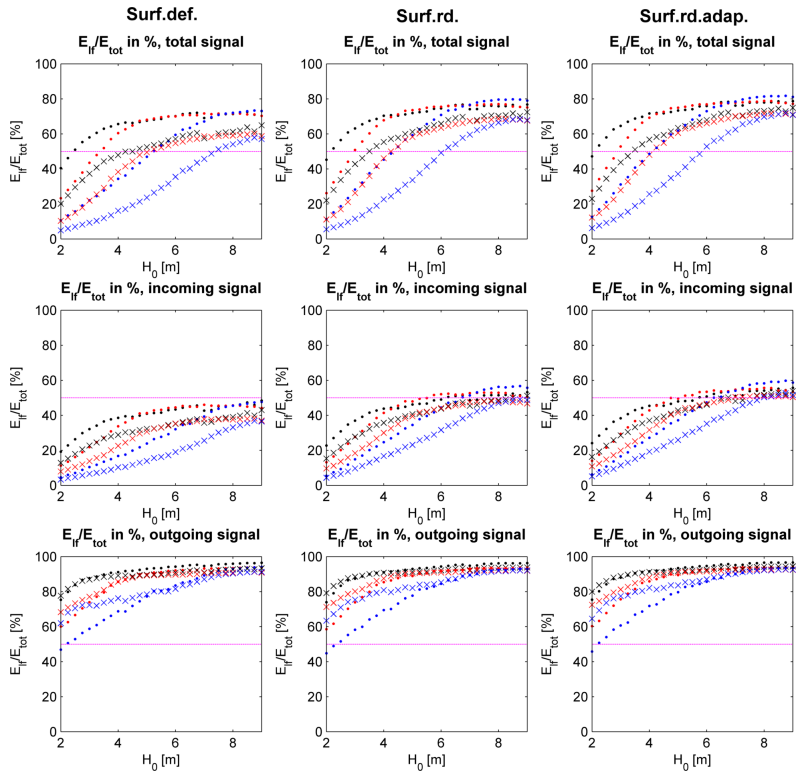

Figure A.15: Behaviour comparison at the toe of all breaker formulations. Left column: Surf-beat, default breaker formulation. Middle column: Surf-beat, Roelvink-Daly (default) formulation. Right column: Surf-beat, Roelvink-Daly, adapted formulation. Top row: total wave signal. Middle row: incoming wave signal. Bottom row: outgoing wave signal. Black markers for $s_0 = 0.01$, red markers for $s_0 = 0.02$ and blue markers for $s_0 = 0.04$, $\cdot = CH$, $\times = CE$

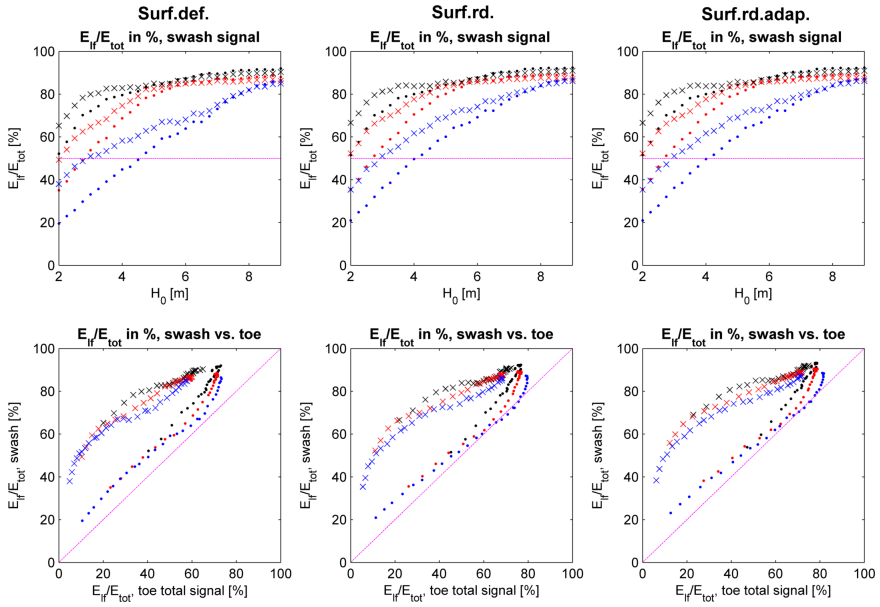

Figure A.16: Behaviour comparison of the swash zone of all breaker formulations. Left column: Surf-beat, default breaker formulation. Middle column: Surf-beat, Roelvink-Daly (default) formulation. Right column: Surf-beat, Roelvink-Daly, adapted formulation. Top row: swash behaviour. Bottom row: swash behaviour against behaviour at the toe. Black markers for $s_0 = 0.01$, red markers for $s_0 = 0.02$ and blue markers for $s_0 = 0.04$, $\cdot = CH$, $\times = CE$

A.2. SURF-BEAT VS. NON-HYDROSTATIC

A.2.1. SURF-BEAT, ROELVINK-DALY

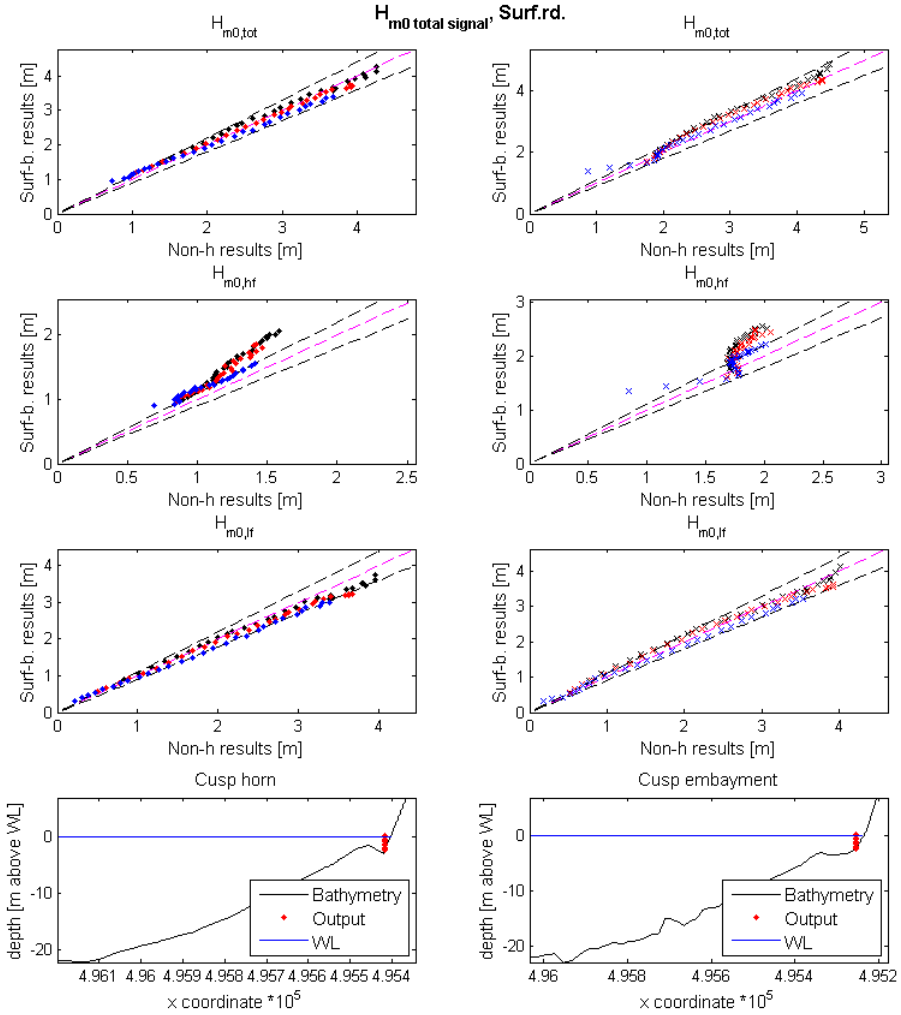

Figure A.17: Surf-beat and Non-hydrostatic scatterplots of the total wave signal at the toe. The black dashed lines (- -) represent a 10% difference between the two modes. The magenta dashed line (- -) represents a 0% difference. Black markers for $s_0 = 0.01$, red markers for $s_0 = 0.02$ and blue markers for $s_0 = 0.04$, $\cdot = CH$, $\times = CE$

Table A.1: RMSE of total wave signal, Surf.rd.

	CH				**CE**			
Total signal	**All**	$s_0 = 1\%$	$s_0 = 2\%$	$s_0 = 4\%$	**All**	$s_0 = 1\%$	$s_0 = 2\%$	$s_0 = 4\%$
$H_{m0,tot}$	**0,123**	0,062	0,059	0,089	**0,196**	0,151	0,096	0,080
$H_{m0,lf}$	**0,191**	0,101	0,114	0,115	**0,141**	0,075	0,088	0,081
$H_{m0,hf}$	**0,258**	0,196	0,144	0,086	**0,325**	0,241	0,185	0,116

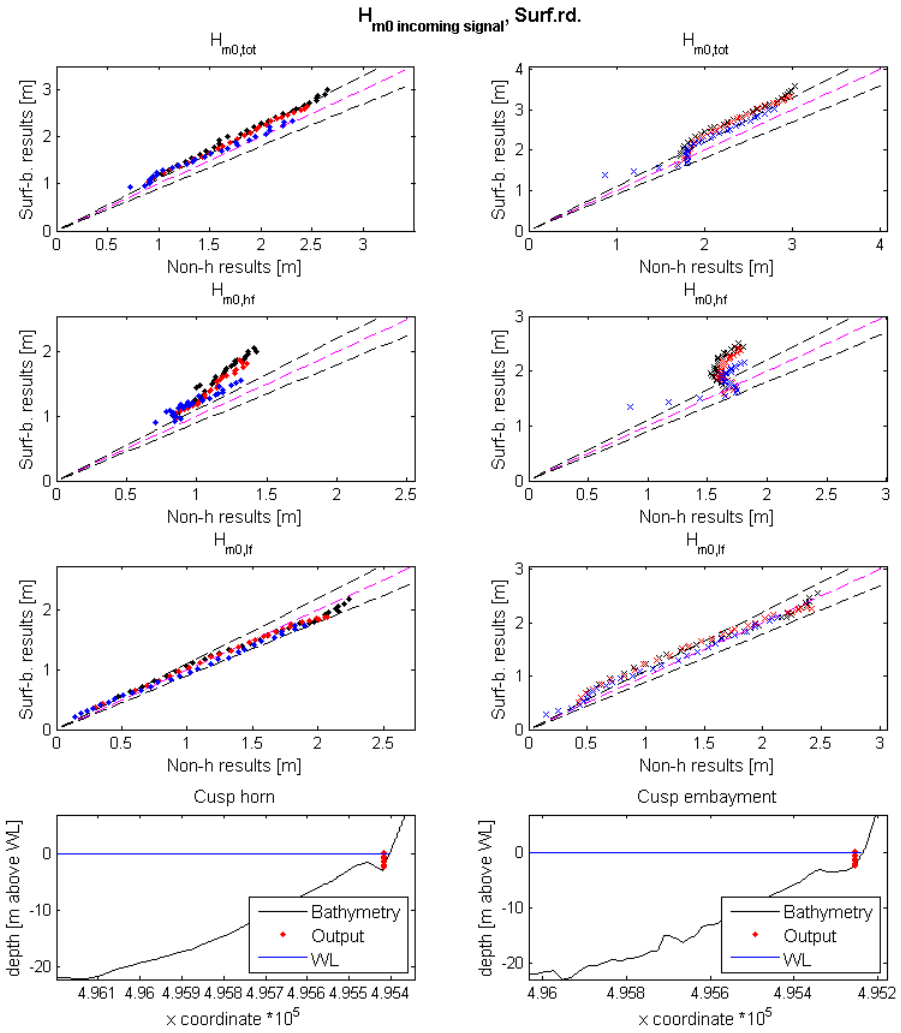

Figure A.18: Surf-beat and Non-hydrostatic scatterplots of the incoming wave signal at the toe. The black dashed lines (- -) represent a 10% difference between the two modes. The magenta dashed line (- -) represents a 0% difference. Black markers for $s_0 = 0.01$, red markers for $s_0 = 0.02$ and blue markers for $s_0 = 0.04$, $\cdot = CH$, $\times = CE$

Table A.2: RMSE of incoming wave signal, Surf.rd.

	CH				**CE**			
Incoming signal	**All**	$s_0 = 1\%$	$s_0 = 2\%$	$s_0 = 4\%$	**All**	$s_0 = 1\%$	$s_0 = 2\%$	$s_0 = 4\%$
$H_{m0,tot}$	**0,203**	0,149	0,108	0,084	**0,331**	0,234	0,192	0,133
$H_{m0,lf}$	**0,082**	0,049	0,044	0,048	**0,131**	0,081	0,087	0,056
$H_{m0,hf}$	**0,347**	0,261	0,189	0,129	**0,423**	0,312	0,241	0,153

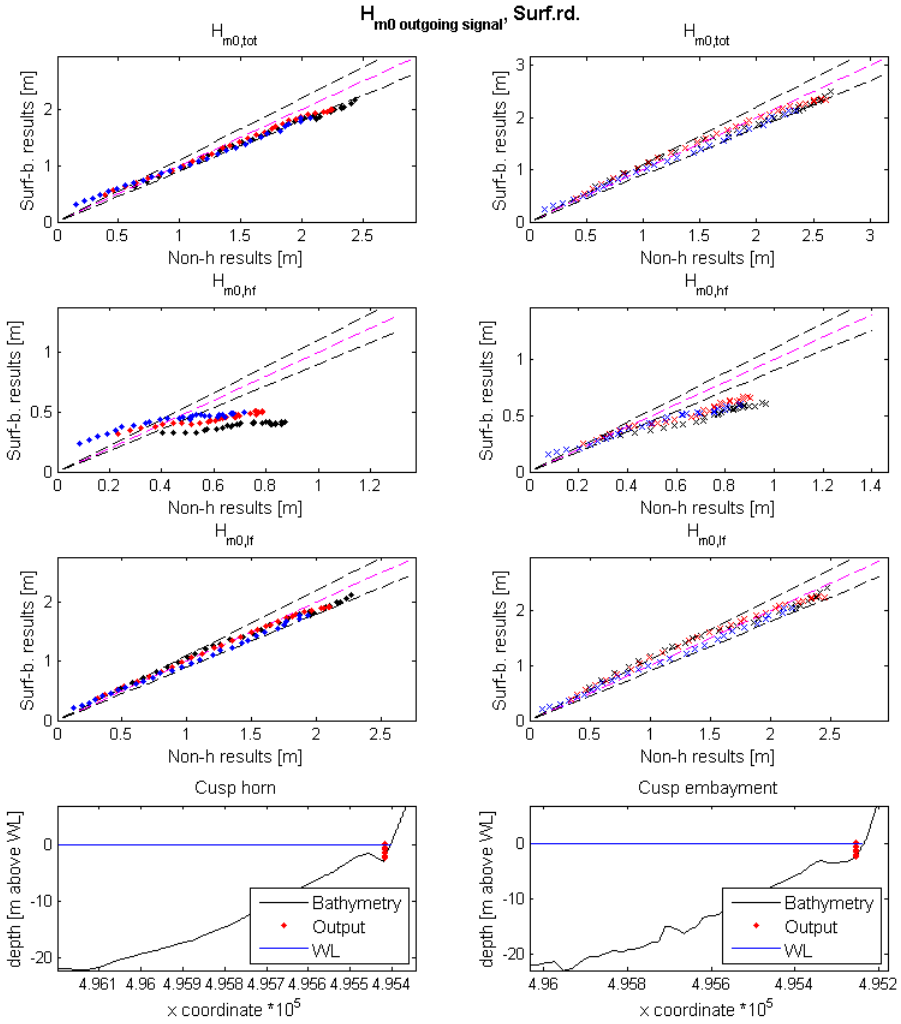

Figure A.19: Surf-beat and Non-hydrostatic scatterplots of the outgoing wave signal at the toe. The black dashed lines (- -) represent a 10% difference between the two modes. The magenta dashed line (- -) represents a 0% difference. Black markers for $s_0 = 0.01$, red markers for $s_0 = 0.02$ and blue markers for $s_0 = 0.04$, $\cdot = CH$, $\times = CE$

Table A.3: RMSE of outgoing wave signal, Surf.rd.

	CH				**CE**			
Outgoing signal	**All**	$s_0 = 1\%$	$s_0 = 2\%$	$s_0 = 4\%$	**All**	$s_0 = 1\%$	$s_0 = 2\%$	$s_0 = 4\%$
$H_{m0,tot}$	**0,145**	0,104	0,068	0,074	**0,124**	0,087	0,060	0,064
$H_{m0,lf}$	**0,089**	0,060	0,041	0,051	**0,101**	0,071	0,059	0,042
$H_{m0,hf}$	**0,233**	0,192	0,111	0,071	**0,191**	0,147	0,092	0,081

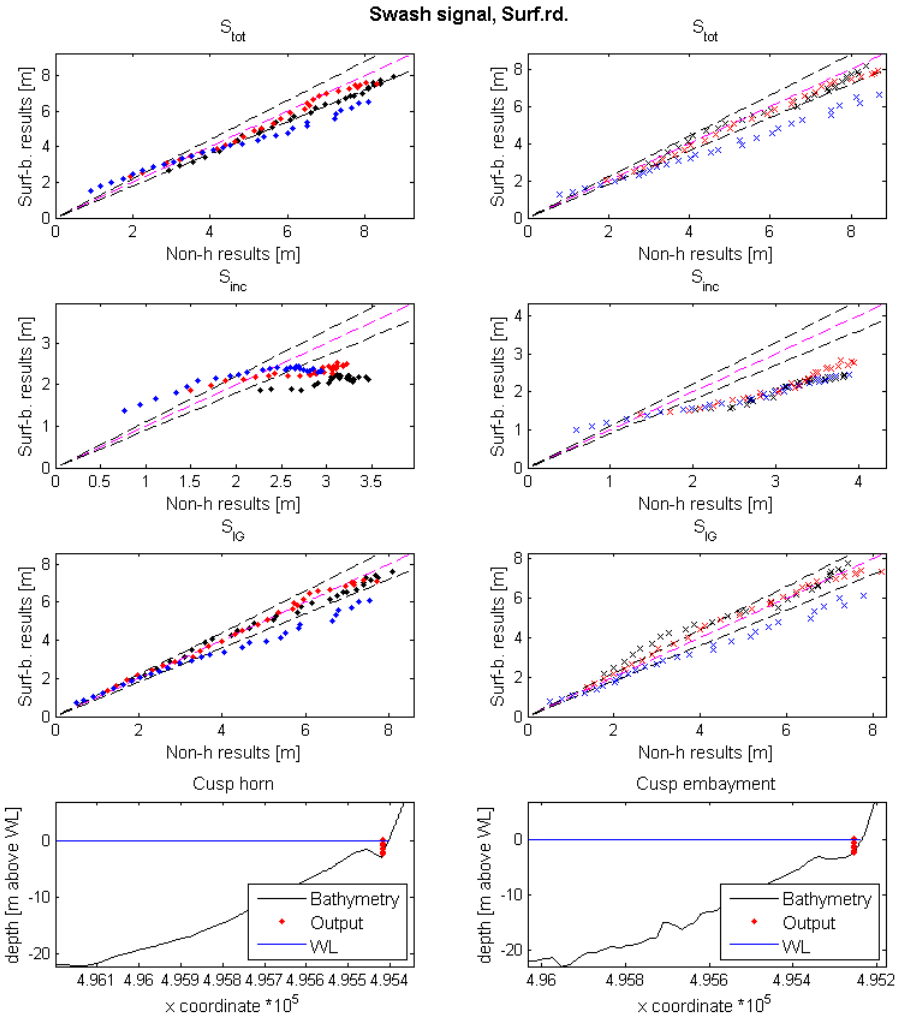

Figure A.20: Surf-beat and Non-hydrostatic scatterplots of the swash height amplitude in the swash zone. The black dashed lines (- -) represent a 10% difference between the two modes. The magenta dashed line (- -) represents a 0% difference. Black markers for $s_0 = 0.01$, red markers for $s_0 = 0.02$ and blue markers for $s_0 = 0.04$, $\cdot = CH$, $\times = CE$

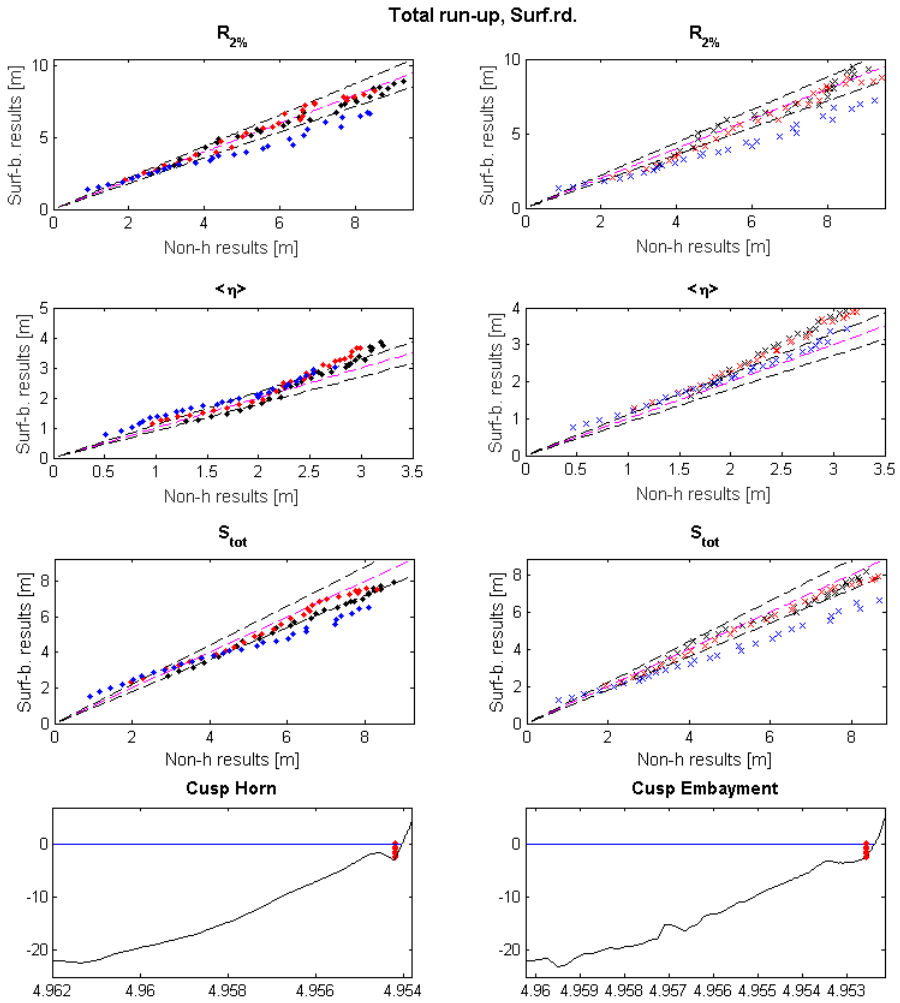

Figure A.21: Surf-beat and Non-hydrostatic scatterplots of the run-up and its components. The black dashed lines (- -) represent a 10% difference between the two modes. The magenta dashed line (- -) represents a 0% difference. Black markers for $s_0 = 0.01$, red markers for $s_0 = 0.02$ and blue markers for $s_0 = 0.04$, $\cdot = CH$, $\times = CE$

Table A.4: RMSE of run-up parameters, Surf.rd

	CH				**CE**			
Run-up signal	**All**	$s_0 = 1\%$	$s_0 = 2\%$	$s_0 = 4\%$	**All**	$s_0 = 1\%$	$s_0 = 2\%$	$s_0 = 4\%$
$R_{2\%}$	**0,636**	0,195	0,151	0,586	**0,864**	0,243	0,241	0,794
$<\eta>$	**0,299**	0,173	0,194	0,148	**0,491**	0,385	0,285	0,106
S	**0,662**	0,356	0,177	0,529	**0,742**	0,200	0,242	0,672
S_{IG}	**0,527**	0,174	0,110	0,486	**0,586**	0,279	0,178	0,484
S_{inc}	**0,705**	0,580	0,323	0,237	**0,983**	0,637	0,531	0,527

ANALYSIS OF THE SCATTERPLOTS OF ROELVINK-DALY, DEFAULT

At the toe , changing to this breaker formulation leads to a small increase in $H_{m0,lf}$ and a significant decrease of $H_{m0,hf}$. This mostly affects the graph of $s_0 = 4\%$, which now lies in the 10% difference range for all LF motions, with the exception of the smallest couple of conditions, where an overestimation of the LF motions occurs. Therefore, the total RMSE for all wave-heights is lower than for the Surf-beat default results, as can be seen in figure 4.20.

In the swash zone , changing the breaker formulation leads to an absolute initial increase in S_{inc}, which diminishes with increasing H_0. This results in a larger overestimation of S_{inc} for the smaller storm conditions, but a lower underestimation for the other storm conditions. Hence, the total RMSE for S_{inc} is slightly lower than for the *default* breaker formulation. The S_{IG} is increased significantly for all storm conditions. This results in a significantly better approximation of $s_0 = 4\%$, but also a better approximation for the other two offshore wave steepnesses. Not only total but also individual RMSE for the different s_0 is lower than the default breaker formulation. This can be seen in figure A.22.

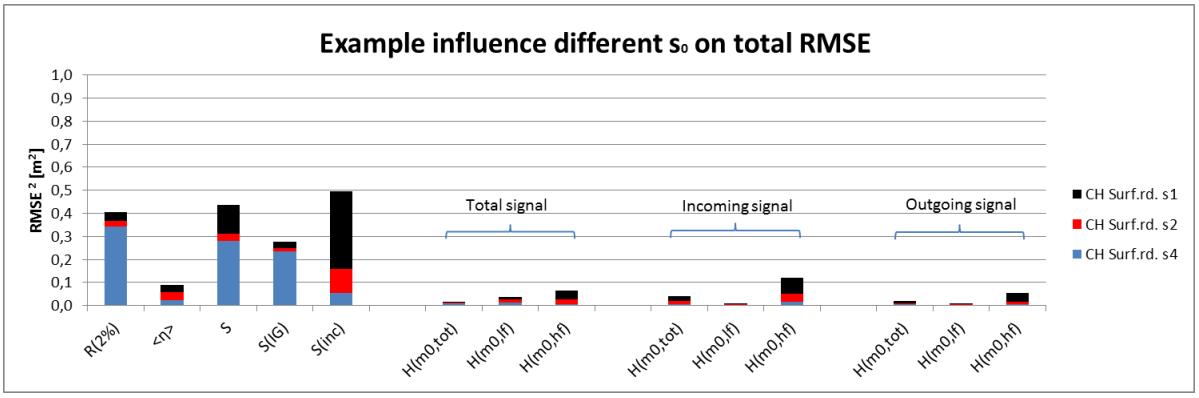

Figure A.22: Contribution to total RMSE by the different offshore wave steepnesses for the Surf-beat Roelvink-Daly breaker formulation. It is a cumulative graph, where the summation of the squares of the RMSE of the different s_0 form the squared total RMSE. The different colours indicate the different offshore steepnesses: Black for $s_0 = 0.01$, red for $s_0 = 0.02$ and blue for $s_0 = 0.04$

The changes in S_{inc} and S_{IG}, lead to a better approximation of S_{tot}. This is only true for the conditions where there is no extreme overestimation of S_{inc}, hence for conditions larger than $H_0 = 2.75$ ($s_0 = 1\%$) and $H_0 = 4$ ($s_0 = 2\%$) at the CH and $H_0 = 3$ ($s_0 = 4\%$) at the CE. For the mean run-up, $< \eta >$, only a small decrease is seen. This results in a minimal decrease of overestimation compared to the Non-hydrostatic results. The combined effects on swash height and mean run-up, result in a better approximation of the $R_{2\%}$, especially for $s_0 = 4\%$.

Overall, this breaker parameter shows a much lower RMSE for both the HF and LF motions, resulting in a better approximation of the run-up at its components.

A.2.2. SURF-BEAT, ROELVINK-DALY, ADAPTED

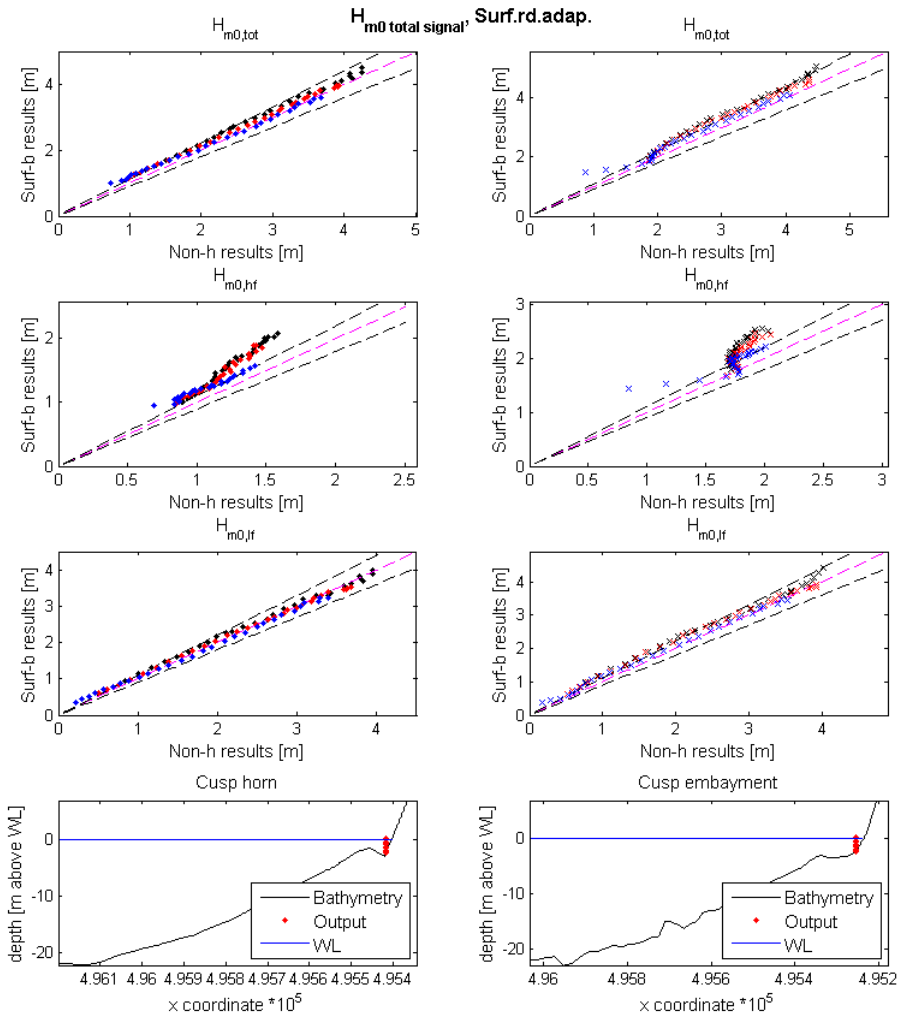

Figure A.23: Surf-beat and Non-hydrostatic scatterplots of the total wave signal at the toe. The black dashed lines (- -) represent a 10% difference between the two modes. The magenta dashed line (- -) represents a 0% difference. Black markers for $s_0 = 0.01$, red markers for $s_0 = 0.02$ and blue markers for $s_0 = 0.04$, $\cdot = CH$, $\times = CE$

Table A.5: RMSE of total wave signal, Surf.rd.adap.

	CH				CE			
Total signal	**All**	$s_0 = 1\%$	$s_0 = 2\%$	$s_0 = 4\%$	**All**	$s_0 = 1\%$	$s_0 = 2\%$	$s_0 = 4\%$
$H_{m0,tot}$	**0,165**	0,121	0,082	0,076	**0,315**	0,236	0,167	0,125
$H_{m0,lf}$	**0,089**	0,057	0,047	0,050	**0,184**	0,135	0,106	0,065
$H_{m0,hf}$	**0,283**	0,208	0,162	0,102	**0,338**	0,249	0,187	0,131

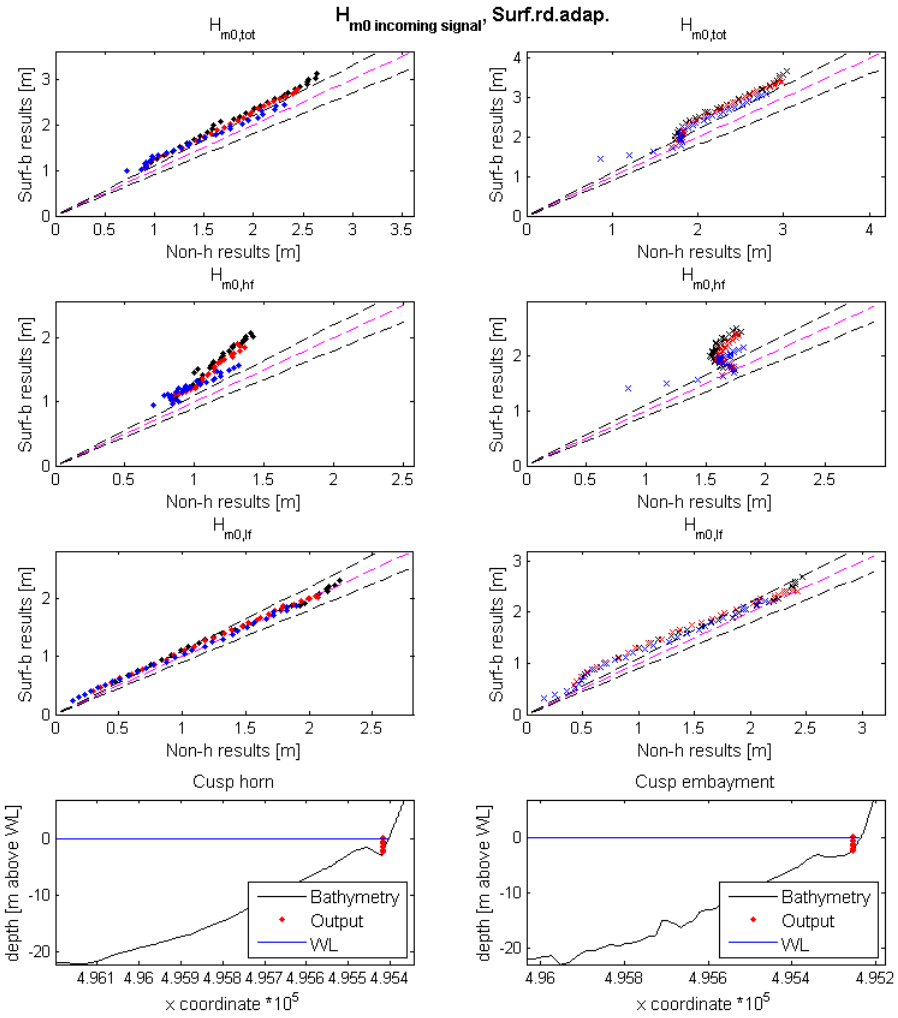

Figure A.24: Surf-beat and Non-hydrostatic scatterplots of the incoming wave signal at the toe. The black dashed lines (- -) represent a 10% difference between the two modes. The magenta dashed line (- -) represents a 0% difference. Black markers for $s_0 = 0.01$, red markers for $s_0 = 0.02$ and blue markers for $s_0 = 0.04$, $\cdot = CH$, $\times = CE$

Table A.6: RMSE of incoming wave signal, Surf.rd.

	CH				**CE**			
Incoming signal	**All**	$s_0 = 1\%$	$s_0 = 2\%$	$s_0 = 4\%$	**All**	$s_0 = 1\%$	$s_0 = 2\%$	$s_0 = 4\%$
$H_{m0,tot}$	**0,278**	0,195	0,156	0,122	**0,408**	0,281	0,234	0,181
$H_{m0,lf}$	**0,074**	0,043	0,043	0,041	**0,202**	0,114	0,128	0,108
$H_{m0,hf}$	**0,372**	0,273	0,206	0,144	**0,434**	0,320	0,242	0,166

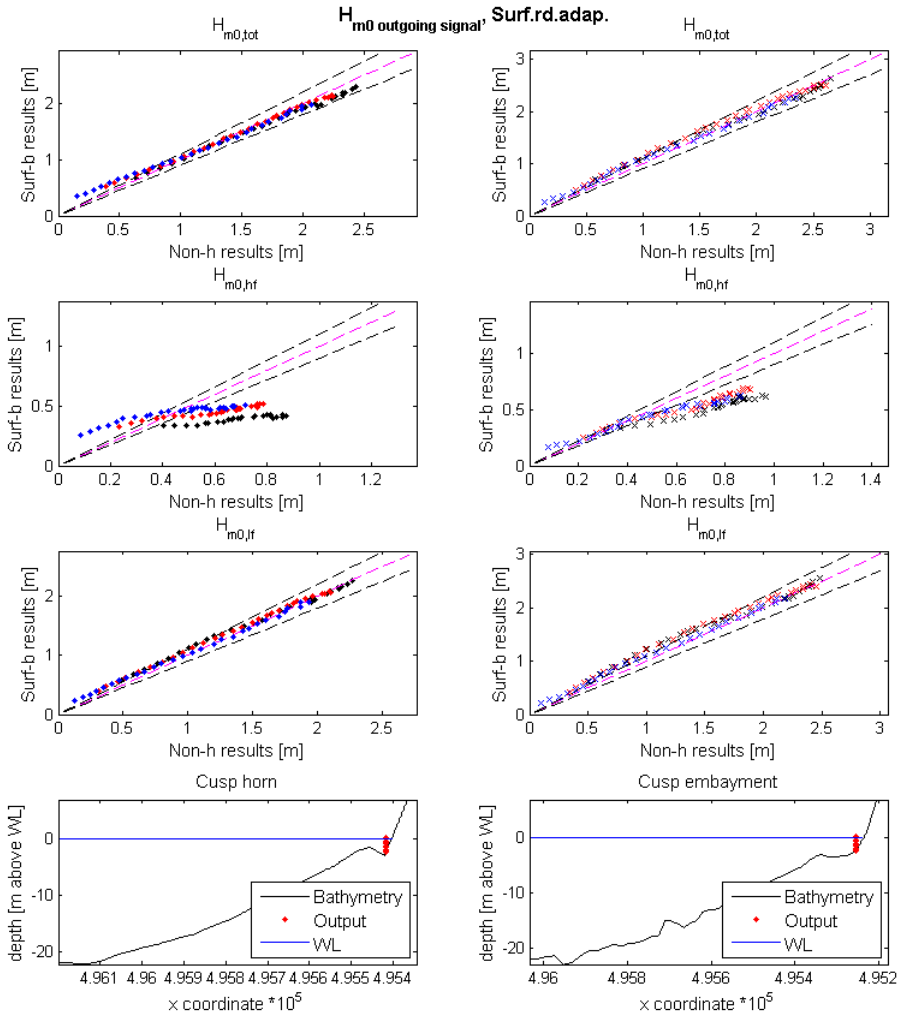

Figure A.25: Surf-beat and Non-hydrostatic scatterplots of the outgoing wave signal at the toe. The black dashed lines (- -) represent a 10% difference between the two modes. The magenta dashed line (- -) represents a 0% difference. Black markers for $s_0 = 0.01$, red markers for $s_0 = 0.02$ and blue markers for $s_0 = 0.04$, $\cdot = CH$, $\times = CE$

Table A.7: RMSE of outgoing wave signal, Surf.rd.adap.

	CH				**CE**			
Outgoing signal	**All**	$s_0 = 1\%$	$s_0 = 2\%$	$s_0 = 4\%$	**All**	$s_0 = 1\%$	$s_0 = 2\%$	$s_0 = 4\%$
$H_{m0,tot}$	**0,086**	0,053	0,035	0,058	**0,094**	0,053	0,062	0,046
$H_{m0,lf}$	**0,071**	0,043	0,042	0,036	**0,124**	0,075	0,086	0,050
$H_{m0,hf}$	**0,228**	0,188	0,106	0,071	**0,181**	0,141	0,085	0,074

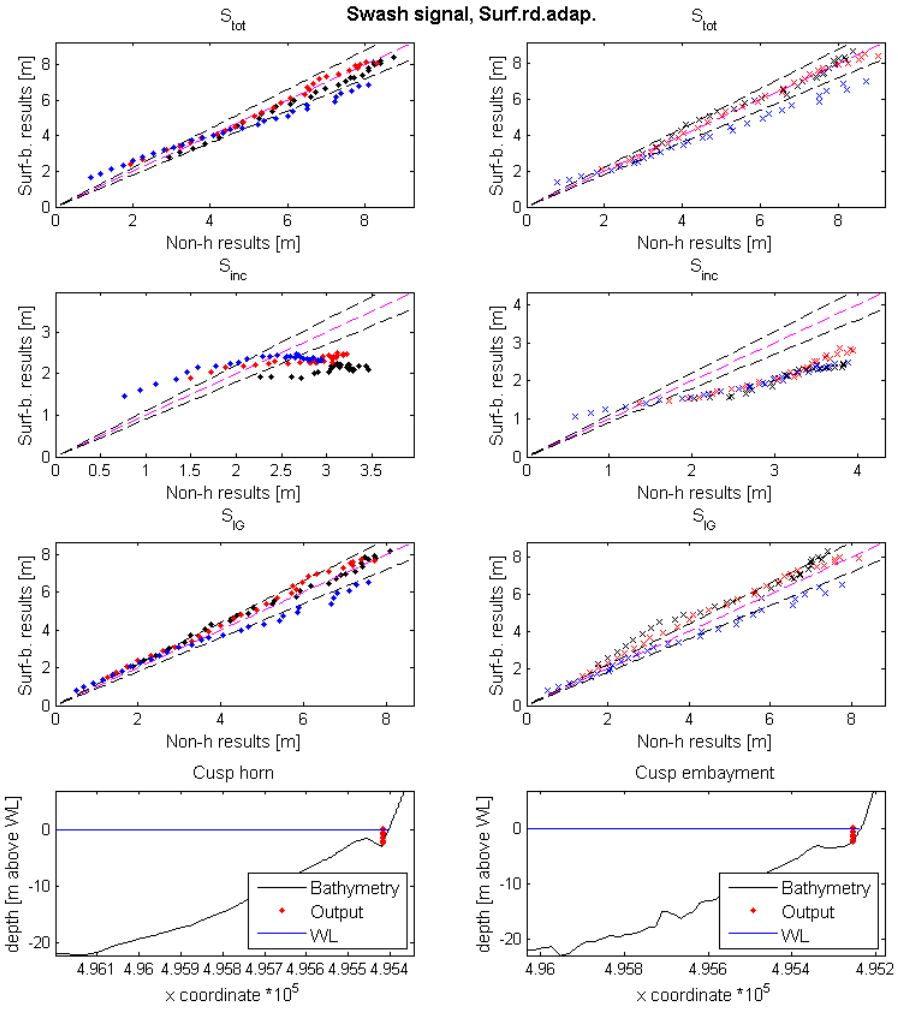

Figure A.26: Surf-beat and Non-hydrostatic scatterplots of the swash height amplitude in the swash zone. Black markers for $s_0 = 0.01$, red markers for $s_0 = 0.02$ and blue markers for $s_0 = 0.04$, $\cdot = CH$, $\times = CE$

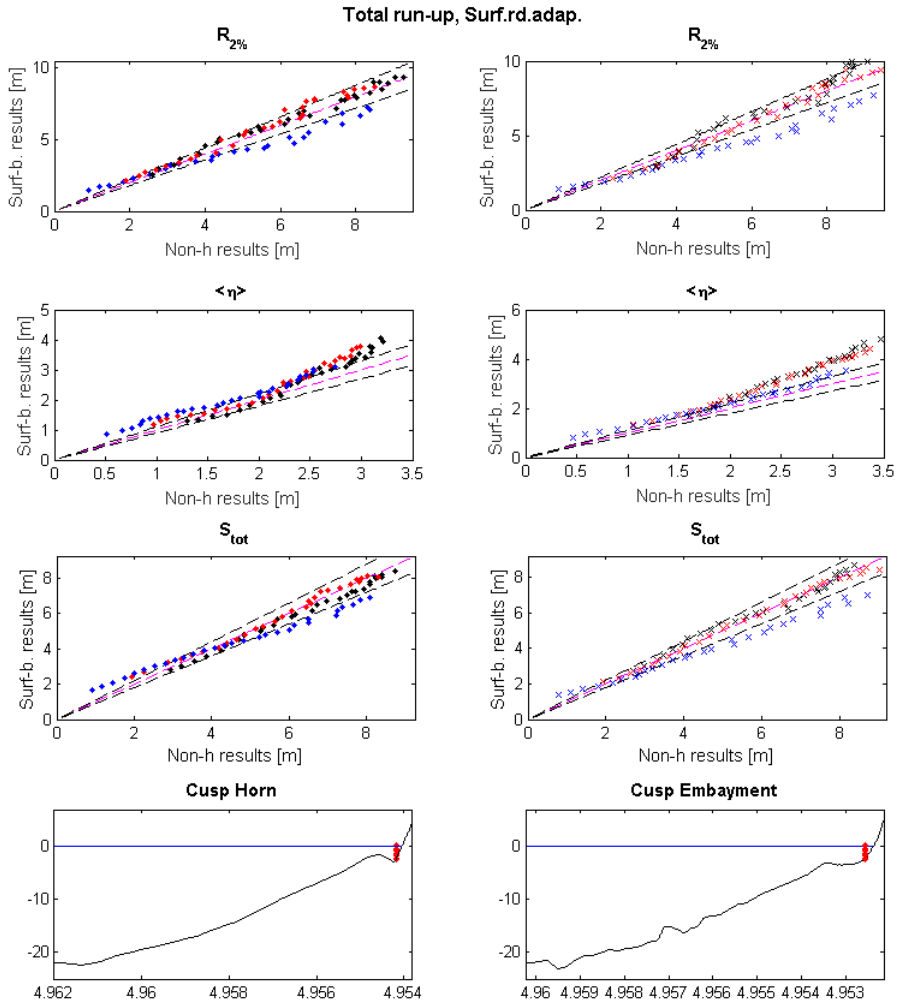

Figure A.27: Surf-beat and Non-hydrostatic scatterplots of the run-up and its components. The black dashed lines (- -) represent a 10% difference between the two modes. The magenta dashed line (- -) represents a 0% difference. Black markers for $s_0 = 0.01$, red markers for $s_0 = 0.02$ and blue markers for $s_0 = 0.04$, $\cdot = CH$, $\times = CE$.

Table A.8: RMSE of run-up parameters, Surf.rd.adap.

	CH				**CE**			
Run-up signal	**All**	$s_0 = 1\%$	$s_0 = 2\%$	$s_0 = 4\%$	**All**	$s_0 = 1\%$	$s_0 = 2\%$	$s_0 = 4\%$
$R_{2\%}$	**0,592**	0,185	0,275	0,490	**0,780**	0,357	0,191	0,666
$<\eta>$	**0,373**	0,221	0,235	0,187	**0,617**	0,462	0,376	0,158
S	**0,475**	0,176	0,127	0,423	**0,548**	0,133	0,094	0,523
S_{IG}	**0,433**	0,144	0,209	0,351	**0,598**	0,412	0,277	0,333
S_{inc}	**0,709**	0,580	0,323	0,248	**0,969**	0,634	0,523	0,513

ANALYSIS OF THE SCATTERPLOTS OF ROELVINK-DALY, ADAPTED

The adaption of the *Roelvink-Daly* formulations leads to an increase of wave motions in general, both HF and LF motions. The most significant increase, however, is for the LF motions. This increase results in a larger overestimation of results that were already overestimated, but a better approximation of the results which were underestimated. By looking at figure 4.20, it can be seen that at the toe, the RMSE of the total and incoming signal are higher than the RMSE for the *Roelvink-Daly,default* breaker formulation.

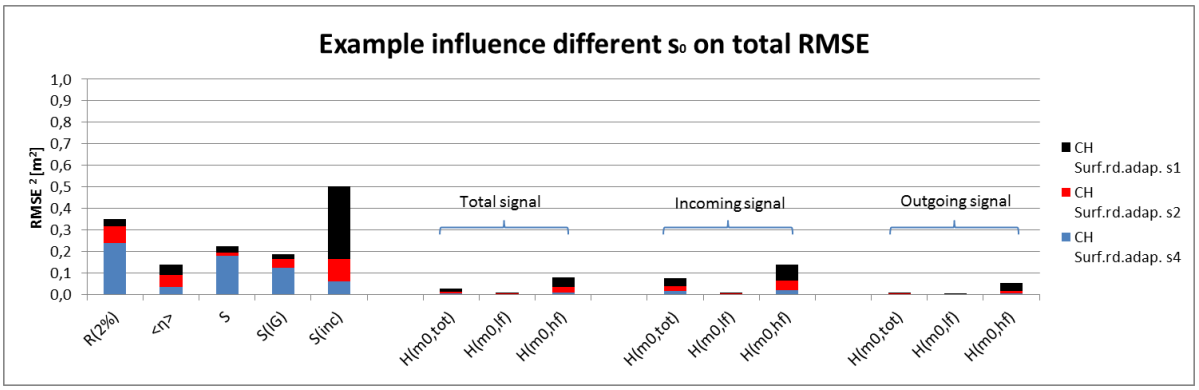

Figure A.28: Contribution to total RMSE by the different offshore wave steepnesses for the Surf-beat Roelvink-Daly (adapted) breaker formulation. It is a cumulative graph, where the summation of the squares of the RMSE of the different s_0 form the squared total RMSE. The different colours indicate the different offshore steepnesses: Black for $s_0 = 0.01$, red for $s_0 = 0.02$ and blue for $s_0 = 0.04$

In the swash zone, again an initial increase of HF motions, S_{inc}, is found. This increase also diminishes with increasing H_0, hence not changing the total RMSE. As all LF motions are increased, so is the S_{IG}. This results in again more overestimation of the smaller conditions. This causes an increase in total RMSE for the CE, but a slight decrease for the CH. Combined however, the S_{tot} has a lower RMSE, as it experiences both over and underestimation. The increased wave heights cause an increase in the mean run-up as well, resulting in higher $R_{2\%}$. This results in a slightly lower RMSE for this breaker formulation, however, it is mostly due to the better approximation of $s_0 = 4\%$. The other two offshore wave steepnesses are affected differently, as can be seen in figure A.28.

The increase in LF motions is mostly beneficial for the results of $s_0 = 4\%$. However, in the swash zone, the results of this offshore wave height still are underestimated by more than 10%. Also, as wave conditions are increased, overestimations worsen by changing from the default breaker model.

B

2D RESULTS

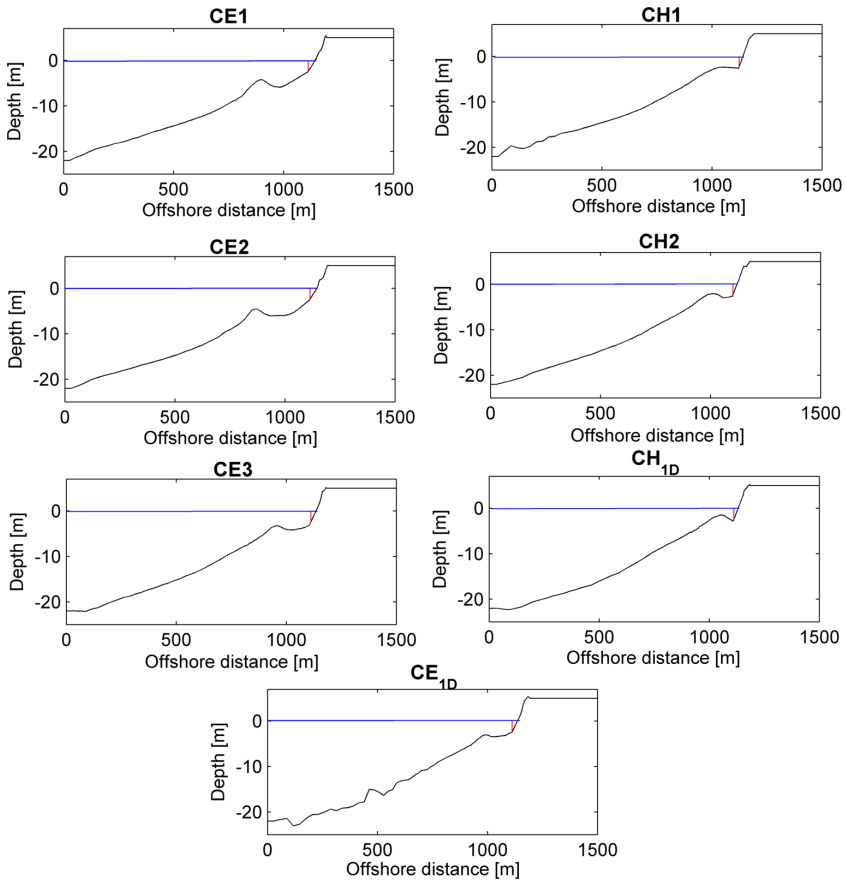

Figure B.1: Cross-sections of the 2D output locations

Table B.1: Beach face slopes of the different cross-sections

	CE1	**CH1**	**CE2**	**CH2**	**CE3**	CH_{1D}	CE_{1D}
β_f	0,093	0,137	0,097	0,121	0,103	0,123	0,096
Bar-depth [m below MSL]	4,26	2,37	4,54	2,07	3,31	1,56	3,03

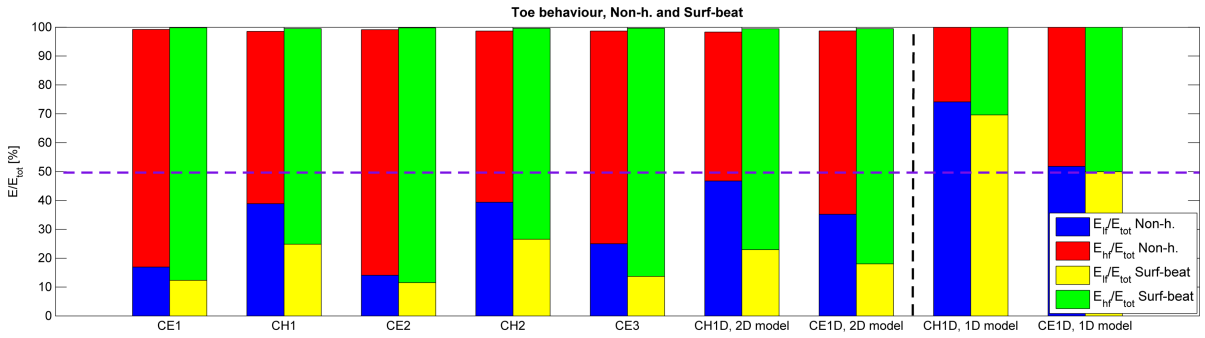

Figure B.2: Comparison of 2D behaviour of the Non-hydrostatic and Surf-beat mode, at the toe

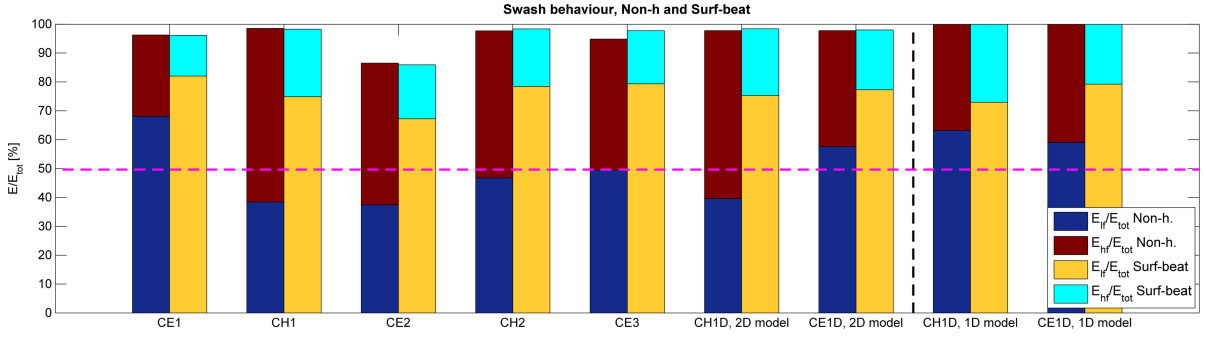

Figure B.3: Comparison of 2D behaviour of the Non-hydrostatic and Surf-beat mode, in the swash zone

C

SWASH-ZONE ANALYSIS

In many studies, a cutoff frequency (f_{cutoff}) is used in the analysis of the run-up signal. It is assumed that any motions above this frequency are wiggles within the system and therefore should not be part of the analysis. An example of this f_{cutoff} is 0.67Hz, a value used by Hughes *et al.* [5]. The analysis of both the 1D and 2D model do not include this cutoff frequency, but have the Nyquist frequency (f_N) as a maximum. This frequency is based on the sample frequency, as visible in equation C.1. Any frequency higher than the $f_{nyquist}$ leads to undersampling or aliasing. This chapter analyses which differences occur if a cutoff frequency would be used instead.

$$f_N = 0.5 f_{sampling} \tag{C.1}$$

C.1. SPECTRAL ANALYSIS

Using a lower maximum frequency in the spectral analysis can affect the total and hf swash height. This section shows the difference in percentage of swash height when a cutoff frequency is used. The difference for the Non-hydrostatic 2D results can be found in table C.1 and analogous the Surf-beat 2D results in table C.2.These tables show that the differences are minimal for the swash height. This could have been expected, as the spectra showed little to no energy within the frequency band higher that the f_{cutoff}. The only exception is the results of location *CE2*, where both the Non-hydrostatic and Surf-beat mode show differences larger than 1%. By looking at the swash spectra, it can be concluded that this location shows more energy in the hf band already for frequencies lower than the f_{cutoff}, compared to the other locations. It can not be said with certainty if this is due to computational error or a physical response to the bathymetry, without any data. Therefore, it is recommended to check if this occurs for other offshore wave heights as well.

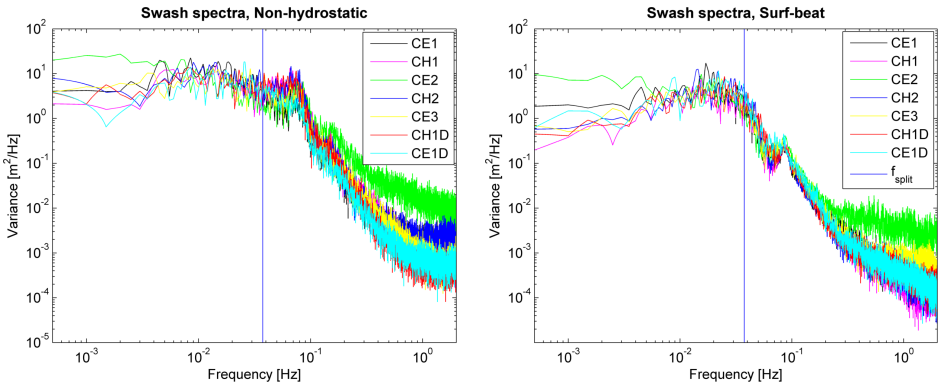

(a) Swash spectra of the 2D Non-hydrostatic mode

(b) Swash spectra of the 2D Surf-beat mode

Figure C.1: Logarithmic graphs with the swash spectra of the Surf-beat and Non-hydrostatic mode.

Table C.1: Effect of f_{cutoff} on swash-height, Non-h.

	S			S_{IG}			S_{inc}		
Location	**Non-h.**	**Non-h. with f_{cutoff}**	**difference [%]**	**Non-h.**	**Non-h. with f_{cutoff}**	**difference [%]**	**Non-h.**	**Non-h. with f_{cutoff}**	**difference [%]**
CE1	2,72	2,72	**0,2**	2,25	2,25	**0,0**	1,45	1,43	**0,8**
CH1	2,93	2,93	**0,2**	1,82	1,82	**0,0**	2,27	2,27	**0,3**
CE2	2,95	2,89	**1,9**	1,80	1,80	**0,0**	2,07	1,99	**3,7**
CH2	3,11	3,10	**0,2**	2,12	2,12	**0,0**	2,22	2,21	**0,5**
CE3	2,63	2,63	**0,1**	1,85	1,85	**0,0**	1,77	1,77	**0,3**
CH1D, 2D model	2,92	2,92	**0,1**	1,84	1,84	**0,0**	2,23	2,22	**0,1**
CE1D, 2D model	2,40	2,40	**0,1**	1,82	1,82	**0,0**	1,52	1,52	**0,3**
CH1D, 1D model	4,64	4,64	**0,0**	3,69	3,69	**0,0**	2,81	2,81	**0,1**
CE1D, 1D model	4,39	4,38	**0,1**	3,37	3,37	**0,0**	2,81	2,80	**0,2**

Table C.2: Effect of f_{cutoff} on swash-height, Surf-b.

	S			S_{IG}			S_{inc}		
Location	**Surf-b.**	**Surf-b. with f_{cutoff}**	**difference [%]**	**Surf-b.**	**Surf-b. with f_{cutoff}**	**difference [%]**	**Surf-b.**	**Surf-b. with f_{cutoff}**	**difference [%]**
CE1	1,69	1,69	**0,1**	1,53	1,53	**0,0**	0,63	0,63	**0,8**
CH1	1,33	1,33	**0,1**	1,15	1,15	**0,0**	0,64	0,64	**0,5**
CE2	1,68	1,66	**1,2**	1,38	1,38	**0,0**	0,73	0,67	**7,2**
CH2	1,73	1,73	**0,1**	1,53	1,53	**0,0**	0,77	0,77	**0,5**
CE3	1,57	1,56	**0,3**	1,40	1,40	**0,0**	0,67	0,66	**1,5**
CH1D, 2D model	1,56	1,56	**0,1**	1,35	1,35	**0,0**	0,75	0,74	**0,6**
CE1D, 2D model	1,70	1,70	**0,1**	1,49	1,49	**0,0**	0,77	0,77	**0,5**
CH1D, 1D model	4,29	4,29	**0,0**	3,67	3,67	**0,0**	2,23	2,23	**0,1**
CE1D, 1D model	4,16	4,15	**0,1**	3,70	3,70	**0,0**	1,90	1,89	**0,3**

C.2. RUN-UP ANALYSIS

The cutoff frequency results in a smoother run-up signal, and therefore it can be expected to have an influence on the $R_{2\%}$ and $<\eta>$. This influence largely depends on where the wiggles occur in the signal; if they occur on the lowest or highest peaks, they respectively lower or increase the $R_{2\%}$ and $<\eta>$. This can be seen in tables C.3 and C.4, where the differences cover a larger range for both the Non-hydrostatic and the Surf-beat mode.

Table C.3: Effect of f_{cutoff} on $R_{2\%}$ and $<\eta>$, Non-h.

	$<\eta>$			$R_{2\%}$		
Location	**Non-h.**	**Non-h. with f_{cutoff}**	**difference [%]**	**Non-h.**	**Non-h. with f_{cutoff}**	**difference [%]**
CE1	1,53	1,39	**9,2**	2,92	2,72	**6,9**
CH1	1,26	1,36	**-7,9**	2,64	2,69	**-1,9**
CE2	1,80	1,78	**1,2**	2,55	2,57	**-0,7**
CH2	1,50	1,50	**-0,5**	2,85	2,90	**-1,6**
CE3	1,49	1,57	**-5,3**	2,84	2,79	**1,5**
CH1D, 2D model	1,29	1,34	**-4,1**	2,63	2,65	**-0,7**
CE1D, 2D model	1,45	1,44	**0,5**	2,92	2,81	**3,7**
CH1D, 1D model	1,93	1,93	**0,1**	4,72	4,72	**0,0**
CE1D, 1D model	2,00	2,00	**0,2**	5,02	5,02	**0,1**

Using a f_{cutoff} does not affect the absolute differences between the two modes for the swash height, as similar changes occur. For the maximum and mean run-up changes do not occur equally for the two modes. Again, this is mostly due to where the wiggles are located within the run-up signal. This shows that the analysis of the maximum run-up is extremely sensitive for small changes within the signal.

Finally, the differences for the 1D model are small. It is suggested this is due to the extremely fine grid. Most wiggles in the 2D run-up signal occur between 2 consecutive grid points, again showing that a finer grid would be desirable in the determination of the maximum run-up.

Table C.4: Effect of f_{cutoff} on $R_{2\%}$ and $<\eta>$, Surf-b.

	$<\eta>$			$R_{2\%}$		
Location	**Surf-b.**	**Surf-b. with f_{cutoff}**	**difference [%]**	**Surf-b.**	**Surf-b. with f_{cutoff}**	**difference [%]**
CE1	1,19	1,36	**-13,6**	2,12	2,42	**-14,0**
CH1	1,05	1,07	**-2,1**	1,82	1,87	**-2,3**
CE2	1,40	1,55	**-11,3**	2,30	2,62	**-14,1**
CH2	1,23	1,12	**8,8**	2,29	2,17	**5,2**
CE3	1,30	1,25	**4,1**	2,15	2,25	**-4,9**
CH1D, 2D model	1,16	0,95	**18,5**	2,06	2,00	**3,0**
CE1D, 2D model	1,25	1,19	**4,8**	2,12	2,06	**2,6**
CH1D, 1D model	1,86	1,86	**0,1**	4,35	4,34	**0,0**
CE1D, 1D model	2,26	2,26	**0,2**	4,61	4,60	**0,2**

D

EXAMPLE OF A 1D XBEACH INPUT FILE

```
%%%%%%%%%%%%%%%%%%%%%%%%%%%%%%%%%%%%
%%%    XBeach parameter settings input file    %%%
%%%    date: 18 - Feb - 2016 10:30:33          %%%
%%%    function: xb_write_params               %%%
%%%%%%%%%%%%%%%%%%%%%%%%%%%%%%%%%%%%

%%%%%%%%Physical processes%%%%%%%%%%%
swave = 1
nonh = 0
morphology = 0
sedtrans = 0
%%%%%%%%Flow boundary condition parameters%%
sprdthr = 0.08
random = 0
%%%%%%%%Flow numerics parameters%%%%%%%%
umin = 0
hmin = 0.200000
%%%%%%%%Flow parameters%%%%%%%%%%%%%%
C = 65
%%%%%%%%Grid parameters%%%%%%%%%%%%%%
gridform = xbeach
xfile = xnew.grd
yfile = ynew.grd
vardx = 1
nx = 1285
ny = 0
depfile = znew.grd
posdwn = -1
thetanaut = 1
thetamin = -45.5
thetamax = 134.5
dtheta = 180
%%%%%%%%Model time%%%%%%%%%%%%%%%%%%
tstop = 3600
CFL = 0.900000
%%%%%%%%Roller parameters%%%%%%%%%%%%%
roller = 1
%%%%%%%%Tide boundary conditions%%%%%%%%%%
tideloc = 1
```

```
zs0file = tide.txt
%%%%%%%%Wave boundary condition parameters%%%
instat = jons_table
bcfile = waves.lst
%%%%%%%%Wave breaking parameters%%%%%%%%
break = 3
gamma = 0.500000
alpha = 1
n = 10
delta = 0
%%%%%%%%Output variables%%%%%%%%%%%%%%
tint = 100
tstart = 0
outputformat = netcdf
nglobalvar = 2
zs
u
npoints = 73
%%%xlocation ylocation name%%%
495821. 4181578.73
495807. 4181563.72
495790. 4181546.71
495149. 4180893. 3
495142. 4180886. 2
495135. 4180879. 1

npointvar = 2
zs
H
tintp = 0.25
nmeanvar = 2
zs
qx
nrugauge = 1
0.0.
```